UNIVERSIDAD DE LA RIOJA

TESIS DOCTORAL

Título
Functional coatings deposited by an Atmospheric Pressure Plasma Jet (APPJ) system over Thermoplastic Elastomer (TPE) substrates
Autor/es
Elisa Sainz García
Director/es
Fernando Alba Elías y Joaquín Bienvenido Ordieres Mere
Facultad
Escuela Técnica Superior de Ingeniería Industrial
Titulación
Departamento
Ingeniería Mecánica
Curso Académico

Tesis presentada como compendio de publicaciones. La edición en abierto de la misma NO incluye las partes afectadas por cesión de derechos

publicaciones.unirioja.es
E-mail: publicaciones@unirioja.es

UNIVERSITY OF LA RIOJA

MECHANICAL ENGINEERING DEPARTMENT

FUNCTIONAL COATINGS DEPOSITED BY AN ATMOSPHERIC PRESSURE PLASMA JET (APPJ) SYSTEM OVER THERMOPLASTIC ELASTOMER (TPE) SUBSTRATES

ELISA SAINZ GARCÍA

Doctoral Dissertation guided by

DR. FERNANDO ALBA ELÍAS

DR. JOAQUÍN ORDIERES MERÉ

in order to apply for the degree of

DOCTOR OF UNIVERSITY OF LA RIOJA

Logroño, March 2017

ABSTRACT

The study of the friction coefficient and the hydrophobic character has long been of great importance in the automotive industry where some areas of the vehicle are subject to slippage. One example is the space between the window channels and the glass. The polymeric materials that are used in these areas, like thermoplastic elastomers (TPEs), involve a high degree of friction. So, in order to decrease the friction coefficient of the TPE, companies are using techniques as flocking. However, its high energy consumption, irregular distribution of fibers, poor adhesion and superhydrophilic character are the main drawbacks. Since TPE is a heat-sensitive material, an Atmospheric Pressure Plasma Jet (APPJ) system with a Dielectric Barrier Discharge (DBD) was used in this thesis.

During the first group of scientific publications, with the objective of reducing the friction coefficient of TPE, the siloxane, aminopropyltriethoxysilane (APTES) was used as precursor. The influence of the plasma power and number of passes was characterized by Profilometry, Atomic Force Microscopy (AFM), Scanning Electron Microscopy (SEM), Attenuated Total Reflectance-Fourier Transform Infrared (ATR-FTIR) Spectroscopy, X-Ray Photoelectron Spectroscopy (XPS), Water Contact Angle (WCA) measurements and friction coefficient. The average surface temperature of the samples and the coating thickness seemed to be the key variables in determining the friction behavior. Successful samples (those that have a lower friction coefficient than those of the current industrial solutions) were coated at an average surface temperature of less than 92 ºC and thickness of the coatings was greater than 1000 nm. Sample coated in six passes and the lowest power proved to have the best friction performance. This sample had a friction coefficient that was 46% lower than that of the flocked seals.

Whereas in the second group of scientific publications, the aim was promoting the adhesion of an antifriction (based on APTES) and hydrophobic (based on a fluorinated precursor) coating by the adhesion promoter, APTES. Different mixtures of APTES with FLUSI (heptadecafluoro-1,1,2,2-tetrahydrodecyl)trimethoxysilane) and PFH (1-perfluorohexene) were applied. The abovementioned characterization techniques together with the lap-shear test were used to study the influence of each precursor percentage. The main difficulty in this work lied in the hydrophilic character of APTES (for example, -NH_2) and the low adhesion of the fluorinated coatings. On one hand, the sample that was coated with 25% of FLUSI and 75% of APTES combined the improvements of both functional properties. It had an average friction coefficient that was 51.5% lower and a WCA that was 4.4% higher than the uncoated TPE sample. A satisfactory stability in humid ambient for twelve months showed a slight decrease of WCA (4.4%) for this sample. On the other hand, the sample coated with a mixture of 50% APTES and 50% PFH was found to be

the best one to satisfy both properties at the same time, despite not having the highest dynamic WCA or the lowest friction coefficient.

Finally, it can be concluded that an APPJ system has been used to deposit a coating over TPE substrates with a friction coefficient lower than the current industrial solutions (flocked seals and polyamide tape) and a hydrophobicity higher than the uncoated TPE. Thus, it is considered that the two proposed objectives have been successfully fulfilled. This allows one to conclude that this technology could be a promising alternative to the current industrial solutions.

ACKNOWLEDGEMENTS

I would like to express my deepest gratitude to my supervisors, Dr. Fernando Alba-Elías and Dr. Joaquín Ordieres-Meré for their excellent guidance and endless encouragement during these years. My heartfelt gratitude to Dr. Ana González-Marcos for her kind advices and support.

I am also thankful to my colleagues Laura Martínez-Martínez, Rodolfo Múgica-Vidal and Cristina Ramírez-Aragón that have created sociable atmosphere in the laboratory.

Last but not least, I express my gratitude to my family for always supporting me in all my endeavors.

This thesis would not have been possible without your help.

Thanks,

Elisa Sainz García

Logroño, March 2017

CONTENTS

LIST OF FIGURES

LIST OF TABLES

ABBREVIATIONS

AFM	Atomic Force Microscopy
APCP	Atmospheric Pressure Cold Plasma
APPJ	Atmospheric Pressure Plasma Jet
APTES	Aminopropyltriethoxysilane
ATR	Attenuated Total Reflectance
ATR-FTIR	Attenuated Total Reflectance – Fourier Transform Infrared Spectroscopy
CVD	Chemical Vapor Deposition
DBD	Dielectric Barrier Discharge
EDX	Energy Dispersive X-ray
EPDM	Ethylen Propylene Diene Monomer
FLUSI	(Heptadecafluoro-1,1,2,2-tetrahydrodecyl)trimethoxysilane
FTIR	Fourier Transform Infrared Spectroscopy
IR	Infrared Spectroscopy
LST	Lap-Shear Strenght
LVDT	Linear Variable Differential Transformer
PE-CVD	Plasma Enhanced – Chemical Vapor Deposition
PFH	1-perfluorohexene
PVD	Physical Vapor Deposition
RF	Radio-Frequency
RMS	Root Mean Square
SD	Standard Deviation
SEM	Scanning Electron Microscopy
TPE	Thermoplastic Elastomer
WCA	Water Contact Angle
XPS	X-ray Photoelectron Spectroscopy

CHAPTER 1

INTRODUCTION

1.1. BACKGROUND

1.1.1. PLASMA TECHNOLOGY

Plasma technology is becoming more and more popular as a way to modify the intrinsic properties of substrate materials by coating or activation [1–3]. Related to the coating deposition, the method is called Plasma Polymerization and it consists of the deposition of thin films on different substrates from a liquid or gas precursor or a mixture of precursors which are exposed to plasma. Moreover, the plasma is generated by ionization. The selection of precursors and the plasma polymerization parameters (plasma power, precursor gas flow, plasma gas, etc.) define the characteristics of the coating and, therefore, of the modified surface [4,5], which can be hydrophilic, hydrophobic, adhesion promoter, anti-adherent, friction-reducing, anticorrosive, absorbance-enhancing of light, etc.

During the last 30 years, plasma equipment for the deposition of solid coatings (for instance, hard coatings for cutting tools) have been commonly employed. These equipment, such as the Chemical Vapor Deposition (CVD) or the Physical Vapor Deposition (PVD), use chamber deposition methods with thermal plasmas in which the coating temperature fluctuate between 200-1000 ºC and they are known of their specific properties, such as their chemical structures and protective coating [6]. However, these coating methods are unsuitable for products that are made from heat-sensitive materials, such as thermoplastic elastomers (TPEs), because of their high processing temperatures [7]. In addition, the low-temperature, Plasma Enhanced Chemical Vapor Deposition (PE-CVD) method is characterized by deposition temperatures that are considerably lower than experienced in other methods [8]. In spite of its excellent coating efficiency, the use of this technique is limited due to the restricted volume of the plasma reactor, the requirement for one or more chemical cycles and the need for a vacuum pressure environment.

This is why, several techniques of cold deposition of solid coatings have been investigated using different sources of Atmospheric Pressure Cold Plasma (APCP) or Atmospheric Pressure Plasma

Jet (APPJ). Compared with thermal plasma, the temperature of the electrons in the cold plasma is much higher than the temperature of the ions and neutral particles, since the energy applied is channeled preferably towards the electrons. Since ions and uncharged particles do not heat as much as electrons, this plasma is called "cold" or "non-thermal". Due to its low temperature, cold plasma treatment is much more careful. The temperature of the ions and neutral atoms does not exceed 100 ºC, while the electrons reach a temperature of about 100.000 ºC. Thus, it can be said that in these techniques the deposition temperature of the coating varies between 30-100 ºC, being the only technique to deposit a solid coating by plasma technology that does not compromise the integrity of any heat-sensitive material, like TPE. As with vacuum techniques (PVC, CVD and PE-CVD), they avoid the use of organic solvents and have a good energy efficiency [5,9,10]. In addition, the use of expensive pumping systems and the construction of air-vacuum chambers are avoided, which makes it possible to reduce costs [10–12]. In this way, the parameters of the plasma polymerization process are easier to control [9]. Therefore, they can be easily implemented in an industrial production line [11,13]. Recent studies have identified and described the types of APCP technology for deposition of coatings [14,15]: [a] Corona Discharge, [b] Dielectric Barrier Discharge (DBD), [c] Radio-Frequency Discharge (RF).

In this thesis an Atmospheric Pressure Plasma Jet system operating in a Dielectric Barrier Discharge configuration is used, since it is particularly suitable for the treatment of heat-sensitive materials, such as TPE [3,13]. In addition, compared to current methods of coating, APPJ has many advantages: [a] a solvent-free process, [b] a clean process, [c] no need vacuum equipment, [d] a lower processing costs, [e] easy scalability for industrial on-line processing, [f] moderate substrate temperature and [g] relatively easy control of plasma parameters (plasma power, gas flow…) [4,11–13].

1.1.2. THERMOPLASTIC ELASTOMERS

The use of elastomer-based materials has increased because of their high performance, relatively low cost and light in weight [12]. Thermoplastic elastomer refers to a series of commercial plastic materials that are both relevant and interesting [16]. TPEs are multifunctional polymeric materials that combine the processability of thermoplastics and the softness, flexibility and resilience of vulcanized rubber. In general, they are biphasic materials that: [a] possess the combined properties of the glassy or semi-crystalline thermoplastics and soft elastomers and [b] enable rubbery materials to be processed as thermoplastics [14–17]. TPEs are characterized by moderate cost, excellent mechanical properties (high elasticity, good flexibility, hardness, etc.), high tensile strength, chemical resistance and hydrophobic character. Furthermore, they offer a wider processing window which makes them ideal for huge industrial applications [14,18].

Nowadays, the global TPEs market is one of the most dynamic markets in the world. The diversity of TPEs means that the market now covers a range of different applications, such as in the automotive industry, wire and cable industry, medical applications, engineering, etc. [18–21]. The use of TPEs in the automotive industry represented over 42% of its market during the period of 2011 to 2013 [20]. In particular, TPEs are widely used in the automotive sealing industry to

produce components for various automotive parts that must be water tight, dust proof and noise proof so, the intrinsically high friction of TPEs is needed [22]. Nevertheless, this high friction coefficient can be a serious problem in some areas of the vehicle in which there is a slippage, such as the space between the window channels and the glass, or between the wind-shield and the wind-shield wipers, where a low friction coefficient is necessary to prevent jams. Furthermore, a high hydrophobicity would be desirable in order to evacuate the stored water in the operation. Currently, with the aim of improving the friction performance, companies are using two different techniques, such as the electrostatic flocking and a polyamide tape affixed to the tape seals. At present, the electrostatic flocking is the most widely used industrial alternative because there is no other technology with better results in terms of friction coefficient**.** This consists of the incorporation of polyamide and polyethylene fibers on the seal surface, which is pretreated by applying adhesives. However, the main drawbacks of this method are: irregular distribution of fibers, poor fiber orientation, poor adhesive distribution, poor performance in the installation, long flocking lines and high energy consumption.

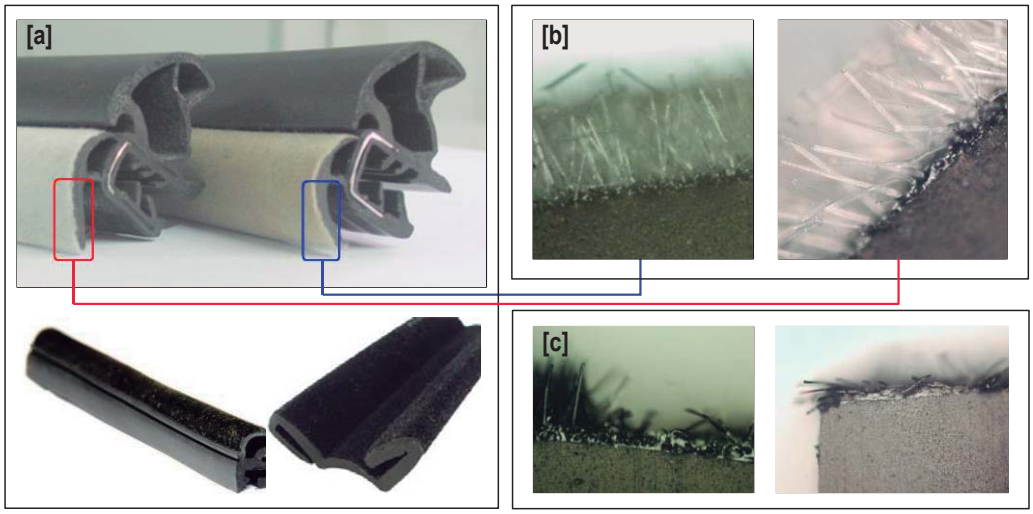

Figure 1.1. [a] Flocked seals, [b] detail micrograph of correct seals and [c] detail micrograph of defective seals.

1.2. MOTIVATION AND OBJECTIVES

Recent advances in APPJ technology have opened a new field in the search of solutions to several industrial problems. The application of functional coatings by this technology allows a simple control of the functional properties that are desired to obtain on the substrate, in addition to an easy implementation of the same in existing production lines on a large scale. In the field of sealing automotive industry, it would be very convenient to replace the current electrostatic flocking technique with a simpler solution with better industrial performance.

Taking the above into account, the main aims of this thesis, including the work of the last four years, are:

OBJECTIVE 1:

Deposition of SiO_x-based functional coatings produced by an Atmospheric Pressure Plasma Jet system over TPE substrates, which have friction coefficients that are similar to, or lower than, the current industrial solutions with the same or greater durability.

OBJECTIVE 2:

Deposition of functional coatings produced by an Atmospheric Pressure Plasma Jet system over TPE substrates to improve both the tribological and hydrophobic properties of the uncoated TPE by using a mixture of two liquid precursors.

1.3. THESIS CONTRIBUTIONS

The two objectives mentioned were achieved and were materialized in four scientific publications that are briefly described below.

1.3.1. SCIENTIFIC PUBLICATIONS

Tribological behavior of plasma-polymerized aminopropyltriethoxysilane films deposited on thermoplastic elastomers substrates. F. Alba-Elías, E. Sainz-García, A. González-Marcos, J. Ordieres-Meré, Thin Solid Films 540 (2013) 125-134.

With an objective of reducing the superficial friction coefficient of TPE, this work analyzes the characteristics of coating films that are based on APTES over a TPE substrate. Since this material is heat-sensitive, it is necessary to use a technology that permits the deposition of coatings at low temperatures without affecting the substrate integrity. Thus, an APPJ system with a DBD was used in this study. After the morphological, chemical and tribological analysis of the coated samples, the studies showed that the coated samples that contain a higher amount of forms of SiOSi and nitrogen-containing groups have lower friction coefficients. The sample coated at a specific plasma power of 550 W and an APTES flow rate of 1.5 slm had the highest values of SiOSi and nitrogen-containing groups peak intensity and atomic percentages of Si2p and SiO_4, and the lowest percentages of C1s and average friction coefficient. The results of this research permit one to conclude that APPJ with a DBD is a promising technique to use in coating SiO_x and nitrogen-containing groups layers on polymeric materials.

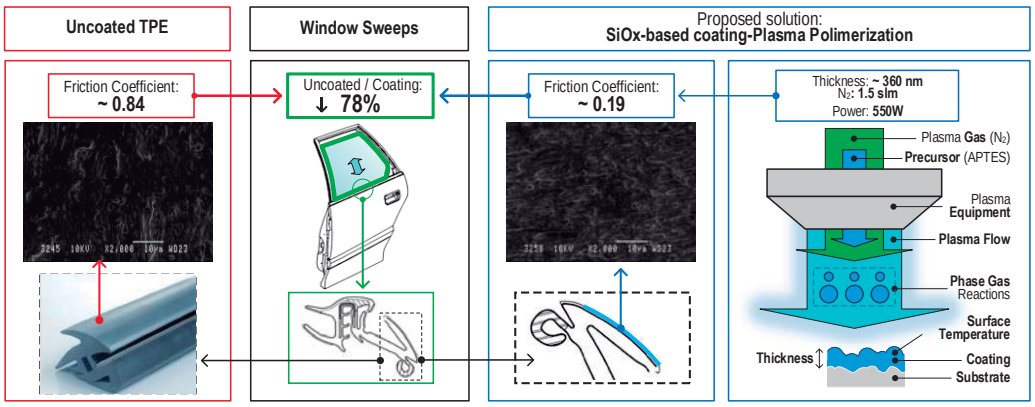

Figure 1.2. Graphical abstract of Alba-Elías et al. [22].

Antifriction aminopropyltriethoxysilane films on thermoplastic elastomer substrates using an APPJ system. E. Sainz-García, F. Alba-Elías, R. Múgica-Vidal, A. González-Marcos, Surface & Coatings Technology 310 (2017) 239-250.

This publication deals with the synthesis and characterization of SiO_x-based coatings that were deposited on TPE substrates that produced by an APPJ with a DBD system. The main purpose was to obtain a coating that had friction coefficients that were similar to, or lower than, the current industrial solutions with the same or greater durability. The influence of the plasma power and number of passes was characterized by morphological, chemical, tribological and wettability analysis. The average surface temperature of the samples and the coating thickness seemed to be the key variables in determining the friction behavior. Successful samples were coated at an average surface temperature of less than 92 ºC and thicknesses of the coatings were greater than 1000 nm. Sample coated in six passes and the lowest power proved to have the best friction performance. This sample has a friction coefficient that is 46% lower than that of the flocked seals. The results of this research allow one to conclude that a promising antifriction technology using APPJ with a DBD could be an alternative to the current industrial solutions.

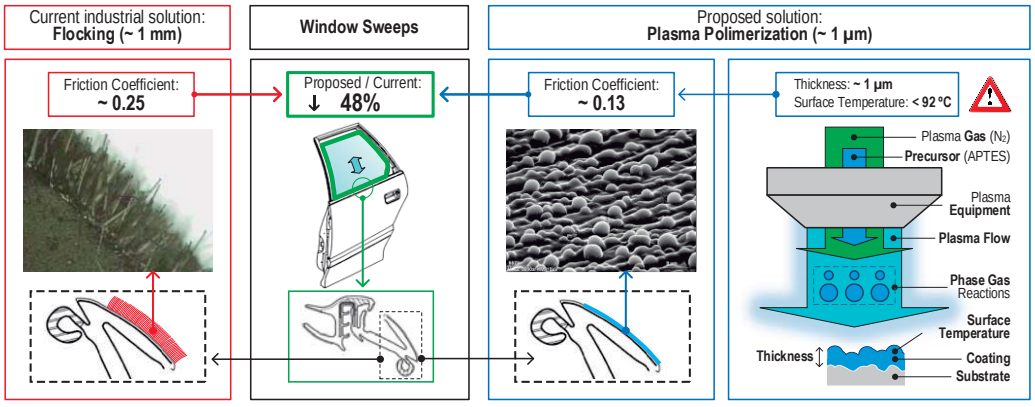

Figure 1.3. Graphical abstract of Sainz-García et al. [23].

Enhanced surface friction coefficient and hydrophobicity of TPE substrates using an APPJ system. E. Sainz-García, F. Alba-Elías, R. Múgica-Vidal, A. González-Marcos, Applied Surface Science 328 (2015) 554-567.

An APPJ system was used to deposit a coating that combines a low friction coefficient with a high Water Contact Angle (WCA) on a TPE that is used in automotive profiling. The main drawback of this research is that groups that improve the hydrophobicity of the surface worsen its tribological properties. To overcome this, this study explored the use of various mixtures of differing proportions of two precursors. They were a siloxane, APTES that was used to reduce the friction coefficient by its content of SiO_x and a fluorinated compound, (heptadecafluoro-1,1,2,2-tetrahydrodecyl)trimethoxysilane (FLUSI) that was used to improve the water-repellency characteristics, due to the presence of CF_2 long chains. After the characterization of the coatings, it was found that an increase of the absorbance area under the SiOSi peak and inorganic groups was related to lower friction coefficients. On the other hand, the higher the CF_2 percentage was, the higher the WCA was. The sample that was coated with 25% of FLUSI and 75% of APTES combined the improvements of both functional properties, the friction coefficient and the WCA. It had an average friction coefficient that was 51.5% lower and a WCA that was 4.4% higher than the uncoated TPE sample. A satisfactory stability in humid ambient for twelve months showed a slight decrease of WCA for this sample. The results of this study permit one to realize the effectiveness of using fluorinated precursors to avoid a significant decrease in the WCA when applying a precursor to antifriction improvement.

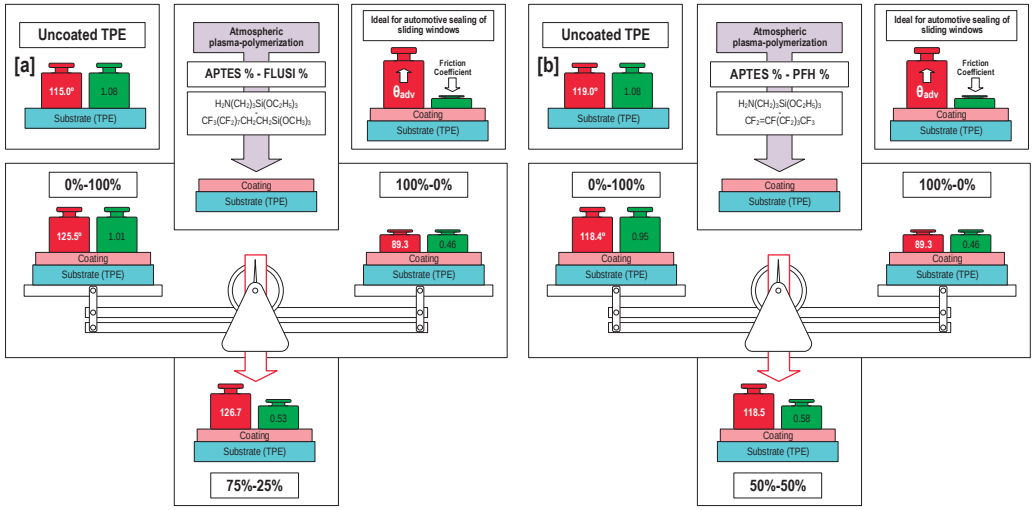

Figure 1.4. [a] Graphical abstract of Sainz-García et al. [24] and [b] graphical abstract of Sainz-García et al. [25].

Promotion of tribological and hydrophobic properties of a coating on TPE substrates by atmospheric plasma-polymerization. E. Sainz-García, F. Alba-Elías, R. Múgica-Vidal, M. Pantoja-Ruiz, Applied Surface Science 371 (2016) 50-60.

This publication's objective is the promotion of adhesion of an antifriction (based on the silane APTES) and hydrophobic (based on the fluorinated precursor 1-perfluorohexene -PFH-) coating by the adhesion promoter, APTES. Different mixtures of APTES and PFH were applied to a TPE substrate by an APPJ system with DBD in order to determine the optimal mixture of precursors. The main difficulty in this work lied in the hydrophilic character of APTES and the low adhesion of the fluorinated coatings. The sample coated with a mixture of 50% APTES and 50% PFH was found to be the best one to satisfy both properties at the same time, despite not having the highest dynamic water contact angle or the lowest friction coefficient.

1.3.2. TOPIC OF THE THESIS

The scientific publications presented are within the scope of the application of functional coatings by APPJ system on TPE substrates used in the automotive sealing industry.

- On the one hand, the first two scientific publications mentioned in the previous section [22,23], are directly related to **OBJECTIVE 1** of this thesis, focused on the deposition of SiO_x-based coatings which have friction coefficients that are similar to, or lower than, the current industrial solutions. In Alba-Elías et al. [22] preliminary results obtained allowed to identify the main variables that control the plasma polymerization process to reduce the coefficient of friction of TPE, whereas in Sainz-García et al. [23], taking into account the optimal variables obtained in the previous publication [22], Objective 1 was successfully achieved.
- On the other hand, the last two scientific publications cited in the previous section [24,25], are directly related to the **OBJECTIVE 2** of this thesis, focused on the deposition of functional coatings to improve both the tribological and hydrophobic properties of the uncoated TPE by using a mixture of two liquid precursors, APTES and a fluorinated compound. In both publications, the antifriction property was improved by the silane, APTES; whereas, the precursor used for the improvement of the water-repellency was different in each work (FLUSI and PFH). The main difference between these fluorinated precursors is related to the type of plasma polymerization that predominates (gas or substrate) which in turn is determined by the flash point of the precursor mixture.

1.4. STRUCTURE OF THE DOCUMENT

In this chapter it has been introduced the background, the motivation and objectives and the scientific publications of this thesis. The rest of the document is organized as follows: Chapter 2 presents the materials and the plasma polymerization system used to coat the samples, as well

as the different techniques of analysis and tests used for the study of coatings obtained. In Chapter 3, the results obtained are discussed. Finally, Chapter 4 shows the conclusions and future lines of research.

CHAPTER 2

EXPERIMENTAL

2.1. MATERIALS

The material used as substrate in this research was produced from pellets of Santorene™ 121-67W175, that has an ISO 18064 code of TPE-(EPDM+PP). This means that the elastic phase is Ethylene Propylene Diene Monomer (EPDM) and the plastic phase is Polypropylene (PP). The raw material was provided by an automotive sealing factory, Kaufil Sealing Technologies SA (Spain). Pellets were injected into a mold to produce sheets of 300 x 200 x 2 mm. The sheets were cut into samples of 100 x 50 x 2 mm.

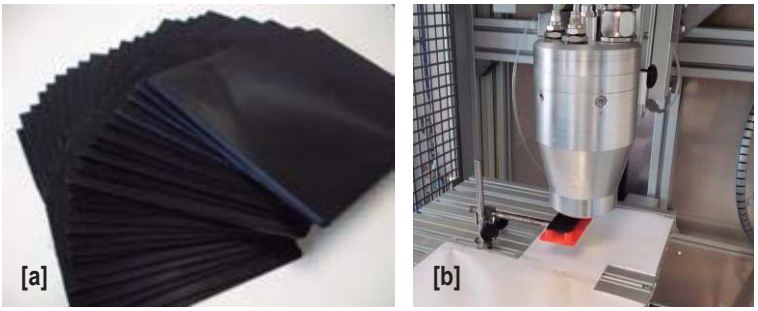

Figure 2.1. [a] TPE sheets and [b] TPE sample during the coating process.

The selection of the liquid precursors used were determined according to the objectives mentioned in this thesis. In this regard, the silane APTES was chosen because of both the antifriction ability of SiO_x groups and its adhesion-promoting action due to the NH_2 group of its molecule [26,27]. On the other hand, related to the wettability, by introducing low surface energy chemical components, such as CF_x groups, an increase in the contact angle of the surface, and hence the hydrophobicity thereof, is achieved. Thus, hydrophobic coatings based on fluorocarbons, ensure the elimination or reduction of adhesion of water, bacteria, grease, oil, dust and other surface contaminants, which is an advantage in many applications [11]. This is the reason why the fluorinated compounds FLUSI and PFH were selected to improve the hydrophobicity of the coated samples. The silane

APTES was provided by Sigma Aldrich and the fluorinated compounds (FLUSI and PFH) were provided by Fluorochem. The chemical structures of these precursors are shown in Figure 2.2.

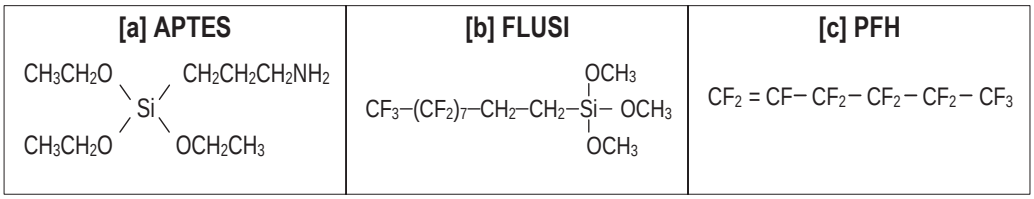

Figure 2.2. Precursor molecules of: [a] APTES, [b] FLUSI and [c] PFH.

2.2. PLASMA POLYMERIZATION PROCESS

Previous work by these authors [28] demonstrated the feasibility of reducing the friction coefficient of EPDM substrates –another popular material used in the automotive sealing industry– with plasma polymerized tetraethoxysilane (TEOS) films that were based on silicon oxides and deposited using an APPJ system [29]. In this research, a different APPJ system and different process parameters (plasma and precursor flow rate, plasma power, ionization gas, number of passes, etc.), substrate (TPE) and precursors (APTES, FLUSI, PFH) were used.

A schematic diagram of the APPJ system of PlasmaSpot® (PlasmaSpot 500, VITO, Belgium) that was used to coat the samples is shown in Figure 2.3 This system consists of an Al_2O_3 dielectric tube between two cylindrical electrodes; the outer electrode is connected to high voltage during operation and the inner electrode is grounded. Between these electrodes circulates the ionization gas which the plasma is generated with. The function of the Al_2O_3 dielectric tube is to prevent disturbances in the plasma jet and to achieve a more homogeneous treatment. In all cases, the jet moved across the sample´s surface at a scanning speed of 6 m/min and a track pitch of 2 mm. The gap between the discharge plasma and the substrate was set at 6 mm. Nitrogen (99.99%) was used as the plasma gas at 80 slm.

For each sample the coating process consisted of two steps, in which the same plasma power at a frequency of 68 kHz was used. In the first step, the sample was scanned once to activate the surface. During this activation step, no precursor was introduced into the jet. Only nitrogen (80 slm, 99.99%) was used as plasma gas. After activation, a process of plasma polymerization with a precursor or a mixed of precursors was carried out. A fine aerosol of liquid precursor was created using an atomizer (model 3076, TSI). The inlet gas for the atomization was nitrogen (99.99%). With the aim of preventing a direct contact of precursor fumes with the plasma operator, owing to its toxicity, the coating process was implemented using a fume hood. The ozone generated from the air during the atmospheric pressure process was evacuated with the same system. The precursor fume from the atomizer was directly transported to the inner electrode via a silicone tube. At the bottom of the inner electrode, the precursor fume contacts with the plasma.

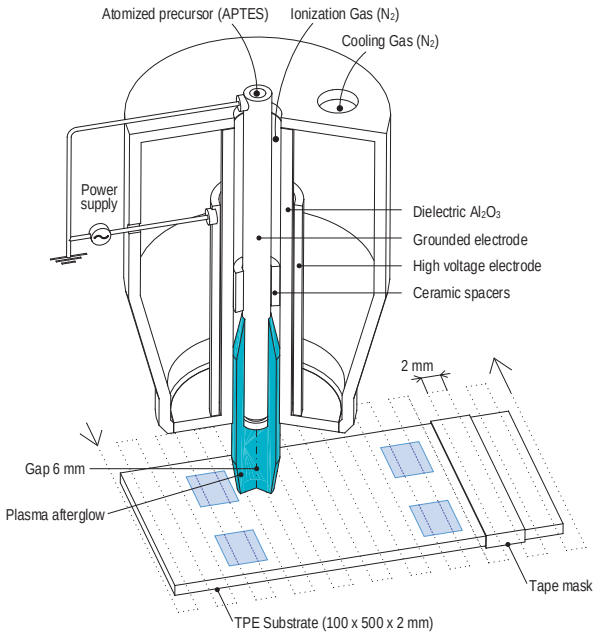

Figure 2.3. PlasmaSpot 500.

Table 2.1 shows the plasma polymerization parameters used for each scientific publication.

	Scientific Publication			
	Alba-Elías et al. [22]	**Sainz-García et al.** [24]	**Sainz-García et al.** [25]	**Sainz-García et al.** [23]
Plasma Power (W)	350-450-550	450	450	350-450-550
Ionization gas	N_2 (99.99%)	N_2 (99.99%)	N_2 (99.99%)	N_2 (99.99%)
Ionization gas flow (slm)	80	80	80	80
Precursor	APTES	APTES + FLUSI	APTES + PFH	APTES
% APTES	100%	100-75-50-25-0%	100-75-50-25-0%	100%
% Fluorinated precursor	0%	0-25-50-75-100%	0-25-50-75-100%	0%
Precursor flow rate (slm)	1-1.5-2	1.5	1.5	1.5
Number of passes (activation)	1	1	1	1
Number of passes (coating)	3	2	2	2-6-12-18

Table 2.1. Process parameters for plasma deposition by APPJ for each scientific publication.

2.3. SAMPLE CHARACTERIZATION TECHNIQUES

2.3.1. THICKNESS MEASUREMENTS

The intrinsic roughness of the uncoated TPE together with the nano-coatings obtained in some samples were a problem in selecting the best method for measuring the thickness of the coated samples. This is the reason why different measurement techniques were tested.

Firstly, in Alba-Elías et al. [22] the thickness of the coatings was measured by optical profilometry (ConScan profilometer, CSM Instruments), using the following procedure. First, the film's surface was partially covered with a mask. Second, the sample was coated with a plasma polymerization process. Finally, the mask was removed and the height of the step was measured by optical profilometry. The thickness range for these samples was 210-810 nm.

In both Sainz-García et al. [24] and Sainz-García et al. [25], silicon wafers were coated using the same process parameters as for coated samples. The coated silicon wafers were fractured by the use of liquid nitrogen. The fractured samples were tilted at an angle of 80° from a horizontal plane inside a SEM chamber (JEOL JSM-840) before taking the images. The thickness of the coated silicon wafers was assumed to be the same as that of the TPE samples. The thickness measurements were between 20-220 nm.

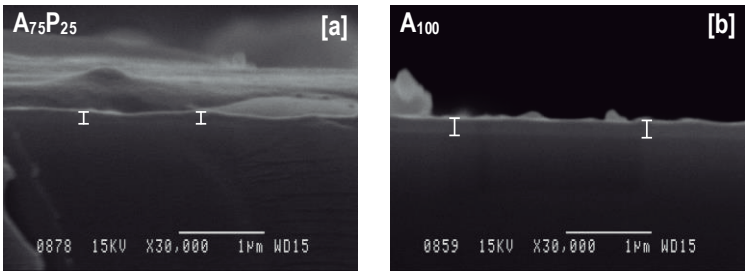

Figure 2.4. SEM cross-section images of samples $A_{75}P_{25}$ and A_{100} on silicon wafers to thickness measurements [25].

Finally, in Sainz-García et al. [23], the thickness of the coatings was evaluated by mechanical profilometry using a Taylor Hobson Surtronic 25 profilometer and the TalyProfile software, which provides data analysis and images captured by scanning. The scanning length that was chosen was 4 mm and the range was 100 µm. Before coating the samples, the TPE´s surface was partially covered by a mask, like in Alba-Elías et al. [22]. After the coating process, the mask was removed and the step´s height was measured by the mechanical profilometer. The average coating thickness of five measurements from each sample was determined. For these samples, the thickness range was 190-2938 nm.

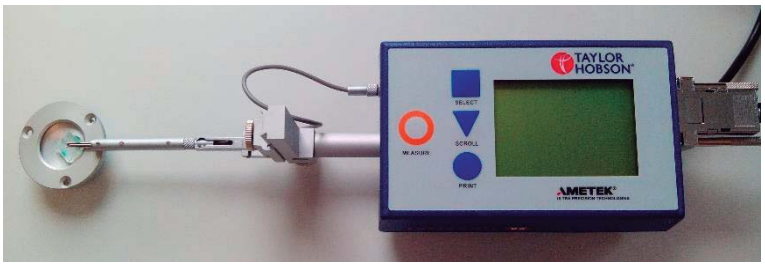

Figure 2.5. Taylor Hobson Surtronic 25 profilometer.

Taking into account the different thickness results, it is concluded that for thicknesses thinner than 1000 nm the procedure of coating an indirect substrate (silicon wafers), fracturing with nitrogen and analyzing the thickness by SEM images seems to be the most appropriate method. By contrast, for coatings that are thicker than 1000 nm, the thickness measurements by mechanical profilometry is a cheaper and easier analysis with a good precision.

2.3.2. SCANNING ELECTRON MICROSCOPY (SEM)

A Scanning Electron Microscope (SEM) examines structure by bombarding the specimen with a scanning beam of electrons and then collecting slow moving secondary electrons that the specimen generates. These are collected, amplified, and displayed on a cathode ray tube (CRT) although now, most are driven by PCs and these computer-generated images are displayed on LCDs. The electron beam is scanned using a raster pattern so that an image of the surface of the specimen is formed. Specimen preparation typically includes drying the sample and making it conductive to electricity, if it is not already. Photographs are taken at a very slow rate of scan in order to boost the signal and capture greater resolution. The SEM is used for conventional samples of normal sizes using the airlock. These specimens are usually mounted on "stubs" and are observed individually.

In the publications of this thesis SEM was used to study the morphology of coatings based on the parameters of plasma polymerization (plasma power, precursor flow, rate, number of passes, APTES percentage in the precursor mixture, etc.), the growth rate mechanisms and the wear track after the friction tests. For this purpose, two different SEM were used.

- A JEOL JSM-840 scanning electron microscope of the Alicante University. This SEM works under an operating voltage of 10-15 kV.
- A HITACHI S-2400 scanning electron microscope of Interquímica (La Rioja). This SEM works under an operating voltage of 18 kV.

As the samples were non-conductive, samples surfaces were coated with a thin gold or gold-palladium layer using a plasma sputtering device before introduction to the SEM chamber to prevent charging during SEM analysis.

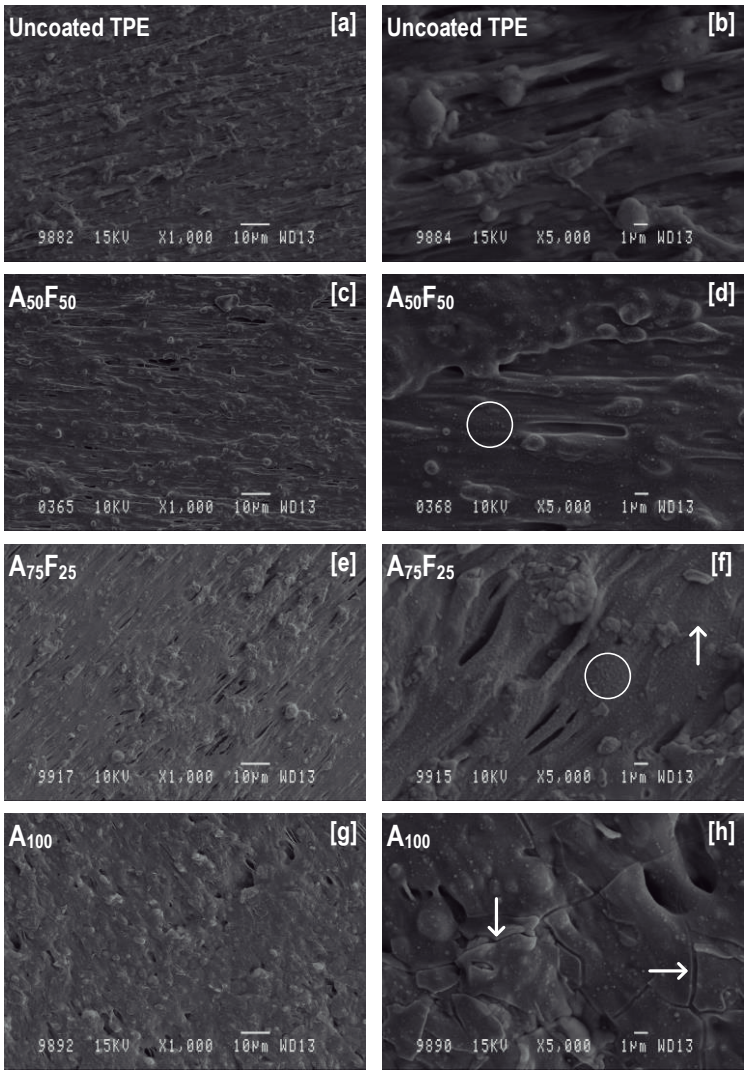

Figure 2.6. SEM images of the surface of [a, b] uncoated TPE and coated samples: [c, d] $A_{50}F_{50}$, [e, f] $A_{75}F_{25}$ and [g, h] A_{100} at magnifications of x1000 and x5000, respectively [24].

2.3.3. ENERGY DISPERSIVE X-RAY SPECTROSCOPY (EDX)

Energy Dispersive X-Ray Spectroscopy (EDX) is an X-ray technique used to identify the elemental composition of materials. EDX systems are attachments to scanning electron microscopy instruments where the imaging capability of the microscope identifies the specimen of interest. The data generated by EDX analysis consist of spectra showing peaks corresponding to the elements making up the true composition of the sample being analyzed. Elemental mapping of a sample and image analysis are also possible.

The energy dispersive X-ray spectroscope Quantax 200 (Bruker) with an XFlash 5010/30 detector and ESPRIT 1.9 microanalysis software that was installed in the HITACHI S-2400 SEM was used

to conduct a qualitative analysis of the chemical composition of the uppermost layer of the wear tracks in Sainz-García et al. [23].

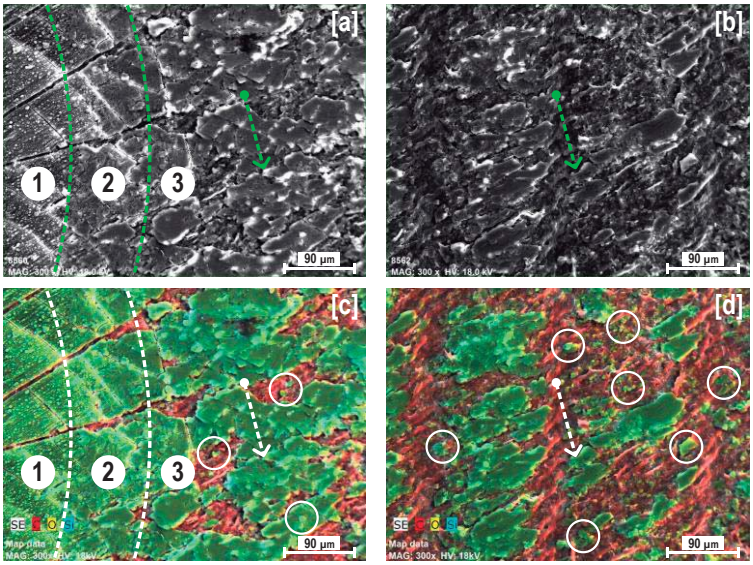

Figure 2.7. SEM (top) and EDX (bottom) images with a magnification of x300 of the wear track of sample S18/550 after a 4000 m friction test: [a] and [c] limited area coating-wear track, [b] and [d] central area of the wear track [23].

2.3.4. ATOMIC FORCE MICROSCOPY (AFM)

Atomic Force Microscopy (AFM) is a technique to obtain images and other information from a wide variety of samples, at extremely high (nanometer) resolution. AFM works by scanning a very sharp probe along the sample surface, carefully maintaining the force between the probe and surface at a set, low level. Usually, the probe is formed by a silicon (Si) or silicon nitride (Si_3N_4) cantilever with a sharp integrated tip, and the vertical bending (deflection) of the cantilever due to forces acting on the tip is detected by a laser focused on the back of the cantilever. The laser is reflected by the cantilever onto a distant photodetector. The movement of the laser spot on the photodetector gives a greatly exaggerated measurement of the movement of the probe. This set-up is known as an optical lever. The probe is moved over the sample by a scanner, typically a piezoelectric element, which can make extremely precise movements. The amount by which the scanner has to move in the z axis to maintain the cantilever deflection is taken to be equivalent to the sample topography. The combination of the sharp tip, the very sensitive optical lever, and the highly precise movements by the scanner, combined with the careful control of probe-sample forces allow the extremely high resolution of AFM.

The most commonly used modes of operation of an AFM are: contact mode, tapping mode and non-contact mode. Contact is often called static mode, and tapping and non-contact called dynamic modes, as the cantilever is oscillated in tapping and non-contact modes. The main difference between tapping mode and non-contact mode is that in tapping mode, the tip of the probe actually touches the sample, and moves completely away from the sample in each

oscillation cycle. In non-contact mode, the cantilever stays close to the sample all the times, and has a much smaller oscillation amplitude.

Two different AFM were used to explore the surface morphology and roughness of the analyzed samples together with the plasma polymerization mechanisms according to the process parameters (plasma power, precursor flow rate, number of passes, APTES percentage in the precursor mixture, etc.).

- A Multimode AFM from Veeco Instruments equipped with a Nanoscope V controller and operated in tapping mode using a phosphorus-doped silicon probe (RTESP) of the Malaga University. Sample areas of 10 μm × 10 μm were processed.
- A XE-70 Atomic Force Microscopy system (Park systems). This AFM was used during my research stay in Ghent University (Belgium). Sample areas of 10 μm x 10 μm and 40 μm x 40 μm were scanned in non-contact mode with a silicon cantilever (NanosensorsTM PPP-NCHR).

The roughness of each sample was obtained from the root mean square (RMS) values of roughness of its AFM images after applying a plane fit algorithm as the average value of the measurements of three different spots per sample by means of NanoScope Analysis 1.4 software.

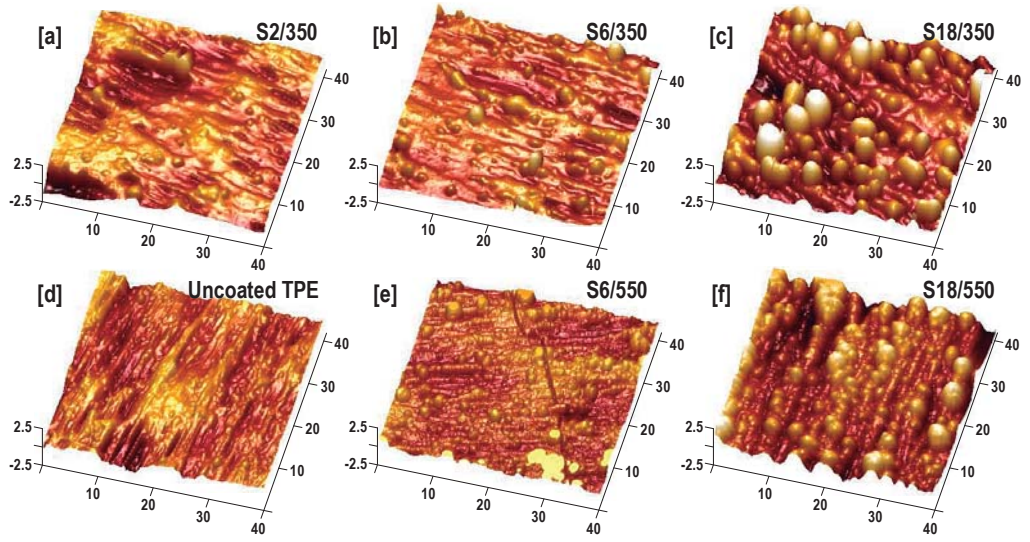

Figure 2.8. AFM images of samples: [a] S2/350, [b] S6/350, [c] S18/350, [d] Uncoated TPE, [e] S6/550 and [f] S18/550 [23].

2.3.5. ATTENUATED TOTAL REFLECTANCE-FOURIER TRANSFORM INFRARED SPECTROSCOPY (ATR-FTIR)

Infrared Spectroscopy (IR) is the analysis of infrared light interacting with a molecule. This can be analyzed in three ways by measuring absorption, emission and reflection. The main use of this technique is in organic and inorganic chemistry to determine functional groups in compounds. Infrared light imposed on a molecule will not create electronic transitions but it does contain

enough energy to interact with a molecule causing vibrational and rotational changes. The possible rotations are around the axis of symmetry for a given molecule or either of the two perpendicular axis. Vibrations can be in the form of a bend or a stretch for each bond. The IR spectrometer with Fourier transform (FTIR) is able to record spectra quickly, accurately and with high signal/noise ratios.

An Attenuated Total Reflection (ATR) accessory operates by measuring the changes that occur in a totally internally reflected infrared beam when the beam comes into contact with a sample. An infrared beam is directed onto an optically dense crystal with a high refractive index at a certain angle. This internal reflectance creates an evanescent wave that extends beyond the surface of the crystal into the sample held in contact with the crystal. This evanescent wave protrudes only a few microns beyond the crystal surface and into the sample. Consequently, there must be good contact between the sample and the crystal surface. In regions of the infrared spectrum where the sample absorbs energy, the evanescent wave will be attenuated or altered. The attenuated energy from each evanescent wave is passed back to the IR beam, which then exits the opposite end of the crystal and is passed to the detector in the IR spectrometer. The system then generates an infrared spectrum.

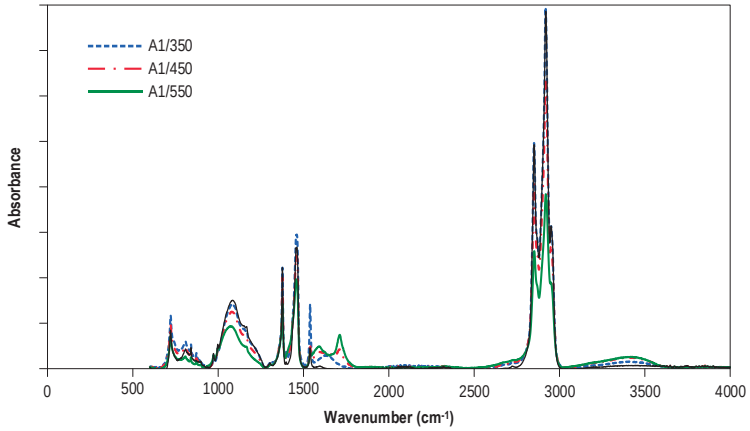

Figure 2.9. ATR-FTIR spectra of the activated samples and the uncoated TPE [23].

With the aim of studying the chemical characteristics of all the analyzed samples two different ATR-FTIR spectroscopes were used:

- A Bruker IFS 66 FTIR spectrometer with a Specac Golden Gate ATR accessory based on a single bounce diamond prism of the University of Alicante. Each spectrum was recorded in the 600-4000 cm^{-1} region with a resolution of 2 cm^{-1} and 64 scans.
- A Bruker Tensor 27 spectrometer that was equipped with a single reflection ATR accessory (Bruker Optik GmbH) of the University of La Rioja. For each spectrum, 32 scans were collected and averaged in the range of 600-4000 cm^{-1} at a 4 cm^{-1} resolution.

Deconvolutions of ATR-FTIR spectra were accomplished by use of the spectral analysis program PeakFit version 4.12 (SPSS Inc.). The ATR-FTIR spectra were fitted with bands described by a mixture of Gaussian and Lorentzian functions.

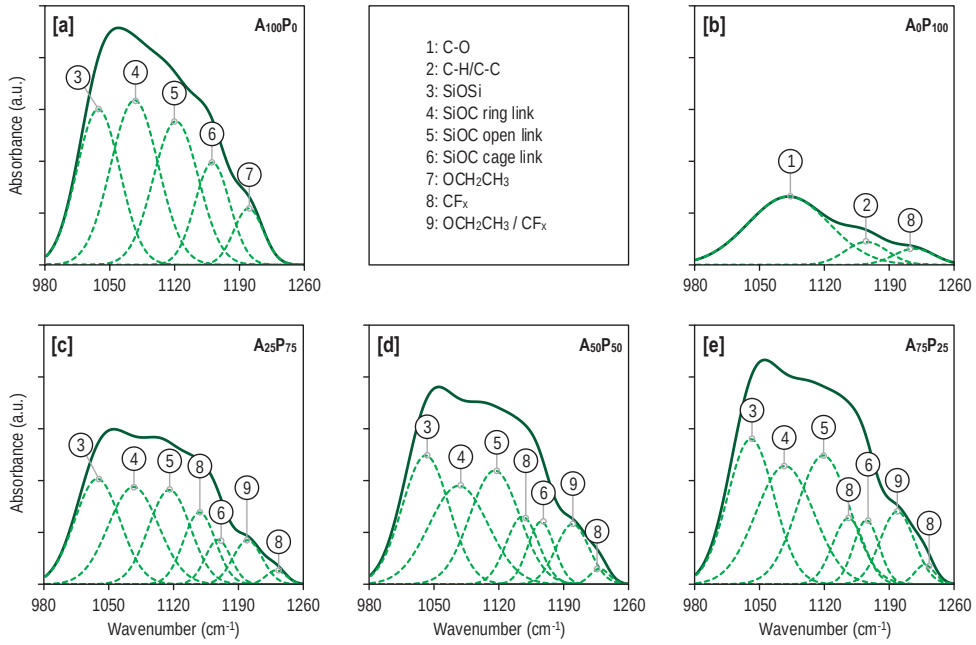

Figure 2.10. ATR-FTIR deconvoluted spectra of Region I of the PFH-based samples [25].

2.3.6. X-RAY PHOTOELECTRON SPECTROSCOPY (XPS)

X-ray Photoelectron Spectroscopy (XPS) is a technique for analyzing the surface chemistry of a material. XPS can measure the elemental composition, empirical formula, chemical state and electronic state of the elements within a material. XPS spectra are obtained by irradiating a solid surface with a beam of X-rays while simultaneously measuring the kinetic energy and electrons that are emitted from the top 1-10 nm of the material being analyzed. A photoelectron spectrum is recorded by counting ejected electrons over a range of electron kinetic energies. Peaks appear in the spectrum from atoms emitting electrons of a particular characteristic energy. The energies and intensities of the photoelectron peaks enable identification and quantification of all surface elements (except hydrogen).

The quantification of the atomic chemical composition of the upper most layer of samples was carried out by a Physical Electronics PHI 5700 spectrometer with a multi-channel hemispherical electron analyzer using a Mg-Kα X-ray source (1253.6 eV) operating at 15 kV and 300 W. The spectra were acquired at a constant pass energy of 29.35 eV and at a pressure that was below 1.33×10^{-7} Pa. The PHI ACCESS ESCA-V8.0C software package was used for acquisition and data analysis. Atomic concentration percentages of the characteristic elements were determined from the spectrum after subtracting a Shirley-type background, and taking into account the corresponding area sensitivity factor for every photoelectron line.

For samples coated with APTES, activated samples and the uncoated TPE, the atomic percentages of C1s, O1s, Si2p and N1s were calculated. For these samples, a value of 285.0 eV for the hydrocarbon C1s core level was used for calibration of the energy scale. For samples coated with a fluorinated compound (FLUSI or PFH), in addition to the abovementioned elements, the F1s atomic percentage was obtained. For these samples, the spectra were corrected for the charging effect by setting the CF_2 component to a binding energy of 291.4 eV. Finally, XPS deconvolutions of C1s, Si2p and F1s were undertaken by means of PeakFit 4.12 (SPSS Inc.) software. The XPS bands were curve-fitted using a mixed Gaussian-Lorentzian functions allowing variable widths of the peaks. The shape and number of peaks were constrained, whereas variable widths were allowed.

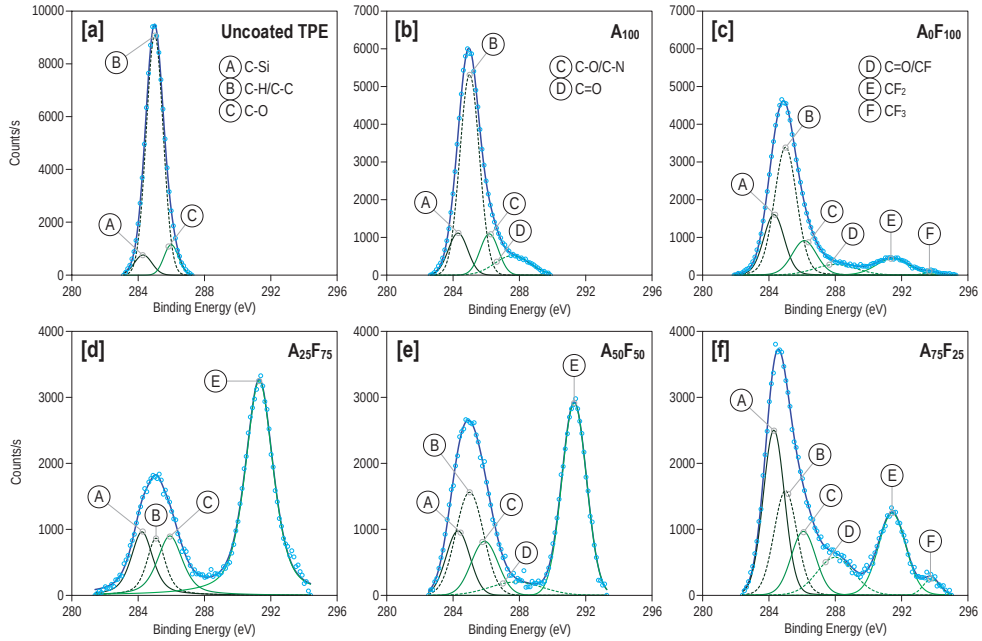

Figure 2.11. Deconvolution of high resolution C1s spectra of FLUSI-based samples [24].

2.3.7. WATER CONTACT ANGLE (WCA) MEASUREMENTS

Contact angle is a quantitative measure of wetting of a solid by a liquid. It is defined geometrically as the angle formed by a liquid at the three phase boundary where a liquid, gas and solid intersect. The well-known Young equation [30] describes the balance at the three phase contact of solid-liquid and gas.

$$\gamma_{lv} \cdot \cos\theta_Y = \gamma_{sv} - \gamma_{sl}$$

where γ_{lv}, γ_{sv}, and γ_{sl} represent the liquid-vapor, solid-vapor, and solid-liquid interfacial tensions, respectively, and θ_Y is the contact angle. From Young's equation applied to a specific liquid-solid system, three thermodynamic parameters, γ_{lv}, γ_{sv}, and γ_{sl}, determine a single and unique contact angle θ_Y.

From Figure 2.12, it can be seen that the low contact angle values indicate that the liquid spreads on the surface while high contact angle values show poor spreading. If the contact angle is less than 90° it is said that the liquid wets the surface, zero contact angle representing complete wetting. If contact angle is greater than 90°, the surface is said to be non-wetting with that liquid. Contact angles can be divided into static and dynamic angles. Static contact angles are measured when droplet is standing on the surface and the three phase boundary is not moving.

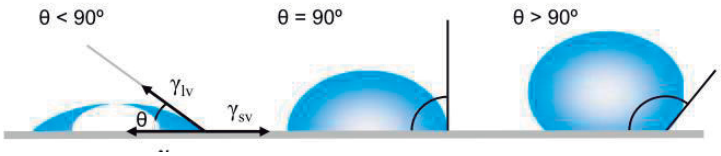

Figure 2.12. Illustration of contact angles formed by sessile liquid drops on a smooth homogeneous solid surface.

When the three phase boundary is moving, dynamic contact angles can be measured, and are referred as advancing (θ_{adv}) and receding angles (θ_{rec}). Contact angle hysteresis (H) is the difference between the advancing and receding contact angles.

$$H = \theta_{adv} - \theta_{red}$$

Contact angle hysteresis arises from the chemical and topographical heterogeneity of the surface, solution impurities absorbing on the surface, or swelling, rearrangement or alteration of the surface by the solvent [31,32]. Advancing and receding contact angles give the maximum and minimum values the static contact angle can have on the surface. Difference between advancing and receding angles can be as high as 50°. Dynamic contact angles and contact angle hysteresis has become a popular topic because of the recent interest in superhydrophobic and self-cleaning surfaces [33].

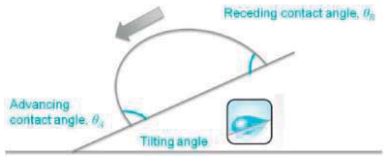

Figure 2.13. Illustration of the advancing (θ_{adv}) and receding (θ_{rec}) contact angles.

Since the equilibrium contact angle cannot be determined on practical polymer surfaces due to their chemical heterogeneity and surface roughness [34,35] in Sainz-García et al. and Sainz-García et al. [24,25], the hydrophobic nature of the surfaces was quantified by measuring the dynamic water contact angle. Due to its simplicity, the “tilting plate” [36] method was selected to measure the advancing (θ_{adv}) and receding (θ_{rec}) contact angles of these samples. The tilting plate method is to slowly tilt a contact angle sample until the sessile drop on it begins to move in the downhill direction. At that time, the downhill contact angle is the advancing angle and the uphill angle the receding contact angle. Thus, after each sample was adhered to the plane, a 10 μL deionized water drop was dropped on the sample surface by using a micropipette. The sample surface was then slowly tilted from 0º to 90º at a rate of 1º/s. A video for the drop was continuously

recorded. All contact angle measurements were performed at ambient temperature. 3-4 deionized water drops were taken and averaged to obtain a value of advancing and receding WCA that were characteristic for each sample.

In Sainz-García et al. [23], since the main objective of this work was not to achieve a coating with high WCA, the determination of the wettability of the samples was performed by the static WCA measurement, instead of the dynamic ones. Thus, after comparing the results obtained for each sample analyzed, we had an idea of the wettability of these samples. Specifically, the static WCAs were measured by the sessile drop method using a digital microwebcam to get the digital images. The WCA value of each sample was calculated as an average of four measurements (10 µL/drop) by image analysis with the ImageJ software.

2.3.8. TRIBOLOGICAL TESTS

The friction coefficient describes the opposition to the movement offered by the surfaces of two bodies in contact, whose result is expressed by a dimensionless value. In a tribological test, a flat, a pin or a sphere is loaded onto the test simple with a precisely known force. The pin is mounted on a stiff lever, designed as a frictionless force transducer. The friction coefficient is determined during the test by measuring the deflection of the elastic arm. This simple method facilitates the study of friction behavior of almost every solid material with or without lubricant. Furthermore, the control of the test parameters such as speed, frequency, contact pressure, time and the environmental parameters (temperature, humidity and lubricant) allows simulation of the real life conditions of a practical wear situation.

Tribometers are instruments designed for force measurement with high precision and can work in two operation modes: linear reciprocating and rotating modes.

- **Linear mode:** The linear mode reproduces the reciprocating motion typical of many real world mechanisms. The instrument produces a friction coefficient for both the forward and backward displacement of the stroke and the software can generate data on Hertzian pressure, static partner and sample wear rates.
- **Rotating mode:** While the disk is rotating, the resulting frictional force acting between the sphere, pin or flat and the disk is measured by the small deflections produced in the elastic arm by a Linear Variable Differential Transformer (LVDT) sensor. The friction coefficient of the sample and the sphere, pin or flat are calculated from the volume of material lost during the test.

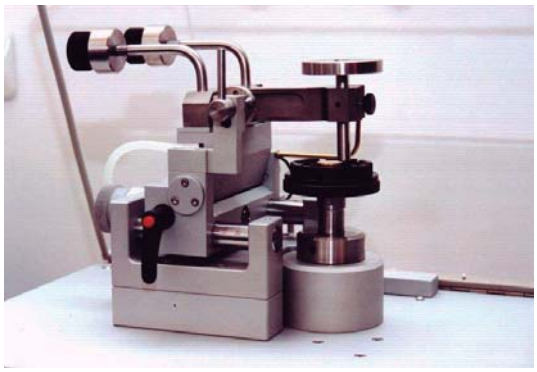

Figure 2.14. CSM Rotative Tribometer.

Tribological tests were conducted to study the tribological behavior of the samples. For this purpose, a ball-on-disk tribometer (CSM Instruments, Switzerland) with a counterpart of Ø6 mm commercial 100 Cr6 steel balls of hardness HRC 60–62 was used. For all tests, the radius was 2.5 mm and the sliding speed was 2 cm/s. However, as one can observe during the scientific publications evolution, test conditions were hardened. The load was increased from 0.25 N in Alba-Elías et al. [22] to 1N in the rest of publications [23–25]. The sliding distance was elongated from 10 m in Alba-Elías et al. [22] to 1000 m in Sainz-García et al. and Sainz-García et al. [24,25] and 4000 m in Sainz-García et al. [23]. During the test, the sample was spun and the steel ball made a circular groove in the sample. The friction coefficient was recorded continuously.

Moreover, in Sainz-García et al. [24] two tribological tests with two different counterparts were performed for each sample. In the first one, a hardened 100Cr6 steel ball (60-62 HRC, 6 mm in diameter) was used as a counterpart and in the second one, a Ø6 glass ball was used.

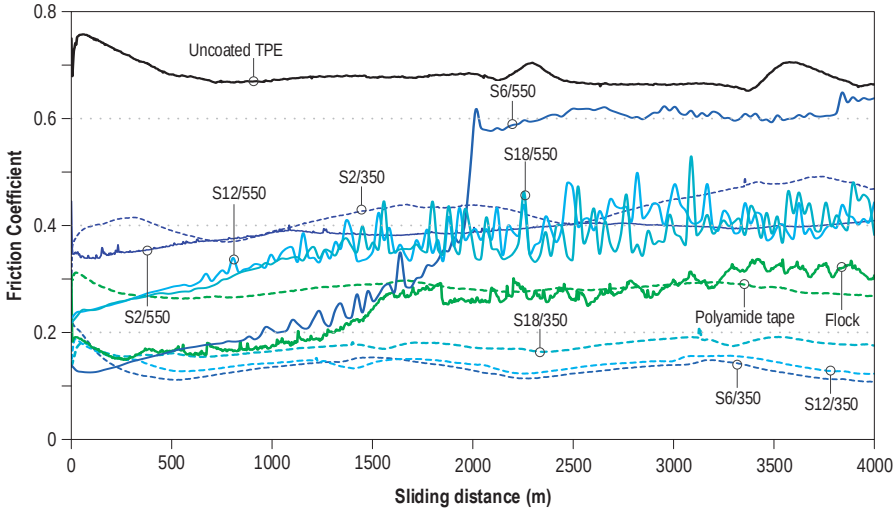

Figure 2.15. Evolution of the friction coefficient of: samples coated at 350 W and 550 W, uncoated TPE, flocked seal and polyamide tape [23].

2.3.9. ADHESION TEST

In order to evaluate the durability of the coatings, in Sainz-García et al. [25], the adhesion properties were evaluated by a tensile lap-shear strength test. The quasi-static lap-shear experiment was based on the UNE-EN 1465:2009. Testing parameters were set on the specimen with a cross-head displacement rate of 0.5 mm/min. The machine used was a TRIAX-50 (Controls) equipped with a 200 N load cell to measure the load for lap-shear fracture. The test specimen was made by affixing 12.5 ± 0.2 mm of the coated sample (1 cm x 2 cm) to the load cell with 3M-600 tape. The control PC software recorded the lap-shear force in newton. For each sample, four specimens sample were tested. Then, the bonding strength was calculated taking into account the tested area. An average of these values was taken as the final bonding strength in MPa.

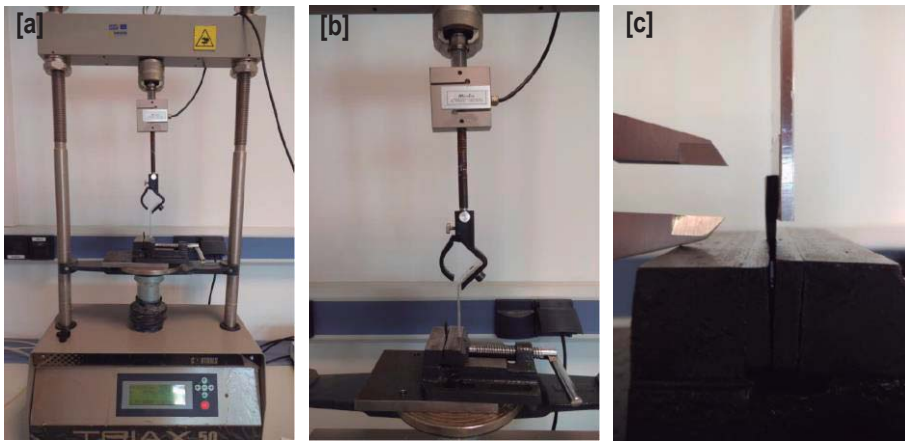

Figure 2.16. [a] TRIAX-50 (Controls) machine, [b] and [c] adhesive union detail.

2.3.10. STABILITY TEST

In order to have a study about the coatings´ stability in humid environment and the durability of the hydrophobic property, in Sainz-García et al. [24] samples were aged in air for twelve months. The test chamber was set at 67% of relative humidity and 15 ºC. At the beginning and upon completion of the test, the repellency toward water was measured and the ATR-FTIR spectrums (Bruker IFS 66) were taken for all the samples. Static water contact angles based on the sessile drop method were recorded using a commercial Contact Angle System OCA15plus system (Dataphysics, Germany) and SCA200 software of the Polytechnic University of Cataluña. A total of 4-5 drops (3 µL/drop) were taken and averaged to obtain a value that was characteristic of the WCA for each sample.

CHAPTER 3

RESULTS AND DISCUSSION

3.1. COATINGS FOR AUTOMOTIVE INDUSTRY: IMPROVEMENT OF TRIBOLOGICAL BEHAVIOR

As already mentioned in section 1.3.2 Topic of the Thesis the publications Alba-Elías et al. [22] and Sainz-García et al. [23], related to the **OBJECTIVE 1** of this thesis, are focused on the deposition of SiO_x-based coatings which have friction coefficients that are similar to, or lower than, the current industrial solutions. In both of them, APTES was used as precursor. In Alba-Elías et al. [22] preliminary results allowed to identify the main parameters to control the plasma polymerization process reducing the friction coefficient of TPE. In particular, the best results against friction performance were found with a precursor flow rate of 1.5 slm. For that reason, the samples studied in Sainz-García et al. [23] were coated with a precursor flow rate of 1.5 slm. Other parameters such as plasma power and number of passes (deposition time) were varied. Thus, the Objective 1 was successfully achieved. Throughout this section the most relevant results obtained in both works have been exposed and discussed.

3.1.1. SAMPLES

Table 3.1 shows the label of each analyzed sample, as well as plasma power, number of passes and APTES flow rate used during the coating process.

Sample label	Power (W) (activation and polymerization)	Number of passes (activation)	Number of passes (polymerization)	APTES flow rate (slm)
S2/350	350	1	2	1.5
S3/350 (1)		1	3	1
S3/350		1	3	1.5
S3/350 (2)		1	3	2
S6/350		1	6	1.5
S12/350		1	12	1.5
S18/350		1	18	1.5

Sample label	Power (W) (activation and polymerization)	Number of passes (activation)	Number of passes (polymerization)	APTES flow rate (slm)
S2/450	450	1	2	1.5
S3/450 (1)		1	3	1
S3/450		1	3	1.5
S3/450 (2)		1	3	2
S6/450		1	6	1.5
S12/450		1	12	1.5
S18/450		1	18	1.5
S2/550	550	1	2	1.5
S3/550 (1)		1	3	1
S3/550		1	3	1.5
S3/550 (2)		1	3	2
S6/550		1	6	1.5
S12/550		1	12	1.5
S18/550		1	18	1.5

Table 3.1. Sample identification and deposition conditions of each sample.

3.1.2. TEMPERATURE MEASUREMENTS

With the aim of evaluating the effect of surface temperature on the properties of the coated samples in Sainz-García et al. [23], the temperature was continuously measured during the coating process using a temperature sensor that was taped to the sample´s surface for the 18-pass samples.

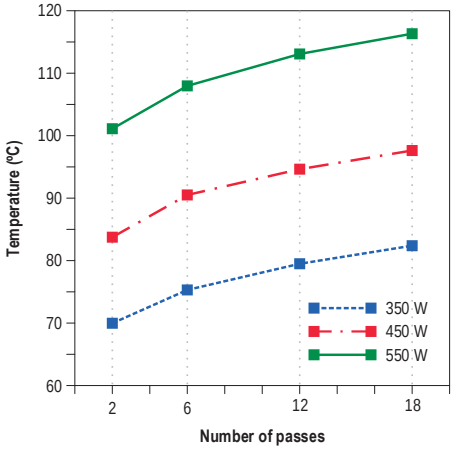

Figure 3.1. Average surface temperature as a function of the number of passes [23].

Figure 3.1 shows clearly that the average surface temperature rises slowly with the number of passes for a given power. This increase is due to the energy stored in the plasma and the coating during the deposition process [37]. The longer the deposition process is, the higher is the surface

temperature that is reached. For a selected number of passes, an increase in the average temperature is observed when the power of the plasma polymerization process is raised [38] because of the greater number of energetic ions, molecules and particulates [39–41]. As some studies have shown [42–45], the surface temperature of the samples and its residence time can have a great impact on chemical composition and structure, surface morphology and mechanical performance of the as-deposited samples, especially when heat-sensitive substrates, such as TPE, are used [46].

3.1.3. SURFACE MORPHOLOGY

Thickness and roughness measurements and SEM and AFM analysis were used to study the relationships between the plasma polymerization parameters. Figure 3.2 depicts the thickness and growth rate of the samples coated in 2, 6, 12 and 18 passes. Figure 3.3 shows the thickness and roughness of the 3-pass samples. Figure 3.4 illustrates the average roughness of the samples coated in 2, 6, 12 and 18 passes.

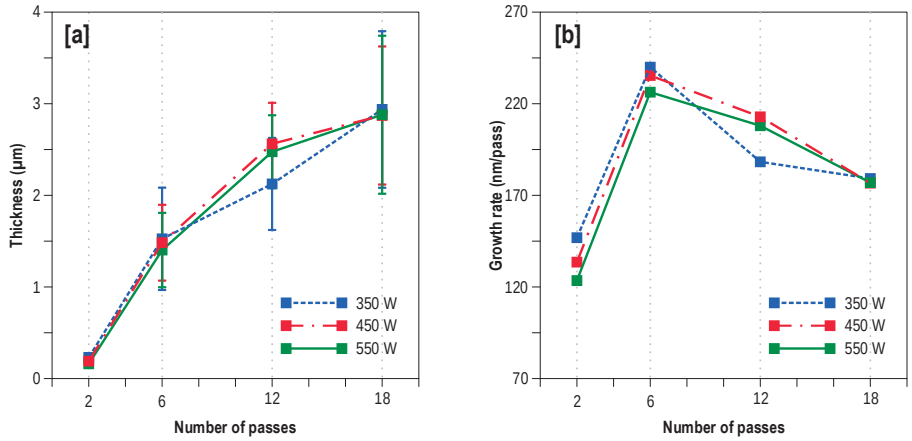

Figure 3.2. [a] Thickness and [b] growth rate of samples coated in 2, 6, 12 and 18 passes [23].

Related to the thickness of the coatings, Figure 3.2 [a] shows that, for a specific power, the coating thickness increases in linear fashion with the number of passes; it is a function of the deposition time. Thus, plasma jet is working longer, which causes further growth of the coatings with a consequent increase in thickness. In Figure 3.3 [a] it can be observed that, in Alba-Elías et al. [22] the values of the thicknesses for the samples coated with 1.5 slm and three passes are thicker than the 2-pass and thinner than the 6-pass of Sainz-García et al. [23].

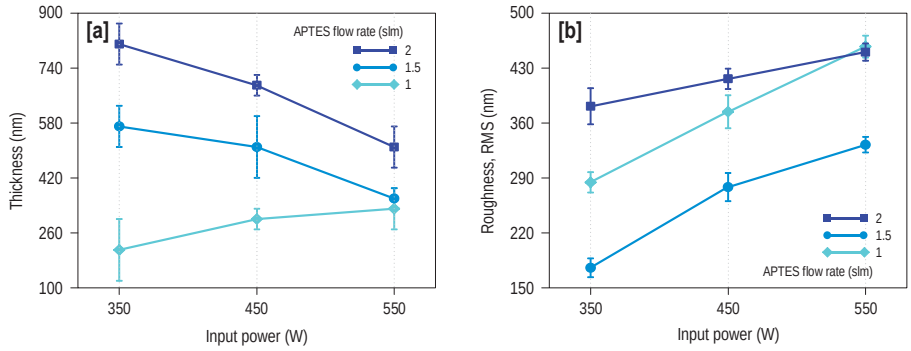

Figure 3.3. [a] Thickness and [b] roughness of the 3-pass samples [22].

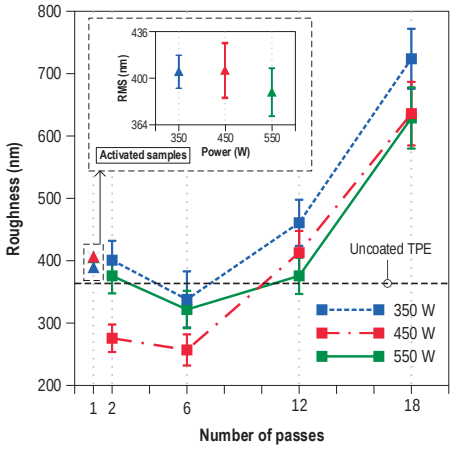

Figure 3.4. Average roughness of samples coated in samples coated in 2, 6, 12 and 18 passes [23].

The curve of the growth rate (Figure 3.2 [b]) for a specified power reaches a maximum at about six passes followed by a linear decrement for up to eighteen passes [47,48]. This behavior seems to be related to the roughness of the samples, since the curve of the roughness (Figure 3.4) shows an inverse shape to that of growth rate. In this respect, when the 2-pass samples are coated, the surface exposed to plasma polymerization appears to be largely determined by the roughness of the uncoated TPE sample. During this process, the cavities of the uncoated TPE are being filled and as the number of passes increases (from 2 to 6 passes), the sample becomes increasingly smooth. That fact is confirmed with the samples coated with 1.5 slm and three passes, since their roughnesses are lower than those of their counterparts coated in two passes, and their greater thicknesses indicating that the cavities of the uncoated TPE are practically filled. In fact, SEM images of these samples, in Figure 3.5, show some cracks, which indicate the incipient growth of a homogeneous coating. This decrease in roughness (from 2 to 6 passes) causes the area exposed to plasma polymerization to be lower, resulting in a higher growth rate. When reaching six passes, the roughness values for these samples are the lowest and therefore the area exposed to the plasma polymerization are the lowest. Given that the precursor flow rate is constant (1.5 slm) throughout the deposition process, a decrease of the area exposed to the plasma

polymerization involves an increase of the growth rate. As the number of passes increases (from 6 to 18 passes), the roughness increases too due to the growth of the particles. This causes an increment of the area exposed to the plasma polymerization which, in turn, results in a decrease in growth rate.

3.1.3.1. EFFECT OF THE PRECURSOR FLOW RATE

With the aim of studying the influence of the precursor flow rate on the morphology of the coatings, several samples were coated in three passes and different precursor flow rates (1, 1.5 and 2 slm) and plasma powers (350 and 550W). Figure 3.5 shows the SEM images of 3-pass samples coated with different precursor flow rates (1.5 and 2 slm) and plasma powers (350 and 550 W).

As Figure 3.3 [a] illustrates, the thickness of the coatings increases with the APTES flow rate for a given power. When the APTES flow rate is equal to 1 slm, there is a positive relationship between the plasma power and the thickness. However, this relationship is the inverse at APTES flow rate values of 1.5 and 2 slm. In Figure 3.3 [b], it can see the higher the plasma power is for a given APTES flow rate, the greater the roughness of the film is. In Figure 3.5, it is possible to identify the direction of the gun movement during the deposition process from the noticeable orientation of the coating fibers. Samples that were coated at 350 W show a more homogeneous surface, whereas samples that were coated at 550 W present a more fibrous and heterogeneous texture.

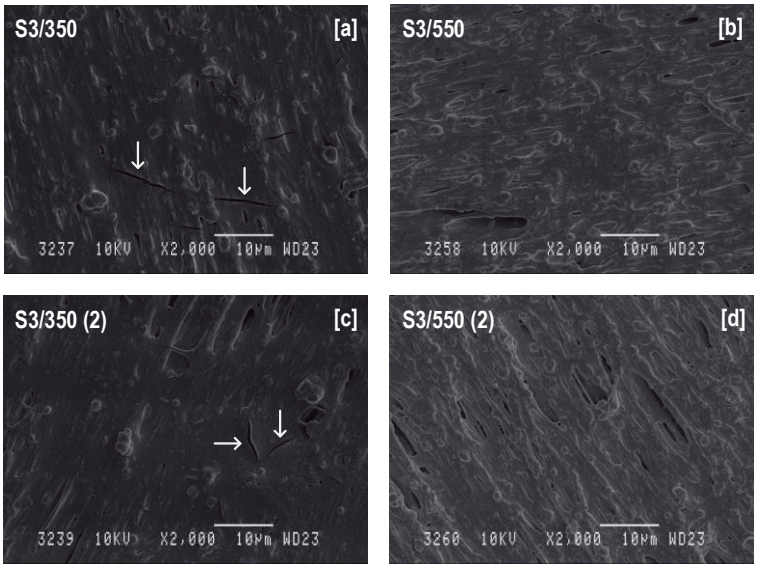

Figure 3.5. SEM images of 3-pass samples coated with different precursor flow rates (1.5 and 2 slm) and plasma powers (350 and 550 W) [22].

Related to the precursor flow rate, for a given plasma power, samples that were coated at 1.5 slm are not as rough as samples that were coated at 1 and 2 slm. In addition, samples that were coated at an APTES flow rate of 1.5 and 2 slm and lower plasma powers (350 W) are thicker, more homogeneous and have a smoother surface. Every characteristic can be explained by the lower number of active species per precursor molecule that are produced at lower plasma powers.

As the number of active species decreases, the plasma polymerization produced on the substrate surface increases. In contrast, when the plasma power is increased, higher precursor decomposition takes place during the gas phase of the plasma, prior to its deposition [49], and a plasma etching of the deposited coating is produced. This causes a greater density of the coatings [50,51], an increment of the fibrous aspect and roughness, and a reduction in the coating thickness [49].

3.1.3.2. EFFECT OF THE NUMBER OF PASSES

In Figure 3.4 one can see that, for a given power, the roughness increases as the number of passes increases. It is noteworthy that, for a specified power, the roughness of samples that were coated in two passes is slighly higher than the roughness of samples that were coated in six passes. However, the surface of 2-pass samples probably has not been completely coated, since such coatings are very thin (160-230 nm) in comparison to TPE´s roughness (RMS: 364±32 nm) and its own roughness (276-401 nm). The reliability of the thickness measurements for 2-pass samples is questionable since it was difficult to identify if the profilometry measurements correspond to the thickness of the coating or to a discontinuity of the raw substrate. As seen in Figure 3.3 and Figure 3.5, something similar happened with the 3-pass samples. Nevertheless, it was found that the use of six passes to coat samples is sufficient to fully cover the TPE´s surface. This provides smoother coatings (257-338 nm) with thicknesses greater than 1000 nm.

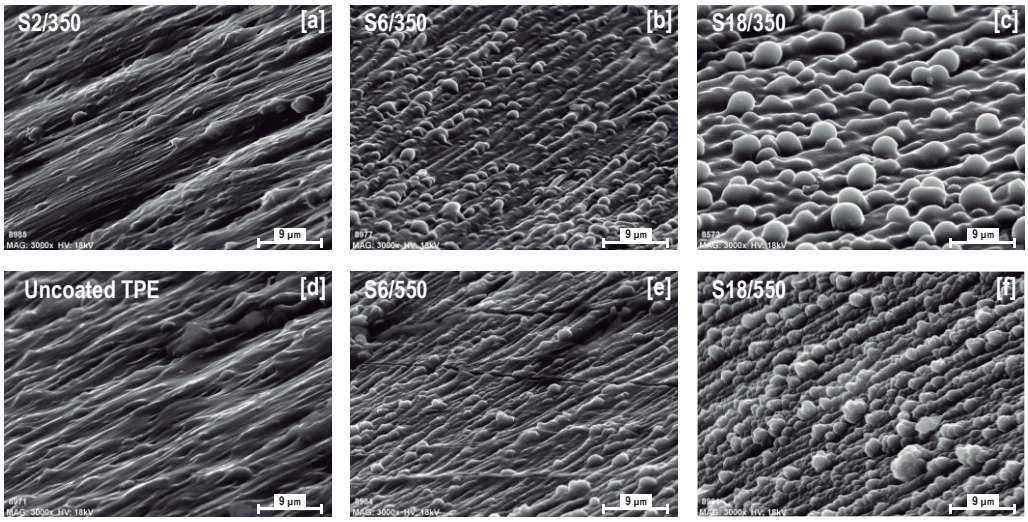

Figure 3.6. Tilted SEM images with a magnification of x3000 of samples: [a] S2/350, [b] S6/350, [c] S18/350, [d] Uncoated TPE, [e] S6/550 and [f] S18/550 [23].

Figure 3.6 illustrates tilted SEM images, whereas Figure 3.7 shows AFM images of samples S2/350, S6/350, S6/550, S18/350, S18/550 and the uncoated TPE. Figure 3.8 illustrates SEM images with cracks of samples coated with 350 W and 550 W.

As can be seen in Figure 3.6 and Figure 3.7, SEM and AFM images of the uncoated TPE substrate exhibit a highly fibrous aspect and some carbon particles of TPE substrate. Samples coated in more than six passes, at 350 W, exhibit a coating that consists of spherical particles that were

deposited on the TPE fibers. It would appear that the morphology of APTES coatings relies heavily on the uncoated TPE´s morphology. In fact, it is believed that both the fibers and carbon particles of TPE substrate probably act as nucleation sites where the coating grows [52]. This agrees with the SEM and AFM images of sample S6/350 that show some spherical particles that have been deposited on both nucleation sites (see Figure 3.6 [b] and Figure 3.7 [b]). An increase in the number of passes results in gas species remaining longer in the plasma jet which favors precursor fragmentation and recombination of different particles during the plasma polymerization process [53]. In turn, this causes an increase in size and number of spherical particulates. Such spherical growth is also promoted by the so-called shadowing effect, which is caused by geometric interaction between the surface roughness of the growing film and the angular direction of the arriving coating species. That is, the deposition rate at the top of spherical particles is higher than at the bottom of the voids [47,52]. As a result of this growth mechanism, an increase in roughness and thickness of the coatings was observed.

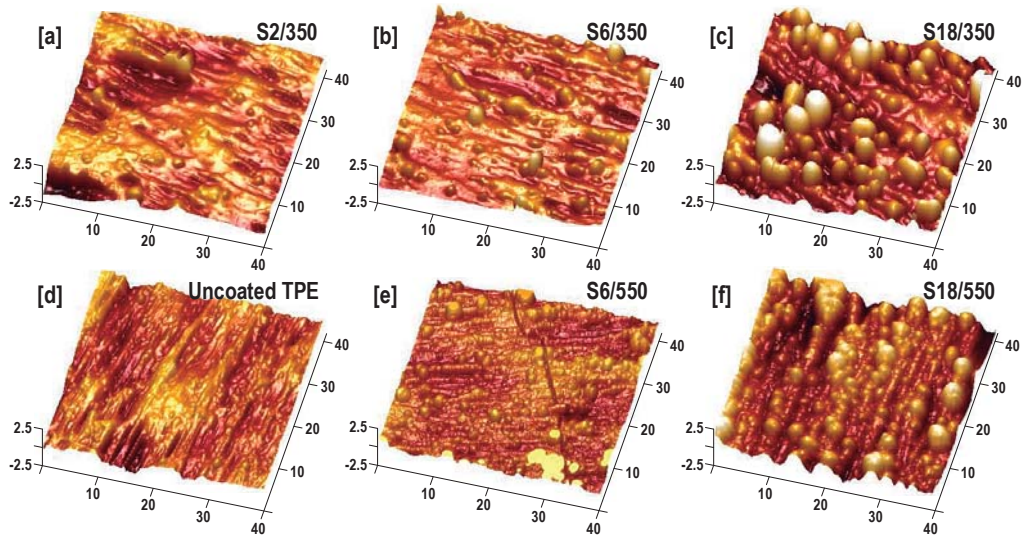

Figure 3.7. AFM images of samples: [a] S2/350, [b] S6/350, [c] S18/350, [d] Uncoated TPE, [e] S6/550 and [f] S18/550 [23].

Cracking has been observed clearly on the surface of samples under SEM analysis in Figure 3.8. The residual thermal stress that is due to differences between the thermomechanical properties of the coating and the TPE substrate [46,54,55], and the coating embrittlement by the higher number of passes may be two of the main causes of cracking [2]. It should be noted that the size of the cracks is the greatest in the samples that were coated in the greatest number of passes. This can be related to the cumulative effect of the surface temperature (see Figure 3.1) due to the longer exposure of the sample to an energetic plasma [56,57].

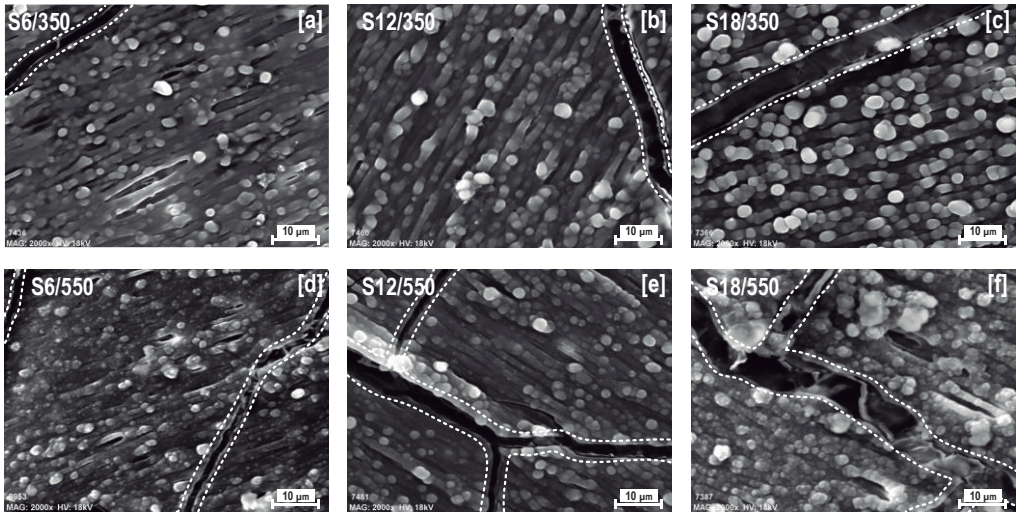

Figure 3.8. SEM images with a magnification of x2000 of samples: [a] S6/350, [b] S12/350, [c] S18/350, [d] S6/550, [e] S12/550 and [f] S18/550 [23].

3.1.3.3. EFFECT OF THE PLASMA POWER

Related to the plasma power effect, the higher the power is, the greater is the precursor decomposition during the gas phase reactions of the plasma and the higher is the number of small particulates on the coating surface [22]. Figure 3.9 shows the AFM profiles of samples that were coated in eighteen passes. In this figure, one can note a higher number of smaller particles on samples that were coated at higher plasma power. This results in a decrease in roughness with increasing power, since spherical particles create a denser and more compact coating that fits the uncoated TPE´s morphology better [28,43].

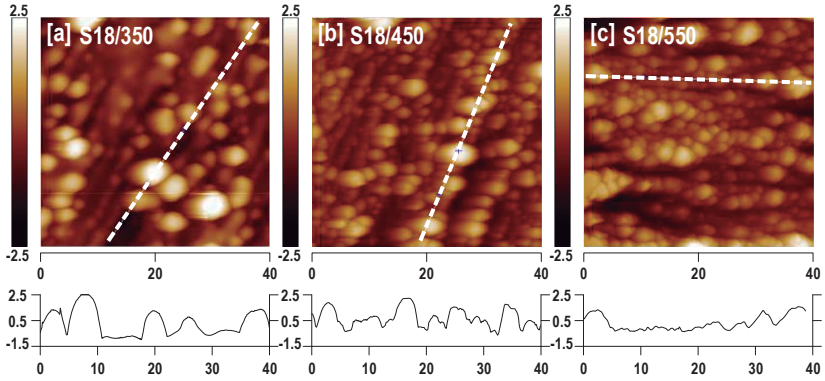

Figure 3.9. AFM images (top) and cross section along the dashed line (bottom) of samples: [a] S18/350, [b] S18/450 and [d] S18/550 [23].

In all cases, the more energetic ions, molecules and particles that are achieved with higher plasma powers cause an increase in the average surface temperature of the samples. In certain cases, these particles may become too powerful and cause a high increase in the temperature of the sample. This increase, if followed by cooling of the sample after the coating process, generates

residual thermal stress. The impact of residual thermal stress will be discussed in section 3.1.7 Tribological Tests. Regarding the crack formation, it can be observed in Figure 3.8 that the higher the power is, the greatest the number of cracks is. This is probably due to the temperature effect, which is similar to what happens with the increment of the number of passes.

Considering the aforementioned, one can conclude that SEM results are in good agreement with the AFM images and confirm that the surface roughness was affected significantly by the deposition conditions. In this regard, Figure 3.10 illustrates a scheme of the growth mechanisms of coating by the plasma power and number of passes. One can see the strong influence of the substrate´s morphology during the early growth stages. As the number of passes increases, the fibrous aspect of the substrate is replaced progressively by a coating that consists of spherical particles from the gas phase reactions. The number and size of the particles depend on the plasma power. Once cavities and holes in the TPE substrate have been covered fully, the coating´s morphology depends, essentially, on the number and size of the spherical particles that have been generated and deposited. This explains the morphology of samples that have been coated in eighteen passes.

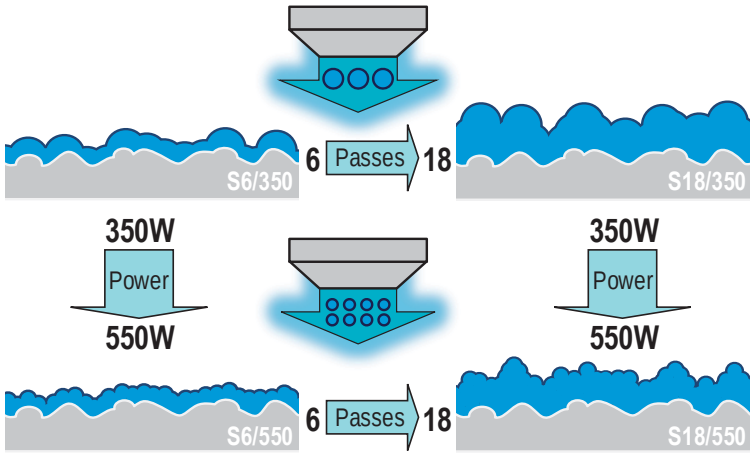

Figure 3.10. Scheme of the growth mechanisms of SiO_x-based coatings [23].

3.1.4. ATR-FTIR ANALYSIS

ATR-FTIR spectroscopy was used to examine the chemical characteristics of all the analyzed samples. The main chemical bonds and frequencies of the uncoated TPE spectrum and the coated samples are described in Table 3.2 and Table 3.3, respectively.

Functional groups	Frequency/range (cm^{-1})	Reference
CH_2 rocking	~721, ~808, ~840	[28]
C-C asymmetric stretching and CH_3 asymmetric rocking	~896, ~973, ~998	[22]
C-O stretching	~1088	[22]

Functional groups	Frequency/range (cm^{-1})	Reference
CH_3 asymmetric rocking, C-H wagging and C-C asymmetric stretching	~1164	[58,59]
CH_2 wagging vibration	~1303	[60]
CH_3 asymmetric stretching	~1377	[28]
CH_2 scissoring	~1460	[28]
saturated hydrocarbons (CH_x)	~2852-2950	[58,61]

Table 3.2. Chemical bonds and frequencies of the uncoated TPE ATR-FTIR spectrum.

Functional groups	Frequency/range (cm^{-1})	Reference
CH_2 rocking	~720	[28,39,57]
Si-C/SiOSi bending	~805	[28,39,57]
CH_3 rocking	~950	[2]
SiOSi stretching	~1050	[24]
SiOC ring link	~1074	[24]
SiOC open link	~1115	[24,62]
SiOC cage link	~1172	[24,62]
OCH_2CH_3	~1200	[24,62]
Si-$(CH_3)_x$ stretching, C-N, C=O and C-C	~1250-1500	[39,57,63]
Amine, amide, C=O and C=C	~1500-1700	[24,63,64]
CH_x stretching	~2900-2950	[2,63]
OH and NH_X stretching	~3000-3600	[42,44,57]

Table 3.3. Chemical bonds and frequencies of the coated samples ATR-FTIR spectrum.

3.1.4.1. EFFECT OF THE PRECURSOR FLOW RATE

The same bands that were observed in the characteristic spectrum of the TPE were also identified in the 3-pass samples. However, the coated samples exhibited a noticeable increase in some of the TPE spectrum peaks, as well as some new bands indicated in Table 3.3. It was noted that the behavior of peaks that are related to these new bands depends largely on the precursor flow rate. Thus Figure 3.11 shows the ATR-FTIR spectra of uncoated TPE and 3-pass samples related to the two main bands (980-1250 cm^{-1} and 1600-1750 cm^{-1}). The resulting spectra after subtracting the uncoated TPE spectrum were deconvoluted into their constituents. Figure 3.12 shows the deconvolution of samples S3/350 and S3/550. Figure 3.13 illustrates the absorption areas of SiOSi and nitrogen-containing groups (N-groups) peaks of the 3-pass samples.

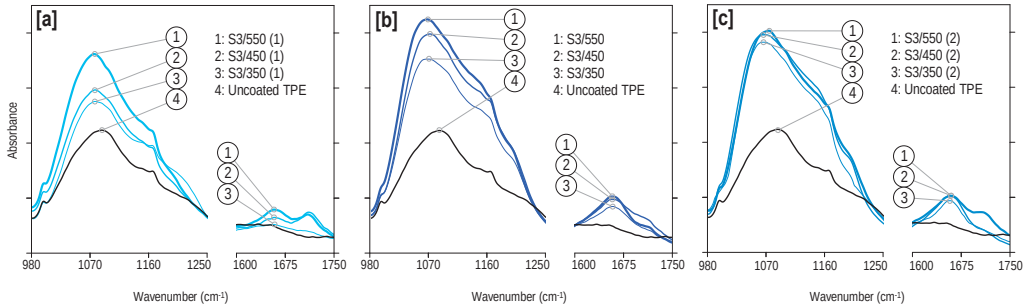

Figure 3.11. ATR-FTIR spectra of the uncoated TPE and plasma polymerized films at APTES flow rate of [a] 1 slm, [b] 1.5 slm and [c] 2 slm at various plasma power values, from 350 to 550 W [22].

In Figure 3.11, it may be noted that, no matter what the APTES flow rate is, the increment of plasma power leads to an increase in the intensity of these bands [50]. In Figure 3.13, it can be seen that, when the precursor flow rate increases for a given plasma power, the absorption area that is below the peak of the analyzed groups also increases for most samples. The absorption areas that were obtained with a precursor flow rate of 1 slm are lower than those obtained with higher APTES flow rates (1.5 and 2 slm). This is probably due to the lower amount of precursor that is available to deposit on the TPE substrate.

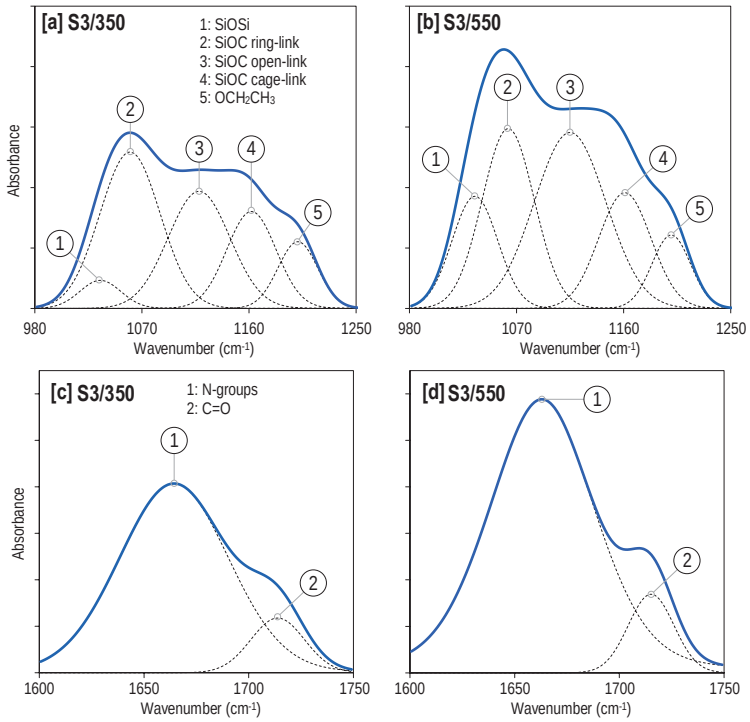

Figure 3.12. Deconvoluted spectra of samples S3/350 and S3/550 obtained in the region of [a] 980-1250 cm^{-1} and [b] 1600-1750 cm^{-1} [22].

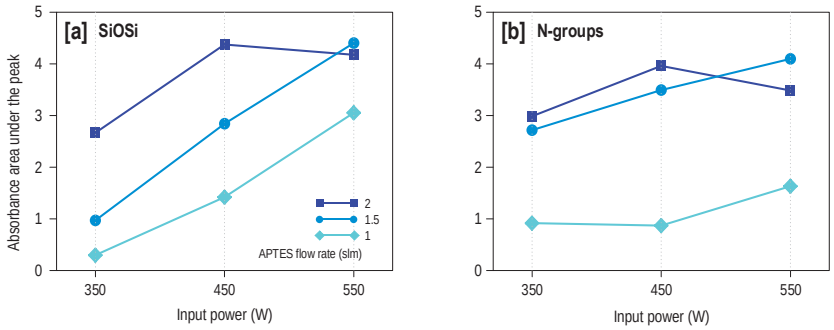

Figure 3.13. Absorption areas under the peak of [a] SiOSi (~1035 cm^{-1}) and [b] nitrogen-containing groups (~1662 cm^{-1}) of 3-pass samples [22].

In Figure 3.13, one can see that, with an APTES flow rate of 1 and 1.5 slm, by increasing the plasma power, an increase of the absorption areas of SiOSi and N-groups takes place. Related to SiOSi groups, this increment may be due to the higher precursor decomposition and, in some cases, the subsequent rearrangement of the bonding structures in the film [65]. For N-groups, this behavior is contrary to what was identified in other works [66,67] where the concentration of primary amines was greater at a low plasma power. Unfortunately, since different groups overlap at a frequency of ~1662 cm^{-1}, it was not possible to identify and quantify the decrement in the content of primary amines by FTIR-ATR analysis [67]. With an APTES flow rate of 2 slm, the absorption area at 450 W is greater than the areas at 350 W and 550 W. This phenomenon, which is also observed in Figure 3.11, is probably due to plasma saturation with the precursor. Thus, for a plasma power of 550 W, an increment in the flow rate from 1.5 to 2 slm reduces the opportunities for active species to react with the precursor. This results in a stabilization of the number of SiOSi groups.

As Figure 3.13 shows, sample S3/550, coated with 1.5 slm and 550 W, provided the maximum absorption area values of both previously mentioned groups. Therefore, it can be said that, for a specific plasma power, an increment of the precursor flow rate does not necessarily lead to an increment of the SiOSi and N-groups.

3.1.4.2. EFFECT OF THE NUMBER OF PASSES

Figure 3.14 depicts the ATR-FTIR spectra of samples that were coated with 350 W in the 0-4000 cm^{-1} range. Chemical bonds for samples coated with more than six passes correspond only to the chemical composition of the coatings, since the thickness of these coatings exceeds the depth of analysis of this technique (<1000 nm).

It is evident in a comparison of the peak intensity of the spectrum of the samples that were coated at 350 W that the lower the number of passes is, the higher the ATR-FTIR spectrum intensity is. This trend is probably explained by the coating morphology. It was seen that a higher number of passes resulted in an increase in the number and size of spherical particles of the coating leading to a greater roughness. Thus, the intensity signal of the functional groups of these samples would be penalized due to the existence of an air gap between the diamond ATR element and the sample

surface. This results in a spectrum with lower intensities that is not representative of the nature of the coating [68–71].

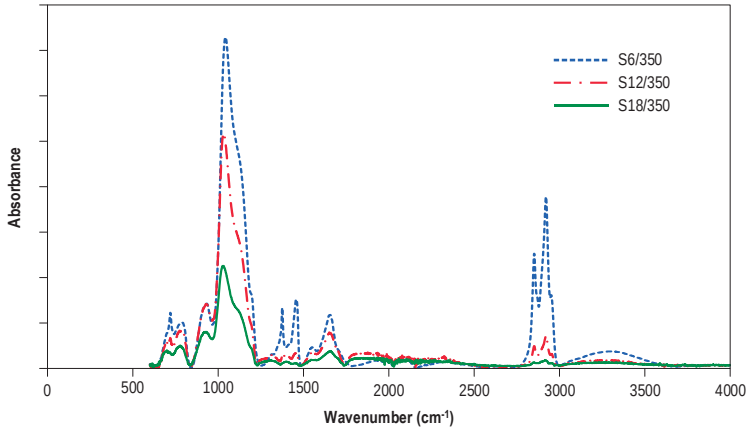

Figure 3.14. ATR-FTIR spectra of samples: S6/350, S12/350 and S18/350 [23].

3.1.4.3. EFFECT OF THE PLASMA POWER

Figure 3.15 and Figure 3.16 depict the ATR-FTIR spectra of samples that were coated in six passes and two passes in the 0-4000 cm^{-1} range, respectively. Considering that the thickness of 2-pass samples is less than 1000 nm, the contribution of the uncoated TPE signal was subtracted from their absorption spectra.

Samples that were coated in six passes have a similar thicknesses and roughnesses (see Figure 3.2 and Figure 3.4). This is the reason why the ATR-FTIR spectra of these samples show similar peaks and intensities in Figure 3.15, with a slight difference in the intensity of the broad band that is found around 1050 cm^{-1}.

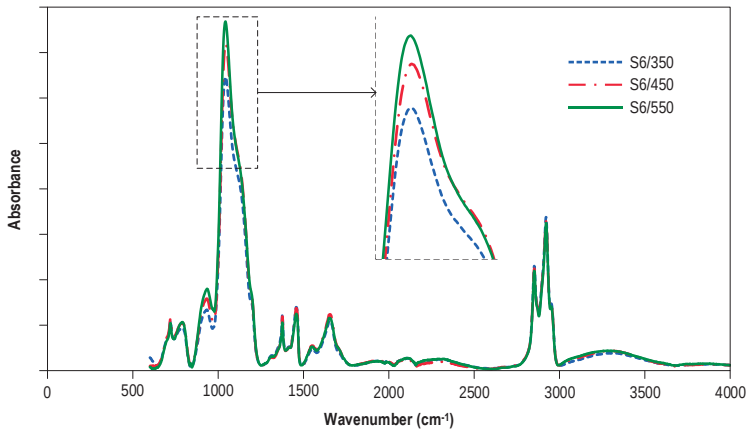

Figure 3.15. ATR-FTIR spectra of samples: S6/350, S6/450 and S6/550 [23].

However, although some authors have identified a relationship between the area under the SiOSi peak and the tribological properties of the coatings [22,24,72], there is no relationship to the 6-

pass samples. This is probably due to the harmful effect of the temperature that is reached during the coating process. This effect will be discussed in section 3.1.7 Tribological Tests.

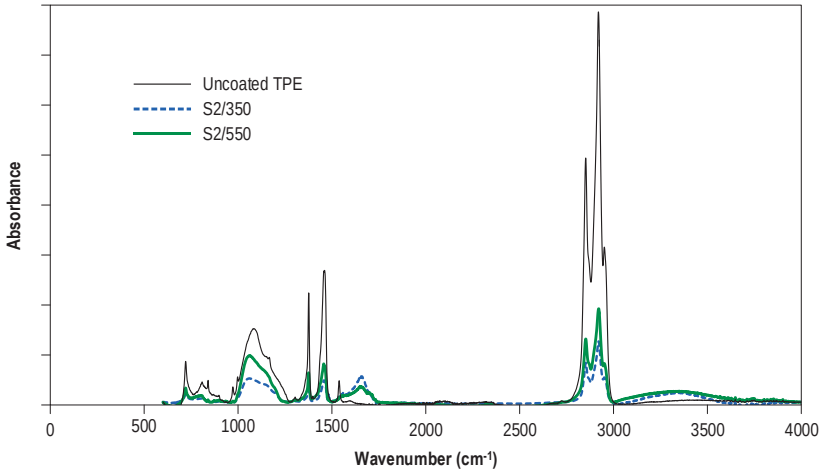

Figure 3.16. ATR-FTIR spectra of samples: Uncoated TPE, S2/350 and S2/550 [23].

Whereas, it appears that temperature does not affect the samples that were coated in less than six passes, since both the average surface temperature of the samples and their residence times have not been sufficiently high to endanger the quality of the coatings. In fact, ATR-FTIR spectra of 2-pass samples in Figure 3.16 show an increase of the area under the SiOSi peak at the power increase that is related to lower friction coefficients, as will be detailed in section 3.1.7 Tribological Tests. This same trend was found for the 3-pass samples in Alba-Elías et al. [22] as one can see in Figure 3.13 [a].

3.1.5. XPS ANALYSIS

In regard to the chemical composition, XPS analysis, with an analysis depth of 10 nm [73,74], was used to quantify the atomic composition of the analyzed samples. Table 3.4 shows the atomic chemical composition (at. %) of all the analyzed samples.

According to the results of Table 3.4, the surface of the uncoated TPE sample is composed mainly of carbon. There are some traces of silicon – which were probably caused by cross contamination– and oxygen. The latter was derived from the oxidation that takes place during the thermal degradation that occurs during the transformation of santoprene pellets into sheets. No presence of nitrogen was observed.

The variations founded in Table 3.4 for C1s, O1s, Si2p and N1s percentages did not allow to justify the tribological behavior as it will be discussed in section 3.1.7 Tribological Tests. However, one can observe the increase in the atomic percentage of Si2p and O1s and the subsequent decrement of C1s percentage of coated samples with respect to the atomic percentages of the uncoated TPE sample. In addition, ATR-FTIR and XPS results of the coated samples showed that the major bond of SiO_x-based films is SiOSi with characteristics peaks at ~805 cm^{-1} and ~1050

cm^{-1}, and the O/Si ratio of the films between 1.7-2.0. The latter is a value that is close to the stoichiometric ratio of silica (O/Si = 2).

Sample	Atomic chemical composition (at. %)			
	C1s	O1s	Si2p	N1s
S2/350	64.2	20.7	11.7	3.4
S3/350 (1)	83.8	11.2	4.6	0.4
S3/350	71.7	17.8	8.6	2.0
S3/350 (2)	65.0	21.5	10.7	2.9
S6/350	55.3	26.5	14.1	4.2
S12/350	58.0	24.9	13.7	3.4
S18/350	56.7	25.2	14.1	4.1
S2/450	60.9	23.6	12.0	3.5
S3/450 (1)	83.1	11.2	5.3	0.4
S3/450	58.7	25.1	12.8	3.5
S3/450 (2)	59.5	24.7	12.3	3.5
S6/450	58.3	24.8	13.3	3.7
S12/450	58.2	24.8	13.6	3.4
S18/450	53.1	28.1	14.8	4.0
S2/550	58.4	24.1	14.4	3.2
S3/550 (1)	70.6	18.7	8.2	2.6
S3/550	57.0	26.1	13.4	3.5
S3/550 (2)	59.6	25.1	12.1	3.2
S6/550	54.0	27.6	15.1	3.3
S12/550	58.3	25.0	13.4	3.4
S18/550	51.4	28.7	16.6	3.3
Uncoated TPE	94.3	4.5	1.2	-

Table 3.4. Atomic chemical composition (at. %) of all the analyzed samples.

3.1.5.1. EFFECT OF THE PRECURSOR FLOW RATE

Deconvolutions of the Si2p signal of the 3-pass samples were undertaken to develop a better quantification of the relative percentages of $(CH_3)_2SiO_2$, CH_3SiO_3 and SiO_4. The binding energies of silicon chemical bonds are shown in Table 3.5 and their relative percentages appear in Table 3.6. For all samples, the predominant chemical bonding was CH_3SiO_3.

	Chemical component	Peak position (eV)	Reference
Si2p	$(CH_3)_4Si$	~100.9	[36 2015]
	$(CH_3)_3SiO$	~101.5	[36 2015]
	$(CH_3)_2SiO_2$	~102.1	[36 2015]
	CH_3SiO_3	~102.8	[36 2015]
	SiO_4	~103.4	[36 2015]

Table 3.5. Assigned chemical components and peak position in Si2p deconvolution.

Figure 3.17 [a] depicts how the absorption area of CH_3SiO_3 increases with the plasma power when the precursor flow rate is 1 slm for the 3-pass samples. In this figure, the same saturation phenomenon of SiOSi groups that was identified in the ATR-FTIR analysis when the precursor flow rate is equal to 1.5 and 2 slm can be observed.

In regards to the SiO_4 (Figure 3.17 [b]), its percentage increases by increasing the plasma power for a given precursor flow rate. It seems that more reactive species of Si and O are formed at a higher power [75]. When comparing the samples and taking into account the plasma power, one may note that the highest values of SiO_4 occur in the samples that were deposited at 1.5 slm, with maximum values of 22.9% for SiO_4 in sample S3/550. As discussed in section 3.1.7 Tribological Tests, for 2 and 3-pass samples, the greater SiO_4 content of this sample, in addition to the ATR-FTIR results, might explain its lower friction coefficient.

Sample	Relative percentage (%)		
	$(CH_3)_2SiO_2$ (~102.1 eV)	CH_3SiO_3 (~102.8 eV)	SiO_4 (~103.4 eV)
S2/350	-	7.9	3.8
S2/550	-	7.4	7.0
S3/350 (1)	-	4.5	0.1
S3/350	-	8.1	0.5
S3/350 (2)	-	10.1	0.6
S3/550 (1)	-	7.1	1.0
S3/550	-	10.3	3.1
S3/550 (2)	-	9.5	2.6
S6/350	2.0	5.0	7.0
S6/550	0.0	5.2	10.0
S12/350	2.0	6.2	5.5
S12/550	1.8	5.8	7.6
S18/350	3.6	3.9	6.6
S18/550	0.0	7.3	9.3

Table 3.6. Relative percentage (%) of $(CH_3)_2SiO_2$, CH_3SiO_3, SiO_4 of samples coated at 350 W and 550 W.

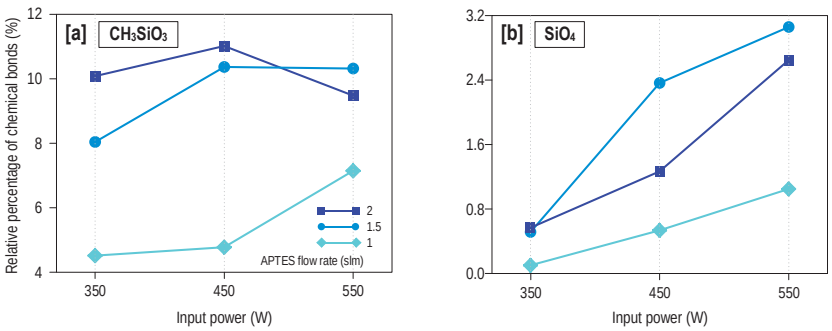

Figure 3.17. Relative percentage of chemical bonds: [a] CH_3SiO_3 and [b] SiO_4 of 3-pass samples coated with different precursor flow rates (1, 1.5 and 2 slm) and plasma powers (350, 450 and 550 W) [22].

3.1.5.2. EFFECT OF THE NUMBER OF PASSES

As can be seen in Table 3.4, no clear relationship was identified between the atomic composition of the analyzed samples when modifying the number of passes.

This fact seems reasonable since, considering that the predominant type of plasma polymerization takes place in the gas phase, a modification of the number of passes practically does not affect the atomic composition of the uppermost layer of the coating. This was not the case in the case of different precursor flow rates or different plasma powers, since these two variables do modify the type of plasma polymerization that takes place and, therefore, the atomic composition of the coating.

3.1.5.3. EFFECT OF THE PLASMA POWER

On the one hand, for the 2 and 3-pass samples, in Table 3.4, the higher the plasma power is for a given precursor flow rate, the lower the C1s atomic percentage is. This is due to the decomposition of the ethoxy groups (OCH_2CH_3) in APTES [51]. On the other hand, the atomic percentages of oxygen increase with plasma power [51]. The atomic percentage of nitrogen is not significant, and can be considered to be constant with changes in plasma power.

Deconvolutions of the Si2p signal of the samples that were coated at 350 and 550 W were undertaken to develop a better quantification of the relative percentages of $(CH_3)_2SiO_2$, CH_3SiO_3 and SiO_4. The binding energies of silicon chemical bonds are shown in Table 3.5 and their relative percentages are shown in Table 3.6. It is noted that, for a selected number of passes, the SiO_4 percentage increases with the plasma power, indicating a more inorganic character of the coatings.

3.1.6. WETTABILITY

To investigate the wettability of the samples, water contact angles of samples were measured. It is known that the wettability of a surface is affected by the chemical composition of the first 3 nm surface layer and the surface roughness of the coatings [39,74]. Figure 3.18 illustrates the WCA of the coated samples, uncoated TPE and the polyamide tape. It was not possible to determine the WCA of the flocked seals, since it consist of polyethylene fibers which absorb the test water drop. Therefore, it can be said that the flocked seals possess a superhydrophilic character.

For the coated samples, changes in WCA seem to be explained by its differences in roughness together with the inorganic character of the coatings. It was discovered in section 3.1.3 Surface Morphology that the growth mechanisms and the roughness of the coatings depended on the number of passes and the plasma power. In addition to this, the inorganic character of the coatings depended on the SiO_4 (Table 3.6). All coated samples, with the exception of sample S6/550, had a WCA that exceeded that of the polyamide tape (85.1º ± 7.4) and the uncoated TPE (86.0º ± 6.4).

3.1.6.1. EFFECT OF THE NUMBER OF PASSES

For any power, as shown in Figure 3.18, WCA usually increases with an increase in the number of passes from 2 to 18. These results can often be explained by the roughness values. Increasing the number of passes from 6 to 18 for a given power increases the roughness and, therefore, the WCA. Similarly, increasing the number of passes from 2 to 6 decreases the roughness and, therefore, the WCA (except for 350 W). The wetting behavior of the coatings can be ascribed to the formation of spherical particles that create a roughness. Therefore, it can be concluded that a rise in WCA is caused by an increase in roughness as other studies have demonstrated [39].

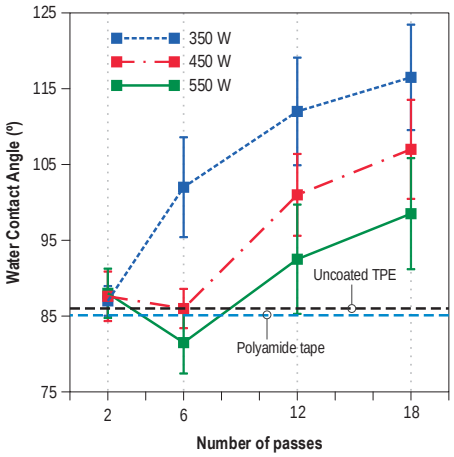

Figure 3.18. Water contact angles of: the coated samples, the uncoated TPE and polyamide tap [23].

3.1.6.2. EFFECT OF THE PLASMA POWER

Despite the high standard deviation (SD) of WCA, it seems that an increase in plasma power from 350 to 550 W results in a lower WCA, for samples that were coated in 6, 12 or 18 passes. This is in agreement with the increasing inorganic character of the samples with higher power as one can see in Table 3.6 since the roughness variations are not so significant to ensure any trend. WCAs of samples that were coated in two passes are practically the same (~87º) and are very similar to the uncoated TPE WCA. It seems that the use of two passes generates an incomplete coverage of the substrate. Thus, there is a minimum number of passes necessary for full-coverage the substrate surface [76]. For samples whose roughness were similar to that of uncoated TPE, differences in WCAs are explained by their chemical composition, since after deposition of an APTES-based coating, the wettability of the sample increased in agreement with the presence of SiO_x groups that are characteristics of the APTES molecule. Finally, it can be concluded that sample S18/350 had the highest WCA (116.5º), that was 37% higher than the WCA of the polyamide tape.

3.1.7. TRIBOLOGICAL TESTS

3.1.7.1. EFFECT OF THE PRECURSOR FLOW RATE

In Alba-Elías et al. [22] the 3-pass samples and the uncoated TPE were subjected to a friction coefficient test applying 0.25 N at 2 cm/s for a sliding distance of 10 m. Table 3.7 presents the measurements of the average friction coefficient of uncoated TPE and 3-pass samples coated using 350 and 550 W. In Figure 3.19, which illustrates the variations of the friction coefficient of the abovementioned samples, one can see a friction coefficient stabilization at the end of the test.

Sample	Average friction coefficient
S3/350 (1)	0.79 ± 0.04
S3/350	0.32 ± 0.04
S3/350 (2)	0.22 ± 0.01
S3/550 (1)	0.49 ± 0.05
S3/550	0.19 ± 0.02
S3/550 (2)	0.20 ± 0.01
Uncoated TPE	0.84 ± 0.03

Table 3.7. Average friction coefficient of the 3-pass samples (350 and 550 W) and the uncoated TPE after a friction test of 10 m [23].

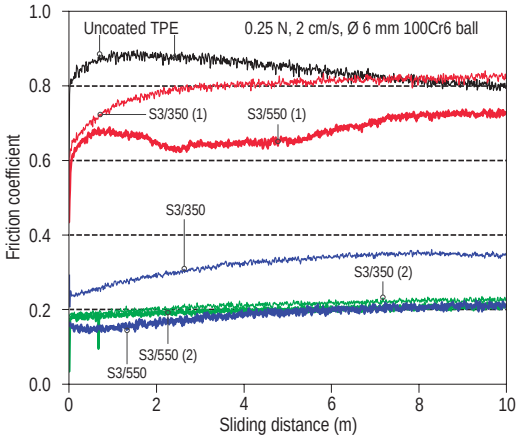

Figure 3.19. Friction coefficient of the uncoated TPE and 3-pass samples coated with different combinations of APTES flow rates (1, 1.5 and 2 slm) and plasma powers (350 and 550 W) [22].

In view of the results that appear in Table 3.7 and Figure 3.19, samples coated with a precursor flow rate of 1.5 and 2 slm had lower friction coefficients than that of the uncoated TPE sample. The friction coefficient of the sample that was coated with a precursor flow rate of 1 slm at a power of 350 W tends towards a value that is similar to that of the uncoated sample. This is probably due to the total loss of its coating during the test. One can also see that the friction coefficient decreases with increasing plasma power, for a given precursor flow rate. An increase of plasma power makes for a chemically and mechanically strong bonding with all fragment molecules, ions, and radicals that turns into a friction coefficient decrement [77]. As was also noted in the ATR-

FTIR and XPS tests, the special behavior of sample S3/550 must be mentioned. This sample possessed the lowest friction coefficient, although the highest precursor flow rate was not used.

With regard to the ATR-FTIR analyses, Figure 3.13 and Figure 3.19 show that the values of the absorption area that are below the peaks of SiOSi and N-containing groups are correlated inversely to the friction coefficient. In regards to the XPS analyses, an inverse relationship between the atomic percentage of Si2p and the relative percentage of SiO_4 chemical bond and average friction coefficient can be seen in Figure 3.17 and Figure 3.19. In turn, the relationship between the average friction coefficient and the atomic percentage of C1s is positive (see Table 3.4). The reduction of carbon content causes an increment in the coating density because there is a diminution in the number of nano-pores in the coating structure. A higher coating density provides an increment in the hardness of the coating, with a consequent friction coefficient reduction [78]. All of these relationships were coherent with previous results [28,67], where an increment in one of the aforementioned groups enabled lower friction coefficients to be obtained.

Taking into account that, in this work, sample with the best friction performance was coated with a precursor flow of 1.5 slm, in Sainz-García et al. [23] all samples were coated with this precursor flow rate (1.5 slm) and the influence of different plasma powers and number of passes was studied.

3.1.7.2. EFFECT OF THE NUMBER OF PASSES

In Sainz-García et al. [23], with the aim of reproducing the rigors of the operation that the coating on a seal of a vehicle undergoes during its lifetime a friction test with a sliding distance of 4000 m was selected. The friction coefficients of samples that were coated at 350 and 550 W together with the uncoated TPE sample and the current industrial solutions (flocked seals and polyamide tape) appear in Figure 3.20. Table 3.8 shows the average friction coefficient of all the analyzed samples.

Figure 3.20 shows that the friction coefficient of the flocked seal gradually increases to 3000 m, reaching a steady state with a friction coefficient of ~0,3. The friction coefficient of the polyamide tape is practically constant during the 4000 m of sliding distance. Finally, it is noted that the friction coefficient of all of the coated samples is lower than the one of the uncoated TPE. As has been mentioned, the higher the plasma power and number of passes are, the higher is the average surface temperature (Figure 3.1) which can have a significant influence on the tribological behavior when a heat-sensitive substrate, like TPE, is coated. The higher the surface temperature, the higher is the residual thermal stress of the coating generated due to difference in the thermal expansion coefficients of TPE and coating [79–81]. As confirmed Zeghni et al. [82], coatings that are subjected to high thermal tensile stress have a poorer friction behavior.

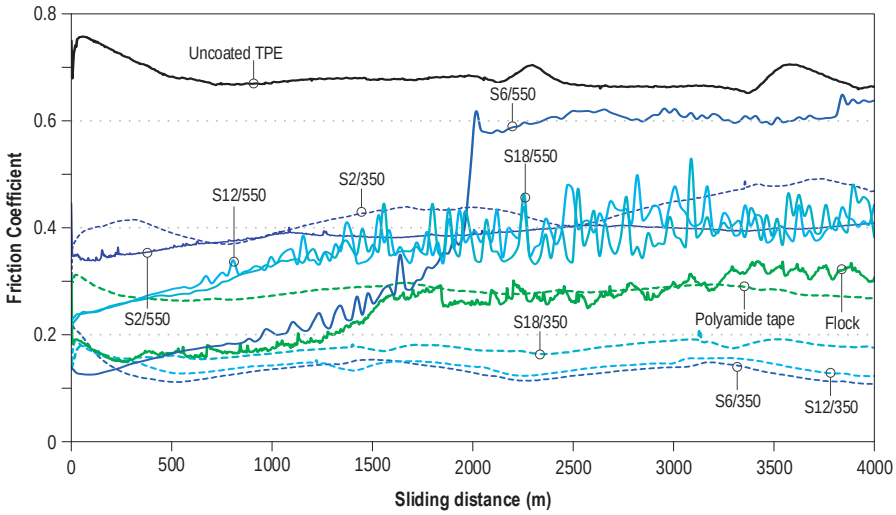

Figure 3.20. Evolution of the friction coefficient of: samples coated at 350 W and 550 W, uncoated TPE, flocked seal and polyamide tape [23].

Sample	Average friction coefficient
S2/350	0.43 ± 0.03
S6/350	0.13 ± 0.02
S12/350	0.14 ± 0.01
S18/350	0.17 ± 0.01
S2/450	0.39 ± 0.04
S6/450	0.24 ± 0.02
S12/450	0.25 ± 0.10
S18/450	0.35 ± 0.19
S2/550	0.39 ± 0.02
S6/550	0.41 ± 0.20
S12/550	0.44 ± 0.05
S18/550	0.36 ± 0.06
Uncoated TPE	0.68 ± 0.02
Flocked seal	0.25 ± 0.06
Polyamide tape	0.28 ± 0.01

Table 3.8. Average friction coefficient of the coated samples, the uncoated TPE, flocked seal and the polyamide tape after a friction test of 4000 m [23].

Figure 3.20 and Table 3.8 indicate that samples coated with 350 W and more than six passes have lower friction coefficients than the current industrial solutions (flock and polyamide tape). These friction coefficients decline slightly with a decrease in the number of passes. The best sample was S6/350 probably because it was subjected to lower process time. This produces a lower average surface temperature, less residual thermal stress and a better friction performance. Otherwise, sample S2/350 had a friction coefficient that exceeds the remaining samples that were coated at 350 W and the current industrial solutions, probably because its surface was not fully

coated. Therefore, it seems that a minimum coating thickness is necessary to enhance a friction coefficient that is lower than those of the current industrial solutions.

Samples that were coated at 550 W had friction coefficients that exceed those of the current industrial solutions. As can be seen in Figure 3.20 and Table 3.8, sample S2/550 had a friction coefficient that was nearly constant and was the lowest of the 550 W-samples. The surface of this sample was not full-coverage, which would cause its friction coefficient to depend not only on the coating, but also on the TPE substrate. In addition to this, its antifriction ability was not significantly affected by the residual thermal stress of this sample. The surface of sample S6/550 was full-coverage with a 1402 nm thickness coating and its friction coefficient showed three different behaviors. During the first stage (0-1000 m), the friction coefficient increased linearly, since the first nanometers of the coating were not subjected to residual thermal stress. In the second stage (1000-2000 m), the friction coefficient fluctuated. This was probably due to successive cycles of the coating breaking and developing tribofilm. Finally, in the third stage (2000–4000 m), there was a sharp increase in the friction coefficient. In this situation, the residual thermal stress was high enough to cause complete detachment of the coating so that tribofilm could not be formed. The TPE surface was exposed to the steel and so the friction coefficient value was similar to that of the TPE. Friction coefficients of samples S12/550 and S18/550 were similar during the entire test. Both samples were subjected to the highest temperatures for the longest time. This caused the highest residual thermal stress in these coatings.

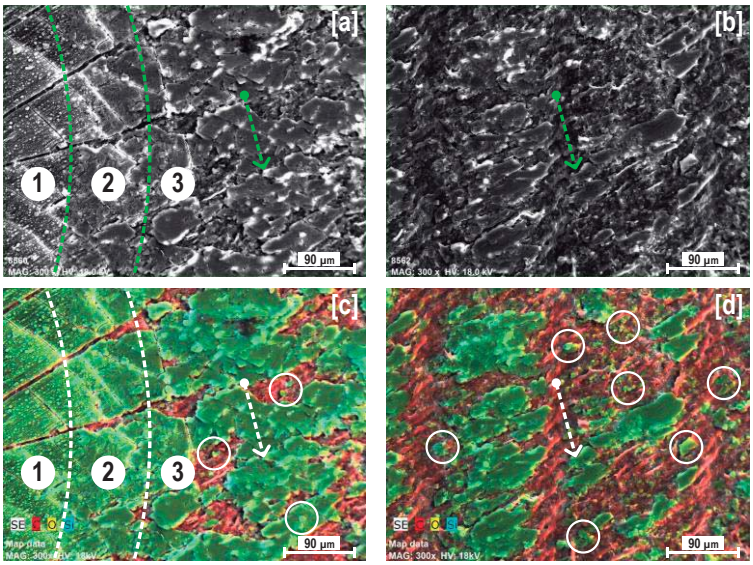

Figure 3.21. SEM (top) and EDX (bottom) images with a magnification of x300 of the wear track of sample S18/550 after a 4000 m friction test: [a] and [c] limited area coating-wear track, [b] and [d] central area of the wear track. The dashed arrows indicate the sliding direction and the white circles indicate coating debris [23].

In order to examine the quality of the coating at the end of the friction test, Figure 3.21 shows SEM wear track images and EDX analyses of sample S18/550 after a friction test of 4000 m. In the EDX maps, the red color corresponds to carbon, the blue color represents the silicon and the

yellow color is associated with oxygen. One can see in Figure 3.21 [a] and [c] different numbered regions of the coating. Region 1 corresponds to an undamaged coating area of spherical particles of SiO_x similar to particles of Figure 3.21 [f]. In fact, its EDX map (Figure 3.21 [c]) evinces a uniformly green coating of SiO_x that was derived from the mixture of silicon (blue) and oxygen (yellow). Region 2 depicts a transition area. This region is shown as a brittle coating where the detected cracks of Region 1 have become wider and the spherical particulates of the surface have been eroded. Region 3, together with Figure 3.21 [b] and [d], represents the central area of the wear track, in which flattened areas of SiO_x (green) of the remaining coating and tribofilm appear. The wear in this region caused the coating to detach, which resulted in areas where the TPE substrate can be observed (red color of carbon). These images show debris of the coating (white circles in Figure 3.21 [c] and [d]) from which the tribofilm is created. These flattened areas of SiO_x at the end of the friction test ensure that the value of the friction coefficient is 50% less than that of the uncoated TPE.

3.1.7.3. EFFECT OF THE PLASMA POWER

Figure 3.20 and Table 3.8 indicate that, for samples that were coated in 6, 12 or 18 passes, the higher the power is, the higher the friction coefficient is for a selected number of passes. This probably is related to the high temperature to which both the coating and the TPE substrate were subjected during the deposition process and results in an increase in the residual thermal stress of the sample. As was discussed earlier, this residual thermal stress has a negative impact on the friction behavior of the samples.

However, the opposite result was found with 2-pass samples. Higher power leds to lower friction coefficient. These samples were subjected to different average surface temperatures for the shortest residence times. This produced a low residual thermal stress that did not affect to their friction behavior. In such a situation, the friction behavior seems to depend on the chemical composition of the coatings as was demonstrated by other authors [22,24,25]. In this regard, the sample that was coated at 550 W (S2/550) had the highest absorption area under the SiOSi peak in the ATR-FTIR spectrum (see Figure 3.16) and the highest SiO_4 percentage after the Si2p deconvolution in XPS analyses (see Table 3.6). This provided a friction coefficient that was less than those of the samples that were coated at a lower power. The same applied to 3-pass samples in Alba-Elías et al. [22], where an increase of plasma power resulted in an increase of both the absorption area of SiOSi peak (ATR-FTIR) and the relative percentage of SiO_4 chemical bond (XPS) leading to a lower friction coefficient.

Finally, it can be concluded that sample coated in six passes and at a power of 350 W proved to have the best friction performance. This sample had a friction coefficient 46% and 53% lower than that of the flocked seals and polyamide tape respectively.

3.2. MULTIFUNCTIONAL COATINGS: IMPROVEMENT OF TRIBOLOGICAL AND WETTABILITY BEHAVIOR

As already mentioned in section 1.3.2 Topic of the Thesis, the publications Sainz-García et al. [24] and Sainz-García et al. [25], related to the **OBJECTIVE 2** of this thesis, are focused on the deposition of functional coatings to improve both the tribological and hydrophobic properties of the uncoated TPE by using a mixture of two liquid precursors, APTES and a fluorinated compound. The key was determining the optimal mixture of precursors that produces a coating that is satisfactory in both characteristics. The main difference between these two publications is related to the different characteristics of the fluorinated precursors used in each case, and more specifically, in its different flash point, which has established the prevailing plasma polymerization (gas or substrate). In Sainz-García et al. [24] the fluorinated precursor FLUSI was used and in Sainz-García et al. [25] PFH. All the analyzed samples were coated with 450 W in a 2-pass coating process. The total flow rate of the mixture of precursors (APTES + fluorinated precursor) was 1.5 slm. Table 3.9 shows the label of each analyzed sample and the percentages of APTES and fluorinated precursor.

Sample label	Fluorinated precursor	% APTES	% fluorinated precursor
A_0F_{100}	FLUSI	0	100
$A_{25}F_{75}$		25	75
$A_{50}F_{50}$		50	50
$A_{75}F_{25}$		75	25
A_0P_{100}	PFH	0	100
$A_{25}P_{75}$		25	75
$A_{50}P_{50}$		50	50
$A_{75}P_{25}$		75	25
A_{100}	-	100	0

Table 3.9. Sample identification according to the proportions of APTES, FLUSI and PFH.

In Sainz-García et al. [24], the chemical modification of the coating surface (due to the CF_x groups) had greater influence in the enhancement of the hydrophobic character of the coating than the modification of the surface roughness. The variations that were observed in the surface morphology depend on the proportions of APTES and FLUSI when they are mixed. They appear to be due to the difference between the flash points of APTES (96 ºC) and FLUSI (168 ºC). The higher the percentage of APTES is, the lower the flash point of the mixture is. The flash point is the lowest temperature at which a liquid can vaporize sufficiently to form an ignitable mixture in air. This determines if a gas phase plasma polymerization predominates for lower flash points, or if there is a higher degree of plasma polymerization on the substrate surface for higher flash points. In this work, the flash point of the mixture of precursors was higher than 114 ºC.

In Sainz-García et al. [25], with the aim of intending a greater influence of the surface morphology of the coating in the hydrophobic properties, increasing the gas phase plasma polymerization, the fluorinated precursor PFH, with a flash point much lower than the one of the FLUSI (PFH: −17 ºC, FLUSI: 168 ºC), was selected. In this way, the flash point of the mixture of precursors was between 12 ºC and 68 ºC. Moreover, and not less important in a potential industrial application, the cost of PFH is substantially lower than that of FLUSI, which is about 3.5 (Synquest Laboratories Inc.) to 6 (TCI Europe) times cheaper.

3.2.1. SURFACE MORPHOLOGY

The thickness and roughness of all coated samples are illustrated in Figure 3.23. Figure 3.24 shows SEM images of the uncoated TPE and samples A_{100}, $A_{75}F_{25}$, $A_{75}P_{25}$, $A_{50}F_{50}$ and $A_{50}P_{50}$. The differences in the thickness, roughness and surface morphology of the samples seem to be determined by the APTES percentage in the precursor mixture. In fact, one can see in Figure 3.23 that the coating thickness is noticeable only on those samples that were coated by the use of APTES. As other authors have noted [5,66], NH_2 groups of APTES play an important role in the adhesion of fluorocarbons on substrates. This is probably why samples A_0F_{100} and A_0P_{100}, which were coated only with FLUSI and PFH respectively, possess the thinnest coatings. In this regard, the higher the percentage of APTES in the mixture of precursors, the greater is the thickness of the coating.

In regard to the roughness (Figure 3.23) and surface morphology of the samples (Figure 3.24), a different trend can be seen for each fluorinated precursor. It appears to be due to the different flash point of the precursor mixture. On the one hand, the flash point of APTES is 96°C and the flash point of FLUSI is 168°C, so the flash point of mixtures of theses precursors are between 96 and 168 ºC. On the other hand, the flash point of PFH is -17 ºC, so a mixture of APTES and PFH will possess a flash point between -17 and 96 ºC. This determines if a gas phase plasma polymerization predominates for lower flash points, or if there is a higher degree of plasma polymerization on the substrate surface for higher flash points [83].

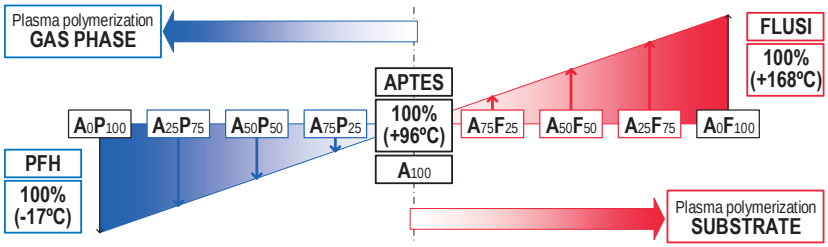

Figure 3.22. Prevailing plasma polymerization depending on the fluorinated precursor percentage.

The surface of the uncoated TPE sample (Figure 3.24 [a]) shows a rough and fibrous appearance. For sample A_{100} (Figure 3.24 [b]), coated only with APTES, the plasma polymerization in the gas phase predominates resulting in higher degree of particle formation. Such particles landed on the surface to grow a smooth layer by the van der Merwe growth mechanism [84]. In addition to this,

this sample's surface reveals typical cracks in coatings that used APTES as precursor [22,24], and they probably were caused by the difference in densities between the TPE substrate and the coating, which leads to uneven shrinkage of the TPE substrate [85].

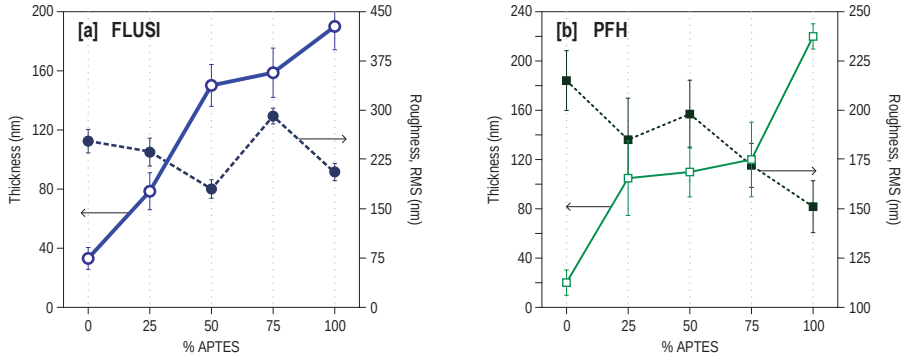

Figure 3.23. Thickness and roughness of the coated samples as a function of the APTES percentage: [a] APTES + FLUSI mixture and [b] APTES + PFH mixture [24,25].

In the case of APTES and FLUSI mixtures, Figure 3.24 [c] shows that the surface of the $A_{75}F_{25}$ sample has an appearance that is similar to the uncoated TPE surface. A high level of spherical particles of 100 nm in diameter is observed to cover practically the entire surface (white circle). These particles were formed as a result of gas phase plasma reactions [86]. Some cracks can be seen on the surface of this image (white arrow in Figure 3.24 [c]) probably caused by the creation of an emerging layer. The $A_{50}F_{50}$ sample (Figure 3.24 [e]), coated with higher FLUSI percentage, shows the smoothest surface of FLUSI-based samples. This suggests that polymerization occurs predominantly in the substrate surface. The polymer film grows by reacting with the monomer fragments that reach the surface [49]. Thus, it can be said that for the FLUSI-based coatings, a decrease in the APTES percentage resulted in an increment of the flash point of the precursor mixture and, therefore, a decrease in the gas phase plasma polymerization (an increase in the substrate plasma polymerization).

The use of mixtures of APTES and PFH leads to the formation of coatings rougher than the A_{100} sample. In this case, contrary to what happens with FLUSI-based samples, the lower the APTES percentage is, the lower is the flash point of the mixture of precursors which results in higher plasma polymerization in the gas phase, and it leads to the formation of spherical particles and agglomerates of these particles. The surface of sample $A_{75}P_{25}$ (Figure 3.24 [d]) has a homogeneous appearance that is similar to that of sample A_{100}, but with a slightly greater roughness. This was likely due to the inclusions in the coating (white circles) caused by the higher degree of plasma polymerization in the gas phase. Also, one can identify cracks that are similar to those observed in the surface of sample A_{100}. On the surface of sample $A_{50}P_{50}$ (Figure 3.24 [f]), one can see some cracks, which indicate the incipient growth of a homogeneous coating (white arrow). In addition, some particles and agglomerates of these particles (white circles) caused by the higher degree of gas plasma polymerization of sample $A_{50}P_{50}$ can be identified, which produces a greater roughness. The surface of sample $A_{25}P_{75}$ exhibits a more fibrous appearance,

with craters and some small particles. Taking into account that the degree of plasma polymerization in the gas phase of this sample is the greatest of all the analyzed samples, one would expect larger agglomerates on its surface. However, this was not the case. This was probably because the lower amine concentration of this sample had prevented some of the agglomerates from adhering to the substrate. All of this caused this sample to possess a lower roughness than that of sample $A_{50}P_{50}$. Finally, the surface of sample A_0P_{100} has a rough and fibrous appearance that is similar to that of the uncoated TPE sample. This is likely due to the extremely low coating thickness of this sample.

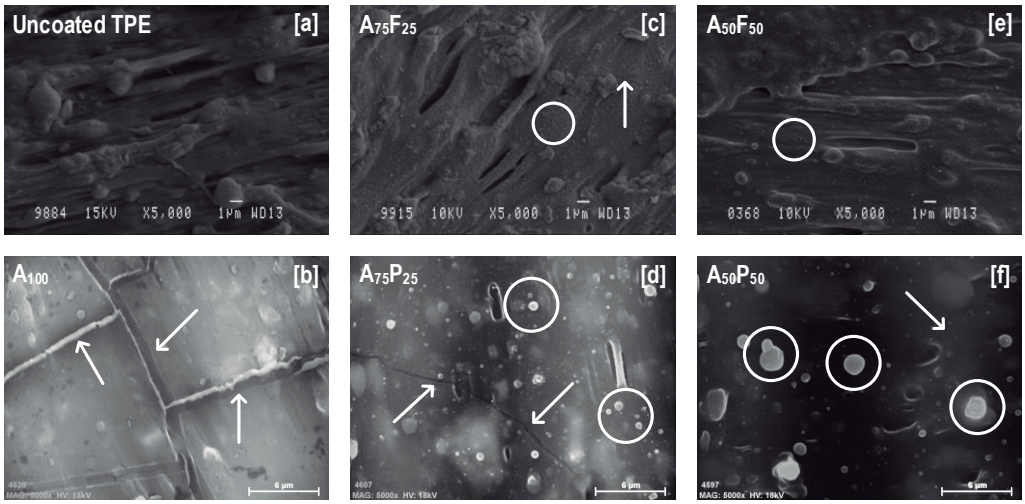

Figure 3.24. SEM images at a magnification of x5000 of samples: [a] uncoated TPE, [b] A_{100}, [c] $A_{75}F_{25}$, [d] $A_{75}P_{25}$, [e] $A_{50}F_{50}$ and [f] $A_{50}P_{50}$.

3.2.2. ATR-FTIR ANALYSIS

The ATR-FTIR spectra of the uncoated TPE and the coated samples in the 600-3800 cm^{-1} range were examined to study the chemical characterization of the coatings. The main chemical bonds of the uncoated TPE spectrum can be seen in Table 3.2. As one can observe in Figure 3.25 and Figure 3.26, some of the bands that were distinguished in the TPE spectrum were also identified in the case of the coated samples. However, a noticeable increase in the intensity of some of these bands in the three main regions can be observed (Region I: 960-1280, Region II: 1500-1800 and Region III: 3000-3800 cm^{-1}).

Table 3.3 shows the chemical bonds for A_{100} sample. The spectra of the fluorinated samples show absorption bands that are similar to the A_{100} bands. In addition, new overlapped peaks were identified in Table 3.10.

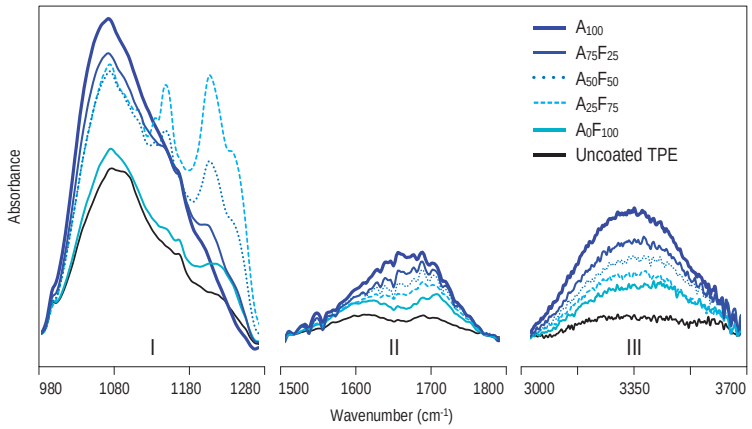

Figure 3.25. ATR-FTIR spectra of the uncoated TPE and the FLUSI-based samples. Three main regions can be identified: Region I (980-1280 cm^{-1}), Region II (1500-1800 cm^{-1}) and Region III (3000-3700 cm^{-1}).

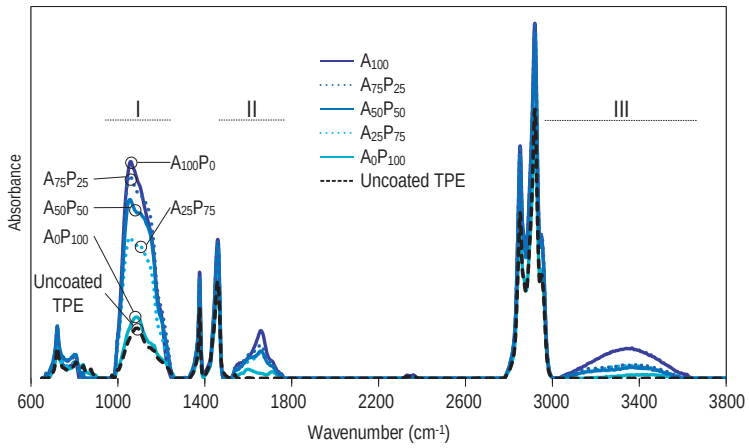

Figure 3.26. ATR-FTIR spectra of the uncoated TPE and the PFH-based samples. Three main regions can be identified: I (960-1280 cm^{-1}), II (1500-1800 cm^{-1}) and III (3000-3800 cm^{-1}).

Functional groups	Frequency/range (cm^{-1})	Reference
CF_x	~1150	[87–89]
CF_x	~1208	[85,88,90]
CF_x	~1242	[87,89,90]
$C=CF_2$	~1700	[85,90]

Table 3.10. Chemical bonds and frequencies of the peaks related to the fluorinated coatings in ATR-FTIR spectrum.

It has been noted that, for all of the coated samples, the ATR-FTIR intensity depends largely on the APTES percentage in the precursor mixture. In order to understand these relationships, a more in-depth study of the bands intensity of Region I, Region II and Region III was conducted. The spectrums of Regions I and Region II of all of the studied samples were deconvoluted into their overlapping peaks. The deconvolution of Region I of FLUSI-based samples can be seen in Figure 3.27.

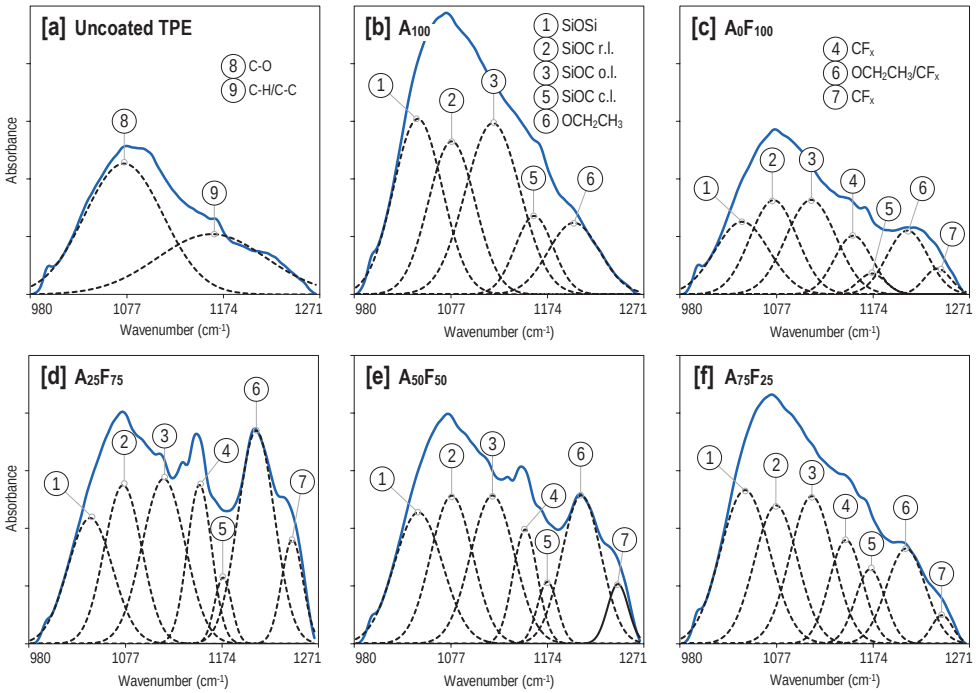

Figure 3.27. ATR-FTIR deconvoluted of Region I for FLUSI-based samples [24].

Figure 3.28 and Figure 3.29 show the absorbance area under the peaks related to SiOSi, CF_x, C=O, OH and N-groups of all of the coated samples. These peaks are associated with enhancement of tribological properties, hydrophobicity and coating adhesion.

Figure 3.28 [a] and Figure 3.29 [a] illustrate the absorbance area of the peaks of Region I with the APTES percentage. In both figures, one can observe that an increment of APTES percentage in the mixture of precursors results in an increment of absorption area under the SiOSi peak. Related to the CF_x groups, the lower the percentage of the fluorinated precursor in the mixture, the lower is the absorbance area. The absorbance area of samples coated just with a fluorinated precursor (A_0F_{100} and A_0P_{100}) is the lowest of those of the fluorinated samples. This fact may be due to the poor adhesion of fluorocarbons to TPE substrates [91,92]. In addition, for sample A_0P_{100}, a volatilization of fluorine compounds, such as CF_x, during the plasma polymerization reactions, could occur [9,93]. The used of higher percentages of PFH should provide more fluorine for the plasma polymerization process, but the lower flash point of PFH makes the material more volatile and more likely to be evacuated.

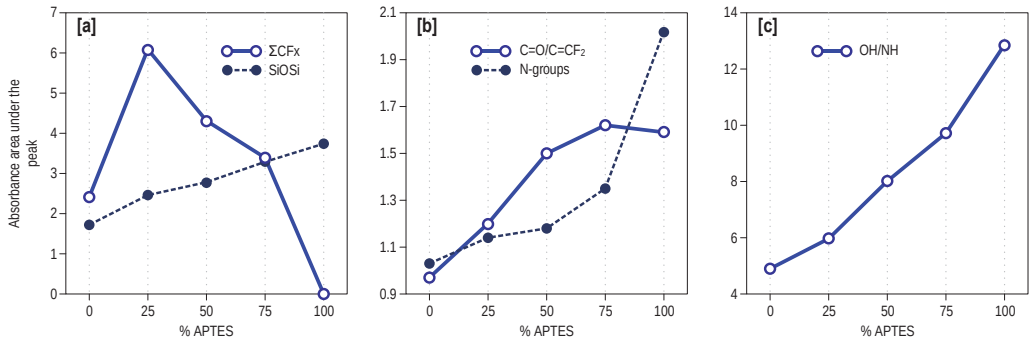

Figure 3.28. Absorption areas under the peak of: [a] SiOSi and CF_x (Region I), [b] C=O/C=CF_2 and N-groups (Region II) and [c] OH/NH (Region III) of FLUSI-based samples [24].

Figure 3.28 [b] and Figure 3.29 [b] illustrate the absorbance area of the peaks of the Region II with the APTES percentage. The higher the APTES percentage, the greater is the absorbance area of N-groups. This is related to amines and dissociation of the amines of APTES molecule [66]. Samples A_0F_{100} and A_0P_{100} contain N-groups due to the nitrogen gas used as supply and carrier gas during the activation and coating phases. Referring to absorption area of the peak related to C=CF_2 groups, for the FLUSI-based samples, this area increases with increasing the APTES percentage. However, there is no clear relationship for the PFH-based samples.

In Figure 3.28 [c] and Figure 3.29 [c], one can observe how, an increase in the APTES percentage results in an increase in the absorbance area of the NH/OH peak. It is known that the APTES molecule contains a NH_2 bond. Therefore, such an increase could be due to the increase in that group, since it is assumed that absorption of OH groups should be similar for all coated samples.

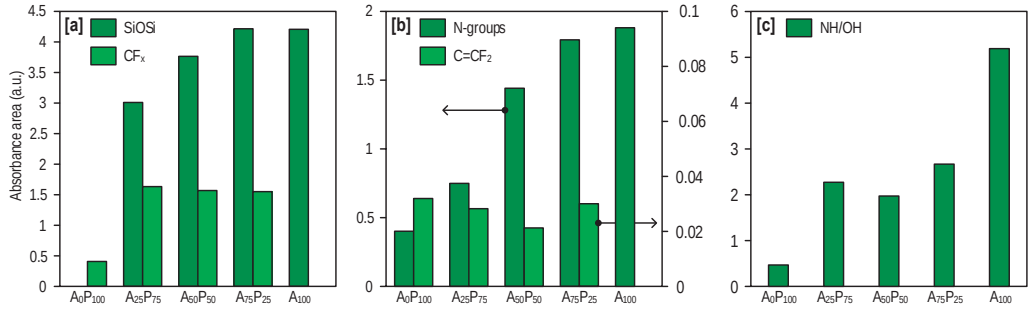

Figure 3.29. Absorption area under the peaks: [a] SiOSi and CF_x (Region I), [b] C=CF_2 and N-groups (Region II) and [c] OH/NH (Region III) of the PFH-based samples [25].

Based on the foregoing, it can be concluded that for both fluorinated precursors, the SiOSi groups (tribological properties) and N-groups (adhesion) are directly related to the APTES percentage. Related to the CF_x groups (hydrophobicity), an inverse relationship with the APTES percentage was identified for the FLUSI-based samples and no clear relationship for the PFH-based samples.

3.2.3. XPS ANALYSIS

A XPS analysis was performed to determine the chemical composition and the atomic percentages of the surface of the uncoated TPE substrate and the coated samples. Table 3.11 shows the atomic percentages of carbon (C1s), oxygen (O1s), silicon (Si2p), fluorine (F1s) and nitrogen (N1s) on the surface of the samples analyzed.

Sample	Atomic chemical composition (at. %)				
	C1s	O1s	Si2p	F1s	N1s
A_0F_{100}	46.6	23.1	14.3	15.5	0.5
$A_{25}F_{75}$	33.3	12.3	7.5	46.2	0.7
$A_{50}F_{50}$	29.8	18.7	10.0	39.8	1.7
$A_{75}F_{25}$	38.0	24.0	11.9	23.1	3.0
A_0P_{100}	82.7	10.9	0.8	4.8	0.8
$A_{25}P_{75}$	51.9	24.0	11.9	7.0	5.2
$A_{50}P_{50}$	50.9	24.9	13.0	6.1	5.1
$A_{75}P_{25}$	57.9	21.2	11.3	5.1	4.6
A_{100}	60.0	23.3	11.8	0.5	3.4
Uncoated TPE	94.3	4.5	1.2	0.0	0.0

Table 3.11. Atomic chemical composition (at. %) of all the analyzed samples.

The uncoated TPE sample contains, in addition to carbon, traces of silicon probably due to cross-contamination and oxygen from the oxidation that takes place during the transformation of the raw material.

On the one hand, for the FLUSI-based samples, atomic concentrations from survey scans of the coatings showed clear differences in the concentrations of chemical groups that were found in the coatings as a function of the APTES percentage. It can be seen that for the $A_{25}F_{75}$, $A_{50}F_{50}$ and $A_{75}F_{25}$ samples, the higher the APTES percentage is, the greater are the oxygen, silicon and nitrogen percentages and the lower is the fluorine percentage. Such variations are due to the decrease in the FLUSI percentage in the precursor mixture. The chemical composition of the A_0F_{100} sample was determined by the absence of the NH_2 groups of APTES. This absence affects mainly the non-adherence of fluorocarbons to the substrate, since SiO_x groups have inherently good adhesion [94]. Therefore, the atomic percentage of fluorine in this sample is the lowest of all FLUSI-based coatings.

On the other hand, the PFH-based samples showed a noticeable percentage of carbon. The fluorine percentage in these was fairly low in comparison with that in FLUSI-based samples, likely due to the two phenomena that were identified in the ATR-FTIR analysis.

In order to study the probable relationships between the hydrophobic character and the chemical composition of the coatings, the deconvolution of the C1s spectra of the FLUSI-based samples were undertaken. Due to the small differences in energy between some functional groups, it was

not possible to get a unique distinction of some peaks [11]. Table 3.12 shows the assigned chemical components and the peak position in the deconvoluted high resolution C1s spectra. Representative, deconvoluted C1s spectrums of FLUSI-based samples are shown in Figure 3.30.

For these samples, in Figure 3.31 [a] and Table 3.11, one can see that an increment in the APTES percentage results in a similar variation of the fluorine atomic percentage and CF_2 relative percentage. In the case of $A_{25}F_{75}$, $A_{50}F_{50}$, $A_{75}F_{25}$ and A_{100} samples, the higher the APTES percentage is, the higher the C=O/CF relative percentage is, that is due to the decomposition of APTES molecules that produce hydrophilic polar groups like C-O, C=O, C-OH, C-N and NH_2 [5,85,88], which are incorporated in the TPE surface by the plasma polymerization process.

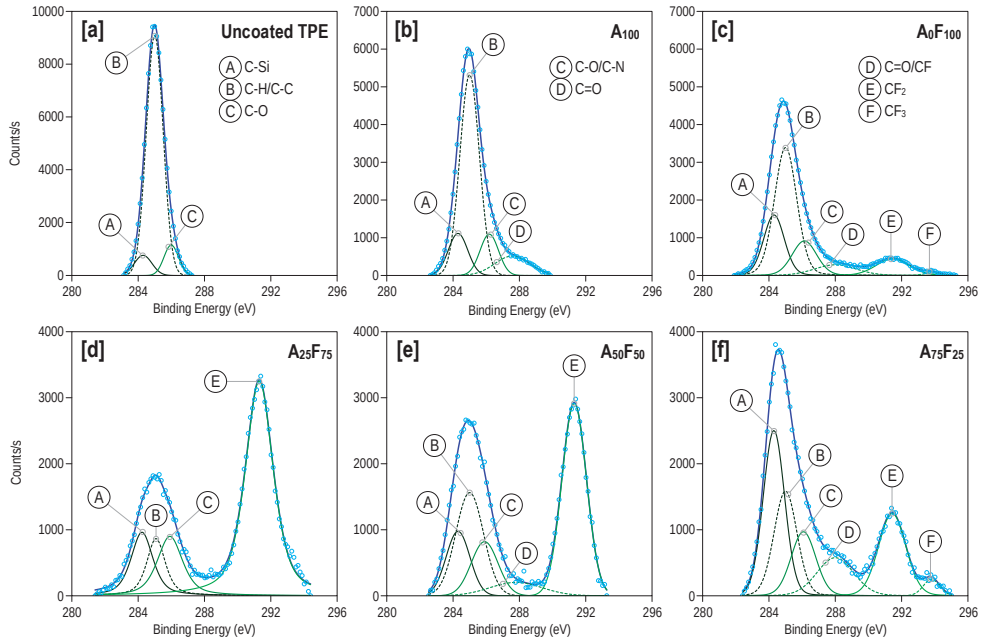

Figure 3.30. Deconvolution of high resolution C1s spectra of FLUSI-based samples [24].

For the PFH-based samples ($A_{25}P_{75}$, $A_{50}P_{50}$ and $A_{75}P_{25}$), it was no possible to identify any relationship between the atomic fluorine percentage and the C-CF/CF relative percentage in the C1s deconvolution, since C-CF groups of PFH were overlapped at ~286 eV with C-N and C-O groups, both provided by APTES, and CF groups of PFH were overlapped at ~288 eV with C=O, provided by APTES.

In order to study the relationship between the tribological properties and the chemical composition of the coatings, Si2p spectrums were deconvoluted into their most representative components that correspond to the main bonding regions. Table 3.12 shows the assigned chemical components and peak position in the deconvoluted high resolution Si2p spectrum.

For the FLUSI-based samples, Figure 3.31 [b] shows the relative percentages of the different silicon chemical bonds and their accumulated proportions of the coated samples. The chemical bonds of $(CH_3)_4Si$, $(CH_3)_3SiO$ and $(CH_3)_2SiO_2$, are referred to as the organic nature, and the

chemical bonds of CH_3SiO_3 and SiO_4 are referred to as the inorganic nature [98]. As can be seen in Figure 3.31 [b], for $A_{25}F_{75}$, $A_{50}F_{50}$, $A_{75}F_{25}$ and A_{100} samples, when the APTES percentage is increased, a high accumulated proportion of chemical bonds CH_3SiO_3 and SiO_4 is obtained. This results in a greater inorganic character and a greater surface hardness of the coatings [98].

	Chemical component	Peak position (eV)	Reference
C1s	C-Si	~284.3	[87,95]
	C-C, C-H	~285	[49,87,95,96]
	C-N, C-O, C-CF	~286	[5,87,96,97]
	C=O, CF	~288	[49,96,97]
	CF_2	~291.4	[49,87]
	CF_3	~293.8	[11,49,87,95]
Si2p	$(CH_3)_4Si$	~100.9	[98]
	$(CH_3)_3SiO$	~101.5	[98]
	$(CH_3)_2SiO_2$	~102.1	[98]
	CH_3SiO_3	~102.8	[98]
	SiO_4	~103.4	[98]

Table 3.12. Assigned chemical components and peak position in C1s and Si2p deconvolutions.

For the PFH-based samples, in Figure 3.31 [c], the higher the APTES percentage is, the greater the SiO_4 percentage is. This is referred to a higher inorganic nature and greater surface hardness [75].

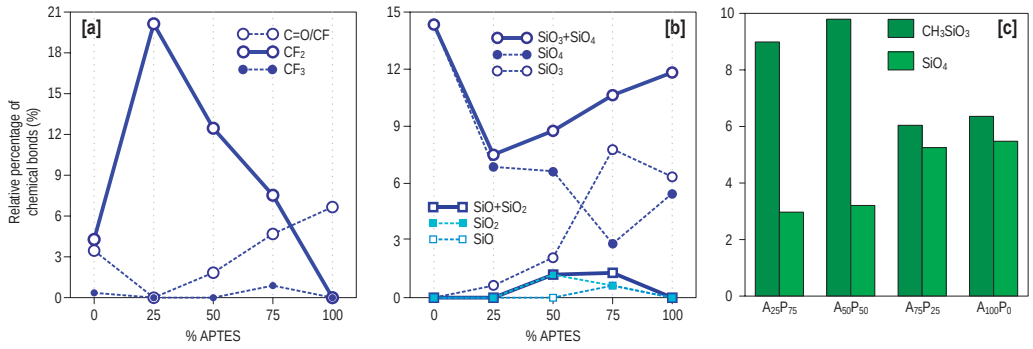

Figure 3.31. Relative percentages of chemical bonds: [a] C=O/CF, CF_2 and CF_3, [b] $(CH_3)_3SiO$, $(CH_3)_2SiO_2$, CH_3SiO_3, SiO_4 and their accumulated proportions of the coated samples of FLUSI-based samples and [c] CH_3SiO_3 and SiO_4 of PFH-based samples [24][25].

3.2.4. WETTABILITY

Since the static water contact angle cannot be determined on practical polymer surfaces due to their chemical heterogeneity and surface roughness [34,35], the hydrophobic nature of the surfaces was quantified by measuring the dynamic WCA. In this way, advancing and receding WCA were measured. It is well established that the advancing contact angle is more sensitive to the low energy components, like CF_x or CH_x, whereas the receding contact angle is more sensitive to the high energy groups, like polar groups [34,35]. In terms of topography, the advancing and

receding WCA can respond differently to increasing surface roughness. An increase in roughness means an increase of the advancing WCA and a decrease of the receding one [34].

Figure 3.32 [a] shows the advancing and receding WCA, relative percentage of the CF_2 and relative percentages of the polar groups: C-O/C-N and C=O of the FLUSI-based samples as a function of the APTES percentage. Figure 3.32 [b] shows the advancing and receding WCA and the roughness of the PFH-based samples with the APTES percentage.

The surface of the uncoated TPE had a hydrophobic character (θ_{adv}=114.9º; θ_{rec}=77.1º), probably due to the long hydrocarbon chains in the polymer backbone [87]. In addition to this, a certain hysteresis is probably a cause of the surface roughness of the substrate. The dynamic WCA for samples A_0F_{100} and A_0P_{100} coated just with FLUSI and PFH respectively, were very close to the uncoated TPE because of its low thickness caused by the lack of amino groups produced by the APTES decomposition. Sample A_{100} had the lowest dynamic WCA of the samples studied (θ_{adv}= 89.3º; θ_{rec}= 68.1º). This sample, besides having almost the lowest roughness, contains the highest absorption areas of polar groups (C=O, N-groups) in the ATR-FTIR analysis and the highest relative percentage of hydrophilic polar groups of APTES decomposition which promote a reduction of the contact angles, primarily the receding WCA [34,35].

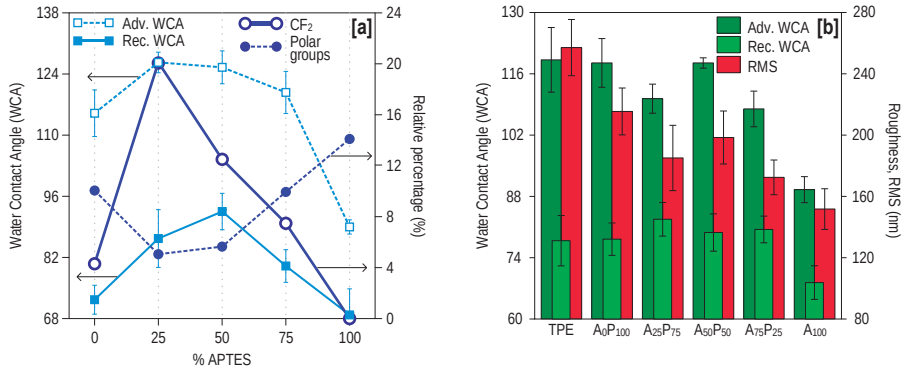

Figure 3.32. [a] Advancing and receding WCA and relative percentage of CF_2 and polar groups for FLUSI-based samples [24] and [b] advancing and receding WCA and roughness for PFH-based samples [25].

On the one hand, for samples coated with an APTES and FLUSI mixture, similar to other studies [11,87] and as Figure 3.32 [a] illustrates, the WCA values, especially the advancing WCA values, are directly correlated to the relative percentage of CF_2. The higher the CF_2, the higher is the advancing WCA. It is known that an ideal hydrophobic fluorine-containing polymer surface should have a structure that is based on CF_2 long chains like PTFE [11]. In addition to this, for $A_{25}F_{75}$, $A_{50}F_{50}$ and $A_{75}F_{25}$ samples, the higher is the APTES percentage, the higher is the relative percentage of hydrophilic polar groups (C-O/C-N and C=O) and the lower is the advancing and receding WCA [12,85,99]. However, this trend is not satisfied for sample $A_{50}F_{50}$, since this sample should have a receding WCA lower than sample $A_{25}F_{75}$. This could be justified by the low roughness of $A_{50}F_{50}$, which contribute to a higher receding WCA for such sample. For these

samples, it can be concluded that the hydrophobicity of the coated samples is directly correlated to CF_2 groups and inversely correlated to polar groups.

On the other hand, once a mixture of APTES and PFH is used, the dynamic WCA are justified solely by the surface roughness of the coatings. It is not possible to relate these results with the chemical composition of the samples, since the absorption area of CF_x is very similar for these samples and the absorption area of $C=CF_2$ groups is practically absent. In addition to this the F1s atomic percentage is very low and similar. For all this, Figure 3.32 [b] shows a direct relationship between the advancing WCA and surface roughness. In this respect, the higher the roughness is, the higher the advancing WCA is. This is attributed to Wenzel´s theory [100], which indicates that, if the surface has contact angles that are greater than 90º, an increase in surface roughness would result in an increase in the WCA. This trend is not satisfied for the receding WCA, since the higher the roughness, the lower the receding WCA. This situation was explained in Li et al. [101], in which the surface roughness of different polymer substrates was increased by sandpapers, resulting in a reduction of receding WCA. In our research, sample $A_{50}P_{50}$ showed a receding WCA lower than the samples $A_{25}P_{75}$ or $A_{75}P_{25}$ probably because its higher roughness.

3.2.5. ADHESION TEST

In order to evaluate the durability of the coatings for the PFH-based samples, the adhesion properties were evaluated by a tensile lap-shear strength test. Figure 3.33 [a] shows the average lap-shear strength (LST) in MPa that was obtained for each coated sample, the thickness as well as the sum of the absorption areas under the peaks of ATR-FTIR that contain NH_x (~1600 cm^{-1} and ~3500 cm^{-1}). The average lap-shear strength of the uncoated TPE sample was $4.1 \cdot 10^{-2}$ MPa, the lowest value.

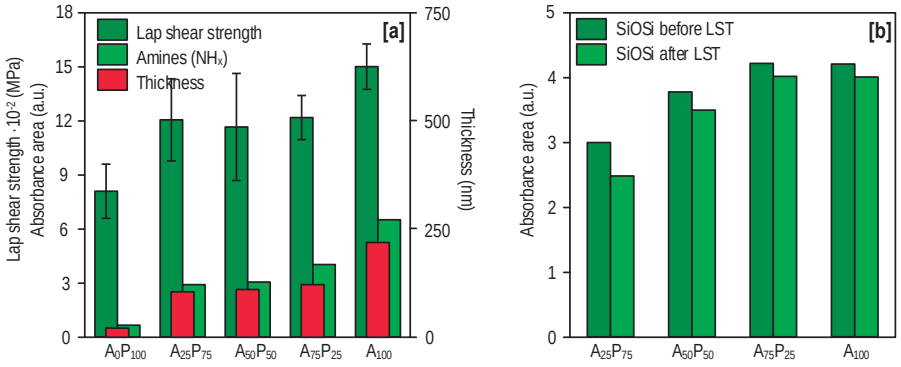

Figure 3.33. [a] Lap-shear strength (MPa), thickness (nm) and sum of the absorption areas under the peaks that contain NH_x groups as a function of the APTES percentage and [b] absorption area of the SiOSi peak before and after the LST test for PFH-based samples [25].

The lap-shear strength value of sample A_0P_{100} was the lowest of all the coated samples mainly because of the poor adhesion of this coating to the TPE substrate, its low thickness and its low content in NH_x groups. Sample A_{100} that was coated only with APTES, had the highest lap-shear strength value because of the good adhesion of silanes with amino functionalities, whose NH_2

groups play an important role in improving the adhesion of the coating to the substrates [5,66,102]. The lap-shear strength values of the remaining samples ($A_{25}P_{75}$, $A_{50}P_{50}$ and $A_{75}P_{25}$) were very similar, like their thickness, and higher than the A_0P_{100} LST value. Taking into account the foregoing, one can conclude that the contribution of NH_x groups is necessary to promote the adhesion of the coating to the TPE substrate which is in accordance with Múgica-Vidal et al. [83]. Figure 3.33 [b] shows the absorption area of the SiOSi peak before and after the test. As one can see, the absorption area after the test sample is lower than before. This means that the failure occurred because of the coating structures [88].

3.2.6. STABILITY TEST

Stability and durability are important properties in evaluating further industrial feasibility. In this regard, FLUSI-based samples were aged in air for twelve months. At the beginning and upon completion of the test, the ATR-FTIR spectrums were taken and the water contact angles were measured for all the samples.

Related to the ATR-FTIR spectrums, Figure 3.34 [a] illustrates the ATR-FTIR spectrums of Region I (980-1280 cm^{-1}) and Region II (1500-1800 cm^{-1}) for the most representative samples (uncoated TPE, $A_{25}F_{75}$ and $A_{75}F_{25}$) at the beginning and at the end of the stability test. In Region I, the decrease in the intensity of the main peak around 1070 cm^{-1} of the uncoated TPE is probably related to the loss of C-O groups for the aging process. It is possible to identify this reduction in the spectrums of $A_{25}F_{75}$ and $A_{75}F_{25}$ samples. For these samples there is no lessening of the intensity of peaks related to fluorinated compounds (~1150 and ~1240 cm^{-1}). The absorption band in Region II is practically unchanged for uncoated TPE, whereas for $A_{25}F_{75}$ and $A_{75}F_{25}$ samples one can note a decrease in the intensity of the peak related to C=O and $C=CF_2$ groups (~1700 cm^{-1}). For $A_{25}F_{75}$ sample, this decrease results in the disappearance of the peak. This reduction is likely due to the humid ambient.

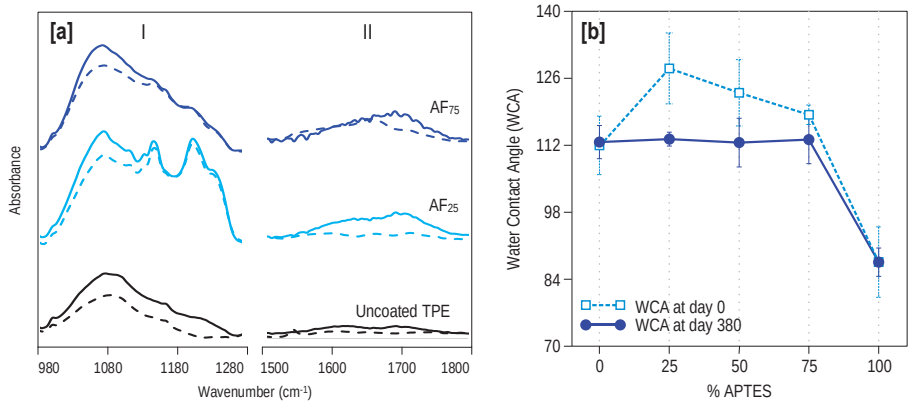

Figure 3.34. [a] ATR-FTIR spectra of Region I and II and [b] static WCA at the beginning and upon completion of the stability test for FLUSI-based samples [24].

Figure 3.34 [b] shows the static WCA obtained from the stability test performed to all the studied samples. On the one hand, the WCA of A_0F_{100} and A_{100} remained unchanged. On the other hand, a decrease in the WCA was produced for uncoated TPE, $A_{25}F_{75}$, $A_{50}F_{50}$ and $A_{75}F_{25}$ samples. This decrease is more marked for lower APTES percentages. This fact seems to be related with the decrease of the intensity of C=O/C=CF_2 peak identified in Figure 3.34 [a].

3.2.7. TRIBOLOGICAL TESTS

This section analyzes the relationship between the APTES percentage, the chemical characteristics and the friction coefficient of all the samples. Table 3.13 presents the measurements of the average friction coefficient and Figure 3.35 illustrates the variation in the friction coefficient with the sliding distance for all samples. These samples were tested by applying 1 N at 2 cm/s for a sliding distance of 1000 m with a steel ball as counterpart.

Sample	Average friction coefficient (steel ball)	Average friction coefficient (glass ball)
A_0F_{100}	1.01 ± 0.07	1.03 ± 0.02
$A_{25}F_{75}$	0.70 ± 0.06	0.97 ± 0.04
$A_{50}F_{50}$	0.80 ± 0.06	0.98 ± 0.02
$A_{75}F_{25}$	0.53 ± 0.05	0.82 ± 0.03
A_0P_{100}	0.95 ± 0.01	-
$A_{25}P_{75}$	0.60 ± 0.04	-
$A_{50}P_{50}$	0.58 ± 0.03	-
$A_{75}P_{25}$	0.54 ± 0.01	-
A_{100}	0.46 ± 0.02	0.62 ± 0.01
Uncoated TPE	1.08 ± 0.02	1.12 ± 0.03

Table 3.13. Average friction coefficient of all the samples.

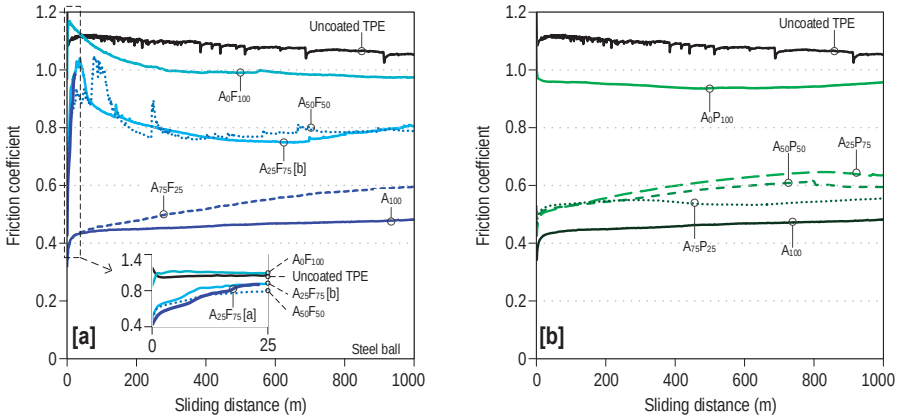

Figure 3.35. Friction coefficients of the: [a] FLUSI-based samples [24] and [b] PFH-based samples together with the uncoated TPE [25] (steel ball tests).

In regards to the $A_{25}F_{75}$ sample, two different stretches are shown, namely $A_{25}F_{75}$ [a] tested during a sliding distance of 22 m and $A_{25}F_{75}$ [b] tested during a sliding distance of 1000 m. In order to

make them easily visible, these tests are presented in a subfigure that shows the first 25 meters of the tribological tests.

SEM micrographs in Figure 3.36 show the wear tracks of the uncoated TPE, $A_{25}F_{75}$ [a], $A_{25}F_{75}$ [b] and A_{100} samples at two different magnifications (x 80 and x 600). Figure 3.36 [a], [c], [e] and [g] show the friction zone outlined by dashed lines. Figure 3.36 [b], [d] and [f] provide a detailed view that corresponds to the white box in Figure 3.36 [a], [c] and [e]. Figure 3.36 [c] – [f] shows the wear tracks of two stretches of the $A_{25}F_{75}$ sample after a sliding distance of 22 m ($A_{25}F_{75}$ [a]) and 1000 m ($A_{25}F_{75}$ [b]). In Figure 3.36 [c] and [d] one can see ridges that formed on the surface of the sample arranged perpendicular to the sliding counterpart movement. These are probably due to delamination wear of both the coating and the surface of the TPE substrate. This wear mechanism seems to be emphasized by hard debris, consisting of SiO_x, which detached from the coating at the beginning of the test. The hard debris results in an increase in the friction coefficient, reaching a maximum value during the running-period (see Figure 3.35 [a]). The friction coefficient gradually decreases while the ridges are being removing from the surface of the track that carries the hard debris. Once the ridges and hard debris disappear, a stabilization of the friction coefficient occurs during the steady-state period (see Figure 3.35 [a]). During this period the exposed surface consists of worm areas of TPE substrate, coated areas (Figure 3.36 [f]) and the soft debris of the remains of ridges (white circles in Figure 3.36 [e]). This agrees with the results obtained by others authors who used polymer substrates [103]. As a result, the surface of the $A_{25}F_{75}$ [b] sample is smoother than that of the $A_{25}F_{75}$ [a] sample. Most of the wear of the $A_{25}F_{75}$ sample takes place at the beginning of the friction test. The absence of hard debris in the wear mechanism of the uncoated TPE sample justifies the non-existence of the maximum peak in the running period of this sample's friction test (Figure 3.35). After 1000 m of sliding distance, ridges originated due to substrate delamination wear can be identified (Figure 3.36 [a] and [b]). In Figure 3.35, one can see that the wear mechanism described above for the $A_{25}F_{75}$ sample is similar to that of the A_0F_{100} and $A_{50}F_{50}$ samples. As mentioned in the XPS analysis, the inorganic character and hardness of the coatings are directly correlated to the APTES percentage. Therefore, the lower the APTES percentage is, the softer the coating is, the higher the wear is and the faster hard debris form resulting in wear delamination of the surface. This is consistent with the delayed onset of the peak of the friction coefficient tests for the A_0F_{100}, $A_{25}F_{75}$ and $A_{50}F_{50}$ samples. The higher the APTES percentage is, the greater is the delay in the growth of the peak.

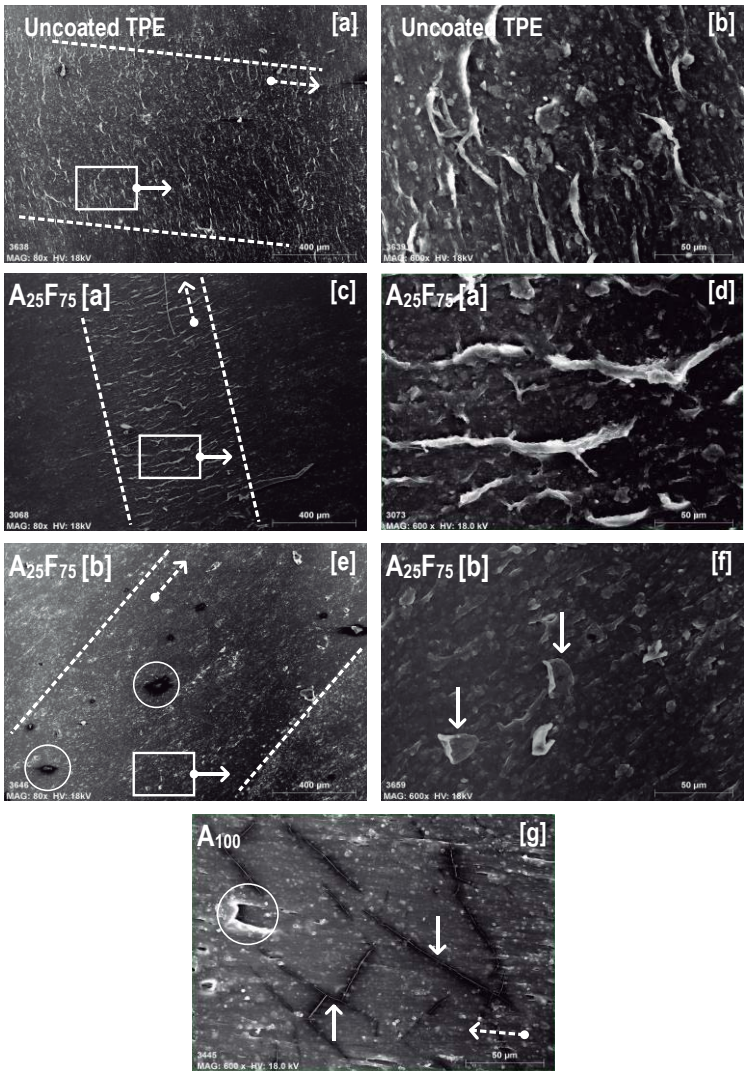

Figure 3.36. SEM images from the wear tracks at different magnification (x 80 and x 600) of samples: [a] and [b] Uncoated TPE, [c], [d], [e] and [f] $A_{25}F_{75}$ and [g] A_{100}. Images [a], [b], [e], [f] and [g] at a sliding distance of 1000 m and [c] and [d] at a sliding distance of 22 m. The tests were done with a steel ball [24].

Related to the friction coefficient tests of $A_{75}F_{25}$ and A_{100} samples (Figure 3.35), it was not possible to identify the characteristic peak of A_0F_{100}, $A_{25}F_{75}$ and $A_{50}F_{50}$ samples at the beginning of the test. The greater wear resistance of $A_{75}F_{25}$ and A_{100} samples prevents delamination wear and a consequent detachment of hard debris of the coating surface which results in noticeably lower friction coefficient than those of the remaining coated samples. Thus, the surface of the track of sample A_{100} after a sliding distance of 1000 m (Figure 3.36 [g]) evinces the typical cracks that were identified on the original coating surface (Figure 3.24 [b]). Therefore, most of the original coating has been maintained during the tribological test. For these samples, the friction coefficient increases gradually with sliding distance due to the increase in the real contact area between the steel counterpart and the surface of the coating [104]. This is also evident in Figure 3.35 [b] for

samples $A_{25}P_{75}$, $A_{50}P_{50}$, $A_{75}P_{25}$ and A_{100} whose friction coefficient are similar. However, they are increasingly lower with increasingly higher APTES percentages. The friction coefficient of sample coated only with PFH (A_0P_{100}) is similar to that of the uncoated TPE. This may be due to the low thickness of the coating, which was damaged during the first meters of the test.

Since for a specific application of such coating to window channels, the materials in contact are the window glass with the TPE sealing, the tribological behavior of all the FLUSI-based samples with a glass ball as counterpart were tested. As one can see in Figure 3.35 [a], Figure 3.37 and Table 3.13, the measurements using a glass ball as counterpart are higher than the ones obtained by using a steel ball. Furthermore, similar relationships between the measurements performed with glass and steel balls were found, that is, the more APTES percentage, the lower friction coefficient.

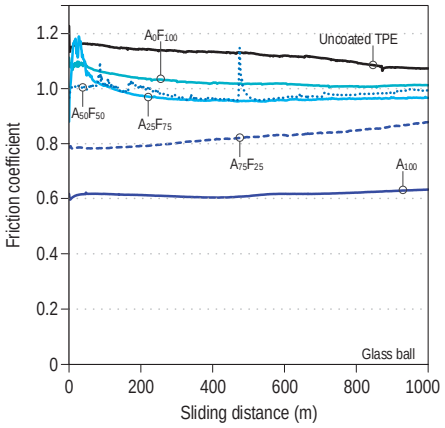

Figure 3.37. Friction coefficients of the uncoated TPE and FLUSI-based samples (glass ball tests) [24].

With the aim of related the chemical structure of the analyzed coatings with the average friction coefficient, an inverse relationship between absorbance areas under the SiOSi peak and the relative percentage of inorganic groups was identified (see Figure 3.10, Figure 3.11 and Table 3.13). It may be noted that an increment of SiOSi peak and a higher proportion of the CH_3SiO_3 and SiO_4 chemical bond are related to an improvement of both the tribological properties and wear resistance of the coating [22,72,75,98].

In regards to the studied functional properties, the results of the following samples are highlighted:

- The A_{100} sample showed the highest values of: [a] SiOSi, [b] polar groups and [c] inorganic groups besides a total absence of CF_2, which seem to justify both the lowest average friction coefficient (0.46 ± 0.02) and advancing WCA (89.0º ± 1.6). These results confirmed that sample A_{100} would perform well in applications in which antifriction is required, but poorly in water-repellency applications.
- The $A_{75}F_{25}$ sample, which was coated by a mixture of 75% APTES and 25% FLUSI, had an average friction coefficient 51.5% lower and an advancing WCA 4.4% higher than the uncoated TPE sample. This sample possessed optimal values in both friction coefficient and

hydrophobicity at the same time, although such values were not the best values of all samples that were studied. In addition, it showed a good behavior in the stability test, since its chemical nature remained unchanged, so that its WCA had just decreased in 4.4% for one year.

- Sample $A_{50}P_{50}$, which was coated by a mixture of 50% APTES and 50% PFH, combined an admissible improvement of both functional properties in comparison to the uncoated TPE substrate. This sample had an advancing WCA equal and a friction coefficient 47.1 % lower than those of the uncoated TPE substrate.

CHAPTER 4

CONCLUSIONS AND FUTURE RESEARCH

6.1. CONCLUSIONS

An Atmospheric Pressure Plasma Jet system over TPE substrates was used to deposit a coating over TPE substrates with a friction coefficient lower than the current industrial solutions (flocked seals and polyamide tape) and a hydrophobicity higher than the uncoated TPE.

Thus it can be concluded that the two proposed objectives have been successfully fulfilled. The specific conclusions to each group of scientific publications are given below.

In relation with the plasma polymerized films of APTES over TPE substrates, the key findings of this research are the following:

- The optimum degree of precursor decomposition relates a certain plasma power and a precursor flow rate.
- It was discovered that the growth mechanisms depend on the plasma power and the number of passes, as determined by the roughness measurements and SEM and AFM images.
- Two key variables that determine the friction performance of the samples are: [a] the average surface temperature of the samples during the coating process (depending on the plasma power and the number of passes) and [b] the coating thickness. If the average surface temperature exceeds a certain value, the residual thermal stress could compromise the antifriction ability. However, it is necessary that the substrate surface be covered entirely.
- Successful samples (those with a friction coefficient that is less than the current industrial solutions) were samples that were coated in 6, 12 or 18 passes and a plasma power of 350 W or coated in six passes and a plasma power of 450 W. The average surface temperature of all of these samples during the coating process did not exceed 92 ºC, and the thickness of the coatings was greater than 1000 nm.

- The wettability of the coated samples depends mainly on the roughness, as no significant chemical variations in the uppermost layer (3 nm) were identified.

Related to the plasma polymerized films of APTES and a fluorinated precursor (FLUSI or PFH) mixture, the following conclusions can be drawn:

- The precursor flash point determines the type of the main plasma polymerization (gas or substrate) that takes place. In the APTES/FLUSI mixtures, an increase in the FLUSI (flash point: 168 ºC) percentage means other increase in the degree of the substrate plasma polymerization. Otherwise, using APTES/PFH mixtures, an increase in the PFH (flash point: -17 ºC) percentage is synonym of a higher plasma polymerization in the gas phase.
- In view of the A_0F_{100} and A_0P_{100} samples characteristics (samples coated just with a fluorinated precursor) it can be stated that NH_x groups must be provided to the coatings to ensure that the fluorocarbons of the fluorinated precursor adhere to the substrate. In this research, the APTES precursor is responsible for providing the NH_x groups.
- In regards to the hydrophobicity, for FLUSI-based samples the relationship between the advancing WCA and the relative percentage of CF_2 and the relative percentage of polar groups is positive and negative respectively. However, the modification of the surface morphology for PFH-based samples justifies their advancing WCA. In this regard, the lower the roughness of these samples is, the lower the advancing WCA is. However, it is not possible to identify any relationship between the surface chemical composition and the dynamic WCAs.
- The friction coefficient of the coatings is directly related to the absorbance areas under the SiOSi peak and the relative percentage of inorganic groups (CH_3SiO_3 and SiO_4), which depends on the APTES percentage in the mixture of precursors. A higher APTES percentage results in a lower friction coefficient.
- It is worth underscoring the effectiveness of using fluorinated precursors as FLUSI or PFH to avoid a significant decrease in the WCA of the surface of samples when applying a precursor (APTES) to antifriction improvement.

6.2. FUTURE RESEARCH

Based on the succesful results achieved in this thesis, it is estimated that the knowledge generated can be applied to other areas. Specifically, it will be undertaken the following for each group of publications.

In relation with the plasma polymerized SiO_x-based functional coatings over TPE substrates:

- Establish the plasma polymerization parameters that provide antifriction properties that are similar to those of the current industrial solutions, but are less costly. The intention will be to

reduce the costs related to the plasma equipment, plasma gas consumption and other consumables in a future industrial process.

- Identified the growth mechanisms of the coatings and their relationship with the process parameters (plasma power, number of passes, precursor flow rate, etc.), the reproduction of “lotus leaf” or “month eye” effects will be studied in order to provide to the antifriction coating other functional properties like hydrophobicity and antireflection, respectively.
- Use of other precursors with antifriction ability (HMDSO, TEOS, PMDS, etc.).
- Verify the effectiveness of the coatings on other substrates like EPDM.

Related to the plasma polymerized films of the plasma polymerized films of mixtures with different proportions of antifriction and hydrophobic precursors:

- Improve the hydrophobic character, friction coefficient and durability of the coatings without worsening of other functional properties.
- Provide the coating with other functional properties: UV stability, ozone stability, etc.

BIBLIOGRAPHY

[1] V. Seitz, K. Arzt, S. Mahnel, C. Rapp, S. Schwaminger, M. Hoffstetter, E. Wintermantel, Improvement of adhesion strength of self-adhesive silicone rubber on thermoplastic substrates - Comparison of an atmospheric pressure plasma jet (APPJ) and a Pyrosil flame, Int. J. Adhes. Adhes. 66 (2016) 65–72. doi:10.1016/j.ijadhadh.2015.12.009.

[2] N. Ghali, C. Vivien, B. Mutel, A. Rives, Multilayer coating by plasma polymerization of TMDSO deposited on carbon steel: Synthesis and characterization, Surf. Coatings Technol. 259 (2014) 504–516. doi:10.1016/j.surfcoat.2014.10.037.

[3] J. Bardon, K. Apaydin, A. Laachachi, M. Jimenez, T. Fouquet, F. Hilt, S. Bourbigot, D. Ruch, Characterization of a plasma polymer coating from an organophosphorus silane deposited at atmospheric pressure for fire-retardant purposes, Prog. Org. Coatings. 88 (2015) 39–47. doi:10.1016/j.porgcoat.2015.06.005.

[4] M. Bashir, J.M. Rees, W.B. Zimmerman, Plasma polymerization in a microcapillary using an atmospheric pressure dielectric barrier discharge, Surf. Coatings Technol. 234 (2013) 82–91. doi:10.1016/j.surfcoat.2013.01.041.

[5] M.F.S. Dubreuil, E.M. Bongaers, P.F.A. Lens, Incorporation of amino moieties through atmospheric pressure plasma: Relationship between precursor structure and coating properties, Surf. Coatings Technol. 206 (2011) 1439–1448. doi:10.1016/j.surfcoat.2011.09.015.

[6] Y. Sawada, S. Ogawa, M. Kogoma, Synthesis of plasma-polymerized tetraethoxysilane and hexamethyldisiloxane films prepared by atmospheric pressure glow discharge, J. Appl. Phys. 28 (1995) 1661–1669. http://stacks.iop.org/0022-3727/28/i=8/a=015?key=crossref.28909a8e171de89fc6a0e574b2567cf2 (accessed January 13, 2017).

[7] C. Huang, C.-H. Liu, C.-H. Su, W.-T. Hsu, S.-Y. Wu, Investigation of atmospheric-pressure plasma deposited SiOx films on polymeric substrates, Thin Solid Films. 517 (2009) 5141–5145. doi:10.1016/j.tsf.2009.03.054.

[8] S.E. Babayan, J.Y. Jeong, V.J. Tu, J. Park, G.S. Selwyn, R.F. Hicks, Deposition of silicon dioxide films with an atmospheric-pressure plasma jet, Plasma Sources Sci. Technol. 7 (1998) 286–288.

[9] H. Biederman, O. Kylian, M. Drabik, A. Choukourov, O. Polonskyi, P. Solar, Nanocomposite and nanostructured films with plasma polymer matrix, Surf. Coatings Technol. 211 (2012) 127–137. doi:10.1016/j.surfcoat.2011.09.011.

[10] N.D. Tran, N.K. Dutta, N.R. Choudhury, Weatherability and wear resistance characteristics of plasma fluoropolymer coatings deposited on an elastomer substrate, Polym. Degrad. Stab. 91 (2006) 1052–1063. doi:10.1016/j.polymdegradstab.2005.07.008.

[11] G. Borcia, N.M.D. Brown, Hydrophobic coatings on selected polymers in an atmospheric pressure dielectric barrier discharge, J. Phys. D. Appl. Phys. 40 (2007) 1927.

doi:10.1088/0022-3727/40/7/015.

[12] A. Bismarck, W. Brostow, R. Chiu, H.E.H. Lobland, K.K.C. Ho, Effects of surface plasma treatment on tribology of thermoplastic polymers, Polym. Eng. Sci. 48 (2008) 1971–1976. doi:10.1002/pen.

[13] D. Merche, N. Vandencasteele, F. Reniers, Atmospheric plasmas for thin film deposition: A critical review, Thin Solid Films. 520 (2012) 4219–4236. doi:10.1016/j.tsf.2012.01.026.

[14] R. Elleuch, K. Elleuch, B. Salah, H. Zahouani, Tribological behavior of thermoplastic polyurethane elastomers, Mater. Des. 28 (2007) 824–830. doi:10.1016/j.matdes.2005.11.004.

[15] I. Luzinov, D. Julthongpiput, V. V. Tsukruk, Thermoplastic elastomer monolayers grafted to a functionalized silicon surface, Macromolecules. 33 (2000) 7629–7638. doi:10.1021/ma000523r.

[16] R.J. Spontak, N.P. Patel, Thermoplastic elastomers: fundamentals and applications, Curr. Opin. Colloid Interface Sci. 5 (2000) 333–340. doi:10.1016/S1359-0294(00)00070-4.

[17] G. Holden, Thermoplastic Elastomers, Elsevier, 1996. doi:10.5772/2038.

[18] S.S. Banerjee, A.K. Bhowmick, Novel nanostructured polyamide 6/fluoroelastomer thermoplastic elastomeric blends: Influence of interaction and morphology on physical properties, Polymer (Guildf). 54 (2013) 6561–6571. doi:10.1016/j.polymer.2013.10.001.

[19] T. Parenteau, E. Bertevas, G. Ausias, R. Stocek, Y. Grohens, P. Pilvin, Characterisation and micromechanical modelling of the elasto-viscoplastic behavior of thermoplastic elastomers, Mech. Mater. 71 (2014) 114–125. doi:10.1016/j.mechmat.2013.06.010.

[20] S. Rapra, TPEs market set to reach 5.1 million tonnes by 2018, Seal. Technol. (2013) 8. doi:10.1016/S1350-4789(13)70363-5.

[21] S. Rapra, TPE 2012 focuses on end-use applications, Seal. Technol. (2012) 6. doi:10.1016/S1350-4789(12)70187-3.

[22] F. Alba-Elías, E. Sainz-García, A. González-Marcos, J. Ordieres-Meré, Tribological behavior of plasma-polymerized aminopropyltriethoxysilane films deposited on thermoplastic elastomers substrates, Thin Solid Films. 540 (2013) 125–134. doi:10.1016/j.tsf.2013.06.028.

[23] E. Sainz-García, F. Alba-Elías, R. Múgica-Vidal, A. González-Marcos, Antifriction aminopropyltriethoxysilane films on thermoplastic elastomer substrates using an APPJ system, Surf. Coatings Technol. 310 (2017) 239–250. doi:10.1016/j.surfcoat.2016.12.079.

[24] E. Sainz-García, F. Alba-Elías, R. Múgica-Vidal, A. González-Marcos, Enhanced surface friction coefficient and hydrophobicity of TPE substrates using an APPJ system, Appl. Surf. Sci. 328 (2015) 554–567. doi:10.1016/j.apsusc.2014.12.084.

[25] E. Sainz-García, F. Alba-Elías, R. Múgica-Vidal, M. Pantoja-Ruiz, Promotion of tribological and hydrophobic properties of a coating on TPE substrates by atmospheric plasma-polymerization, Appl. Surf. Sci. 371 (2016) 50–60. doi:10.1016/j.apsusc.2016.02.186.

[26] A.R. Yadav, R. Sriram, J.A. Carter, B.L. Miller, Comparative study of solution-phase and vapor-phase deposition of aminosilanes on silicon dioxide surfaces, Mater. Sci. Eng. C. 35 (2014) 283–290. doi:10.1016/j.msec.2013.11.017.

[27] M. Masuko, H. Miyamoto, A. Suzuki, Tribological characteristics of self-assembled monolayer with siloxane bonding to Si surface, Tribol. Int. 40 (2007) 1587–1596. doi:10.1016/j.triboint.2007.02.017.

[28] F. Alba-Elías, J. Ordieres-Meré, A. González-Marcos, Deposition of thin-films on EPDM substrate with a plasma-polymerized coating, Surf. Coatings Technol. 206 (2011) 234–242. doi:10.1016/j.surfcoat.2011.06.054.

[29] J. Ihde, R. Wilden, J. Degenhardt, A. Knospe, C. Buske, Atmospheric Pressure Plasma Method for profucing surface-modified particles and coatings, WO 2011/042459 A1, 2011.

[30] T. Young, An Essay on the Cohesion of Fluids, Philos. Trans. R. Soc. London. 95 (1805) 65–87. doi:10.1098/rstl.1805.0005.

[31] A. Marmur, Thermodynamic aspects of contact angle hysteresis, Adv. Colloid Interface Sci. 50 (1994) 121–141. doi:10.1016/0001-8686(94)80028-6.

[32] L. Gao, T.J. McCarthy, Contact angle hysteresis explained, Langmuir. 22 (2006) 6234–6237. doi:10.1021/la060254j.

[33] L. Feng, S. Li, Y. Li, H. Li, L. Zhang, J. Zhai, Y. Song, B. Liu, L. Jiang, D. Zhu, Super-hydrophobic surfaces: From natural to artificial, Adv. Mater. 14 (2002) 1857–1860. doi:DOI 10.1002/adma.200290020.

[34] S. Kirk, M. Strobel, C.-Y. Lee, S.J. Pachuta, M. Prokosch, H. Lechuga, M.E. Jones, C.S. Lyons, S. Degner, Y. Yang, M.J. Kushner, Fluorine plasma treatments of polypropylene films, 1-Surface characterization, Plasma Process. Polym. 7 (2010) 107–122. doi:10.1002/ppap.200900111107.

[35] M. Strobel, C.S. Lyons, An essay on contact angle measurements, Plasma Process. Polym. 8 (2011) 8–13. doi:10.1002/ppap.201000041.

[36] www.firsttenangstroms.com, Tilting Plate Example, First Ten Angstroms. (2004) 1–4.

[37] X. Landreau, C. Dublanche-Tixier, C. Jaoul, C. Le Niniven, N. Lory, P. Tristant, Effects of the substrate temperature on the deposition of thin SiOx films by atmospheric pressure microwave plasma torch (TIA), Surf. Coatings Technol. 205 (2011) S335–S341. doi:10.1016/j.surfcoat.2011.03.123.

[38] L. Körner, A. Sonnenfeld, P.R. Von Rohr, Silicon oxide diffusion barrier coatings on polypropylene, Thin Solid Films. 518 (2010) 4840–4846. doi:10.1016/j.tsf.2010.02.006.

[39] E. Kedronova, L. Zajjickova, D. Hegemann, M. Kllima, M. Michlicek, A. Manakhov, Plasma Enhanced CVD of Organosilicon Thin Films on Electrospun Polymer Nanofibers, Plasma Process. Polym. 12 (2015) 1231–1243. doi:10.1002/ppap.201400235.

[40] M.R. Amirzada, A. Tatzel, V. Viereck, H. Hillmer, Surface roughness analysis of SiO2 for PECVD, PVD and IBD on different substrates, Appl. Nanosci. 6 (2015) 215–222. doi:10.1007/s13204-015-0432-8.

[41] D.S. Wuu, W.C. Lo, C.C. Chiang, H.B. Lin, L.S. Chang, R.H. Horng, C.L. Huang, Y.J. Gao, Plasma-deposited silicon oxide barrier films on polyethersulfone substrates: Temperature and thickness effects, Surf. Coatings Technol. 197 (2005) 253–259. doi:10.1016/j.surfcoat.2004.09.033.

[42] L. Zhou, G.-H. Lv, H. Pang, G.-P. Zhang, S.-Z. Yang, Comparing deposition of organic and inorganic siloxane films by the atmospheric pressure glow discharge, Surf. Coatings Technol. 206 (2012) 2552–2557. doi:10.1016/j.surfcoat.2011.11.011.

[43] B. Verheyde, D. Havermans, A. Vanhulsel, Characterization and tribological behaviour of siloxane-based plasma coatings on HNBR rubber, Plasma Process. Polym. 8 (2011) 755–762. doi:10.1002/ppap.201000136.

[44] L. Marcinauskas, M. Silinskas, A. Grigonis, Influence of standoff distance on the structure and properties of carbon coatings deposited by atmospheric plasma jet, Appl. Surf. Sci. 257 (2011) 2694–2699. doi:10.1016/j.apsusc.2010.10.047.

[45] M. Bedjaoui, B. Despax, Physicochemical and structural properties of ultra thin films with embedded silicon particles, Surf. Coatings Technol. 201 (2007) 9179–9183. doi:10.1016/j.surfcoat.2007.04.006.

[46] L. Korner, Diffusion Barrier Coatings for Polymer Containers processed by Plasma Enhanced Chemical Vapor Deposition, 2010. http://e-collection.library.ethz.ch/eserv/eth:1657/eth-1657-02.pdf.

[47] B.U. Borer, SiOx in a Thin Film Deposition on Particles by Plasma Enhanced Chemical Vapor Deposition Circulating Fluidized Bed Reactor, 2005. http://e-collection.library.ethz.ch/eserv/eth:28482/eth-28482-02.pdf.

[48] A. Manakhov, M. Moreno-Couranjou, N.D. Boscher, V. Rogé, P. Choquet, J.-J. Pireaux, Atmospheric pressure pulsed plasma copolymerisation of maleic anhydride and vinyltrimethoxysilane: Influence of electrical parameters on chemistry, morphology and deposition rate of the coatings, Plasma Process. Polym. 9 (2012) 435–445. doi:10.1002/ppap.201100184.

[49] L. Sandrin, M.S. Silverstein, E. Sacher, Fluorine incorporation in plasma-polymerized octo fluuorocyclobutane , hexafluoropropylene and trifluoroethylene, Polymer (Guildf). 42 (2001) 3761–3769.

[50] C.-H. Lo, W.-S. Hung, S.-H. Huang, M. De Guzman, V. Rouessac, K.-R. Lee, J.-Y. Lai, Plasma deposition of tetraethoxysilane on polycarbonate membrane for pervaporation of tetrafluoropropanol aqueous solution, J. Memb. Sci. 329 (2009) 138–145. doi:10.1016/j.memsci.2008.12.029.

[51] K. Sever, Y. Seki, H.A. Güleç, M. Sarikanat, M. Mutlu, I. Tavman, Preparation and characterization of thin films by plasma polymerization of glycidoxypropyltrimethoxysilane at different plasma powers and exposure times, Appl. Surf. Sci. 255 (2009) 8450–8457. doi:10.1016/j.apsusc.2009.05.153.

[52] B. Borer, A. Sonnenfeld, P. Rudolf von Rohr, Influence of substrate temperature on morphology of SiOx films deposited on particles by PECVD, Surf. Coatings Technol. 201 (2006) 1757–1762. doi:10.1016/j.surfcoat.2006.03.001.

[53] A. Soum-Glaude, L. Thomas, E. Tomasella, Amorphous silicon carbide coatings grown by low frequency PACVD: Structural and mechanical description, Surf. Coatings Technol. 200 (2006) 6425–6429. doi:10.1016/j.surfcoat.2005.11.066.

[54] B. Verheyde, M. Rombouts, A. Vanhulsel, D. Havermans, J. Meneve, M. Wangenheim, Influence of surface treatment of elastomers on their frictional behaviour in sliding contact, Wear. 266 (2009) 468–475. doi:10.1016/j.wear.2008.04.040.

[55] C. Sarra-bournet, Fonctionnalisation de surface de polymères par plasma à la pression atmosphérique. Amination de surface et dépôt de couches minces par un procédé de décharge par barrière diélectrique, Université Laval, 2009.

[56] S. Bhattacharya, A. Datta, J.M. Berg, S. Gangopadhyay, Studies on Surface Wettability of Poly (Dimethyl) Siloxane (PDMS) and Glass Under Oxygen-Plasma. Treatment and Correlation with Bond Strength, J. Microelectromechanical Syst. 14 (2005) 590–597. doi:10.1109/JMEMS.2005.844746.

[57] J. Petersen, J. Bardon, A. Dinia, D. Ruch, N. Gherardi, Organosilicon coatings deposited in atmospheric pressure townsend discharge for gas barrier purpose: Effect of substrate temperature on structure and properties, ACS Appl. Mater. Interfaces. 4 (2012) 5872–5882. doi:10.1021/am3015229.

[58] S.-G. Hong, C.-M. Liao, The surface oxidation of a thermoplastic olefin elastomer under ozone exposure: ATR analysis, Polym. Degrad. Stab. 49 (1995) 437–447. doi:10.1016/0141-3910(95)00127-8.

[59] J.H. Ku, I.H. Jung, K.Y. Rhee, S.J. Park, Atmospheric pressure plasma treatment of polypropylene to improve the bonding strength of polypropylene/aluminum composites, Compos. Part B Eng. 45 (2013) 1282–1287. doi:10.1016/j.compositesb.2012.06.016.

[60] J. Kim, P. Seidler, L.S. Wan, C. Fill, Formation, structure, and reactivity of amino-terminated organic films on silicon substrates, J. Colloid Interface Sci. 329 (2009) 114–119. doi:10.1016/j.jcis.2008.09.031.

[61] S. Bulou, L. Le Brizoual, P. Miska, L. de Poucques, R. Hugon, M. Belmahi, J. Bougdira, The influence of CH4 addition on composition, structure and optical characteristics of SiCN thin films deposited in a CH4/N2/Ar/hexamethyldisilazane microwave plasma, Thin Solid Films. 520 (2011) 245–250. doi:10.1016/j.tsf.2011.07.054.

[62] C.S. Yang, Y.H. Yu, K.-M. Lee, H.-J. Lee, C.K. Choi, Investigation of low dielectric carbon-doped silicon oxide films prepared by PECVD using methyltrimethoxysilane precursor, Thin Solid Films. 506–507 (2006) 50–54. doi:10.1016/j.tsf.2005.08.032.

[63] N.S.K. Gunda, M. Singh, L. Norman, K. Kaur, S.K. Mitra, Optimization and characterization of biomolecule immobilization on silicon substrates using (3-aminopropyl)triethoxysilane (APTES) and glutaraldehyde linker, Appl. Surf. Sci. 305 (2014) 522–530. doi:10.1016/j.apsusc.2014.03.130.

[64] M. Touzin, P. Chevallier, F. Lewis, S. Turgeon, S. Holvoet, G. Laroche, D. Mantovani, Study on the stability of plasma-polymerized fluorocarbon ultra-thin coatings on stainless steel in water, Surf. Coatings Technol. 202 (2008) 4884–4891. doi:10.1016/j.surfcoat.2008.04.088.

[65] R. Navamathavan, R. Nirmala, C.Y. Kim, C.-R. Lee, C.K. Choi, A study on structural and electrical properties of low dielectric constant SiOC(–H) thin films deposited via PECVD, J. Phys. Chem. Solids. 73 (2012) 641–645. doi:10.1016/j.jpcs.2012.01.002.

[66] C. Volcke, R.P. Gandhiraman, V. Gubala, J. Raj, T. Cummins, G. Fonder, R.I. Nooney, Z. Mekhalif, G. Herzog, S. Daniels, D.W.M. Arrigan, A.A. Cafolla, D.E. Williams, Reactive amine surfaces for biosensor applications, prepared by plasma-enhanced chemical vapour modification of polyolefin materials, Biosens. Bioelectron. 25 (2010) 1875–1880. doi:10.1016/j.bios.2009.12.034.

[67] E. Gallino, S. Massey, M. Tatoulian, D. Mantovani, Plasma polymerized allylamine films deposited on 316L stainless steel for cardiovascular stent coatings, Surf. Coatings Technol. 205 (2010) 2461–2468. doi:10.1016/j.surfcoat.2010.09.047.

[68] A. Ramamoorthy, M. Rahman, D.A. Mooney, J.M. Don MacElroy, D.P. Dowling, The influence of process parameters on chemistry, roughness and morphology of siloxane films deposited by an atmospheric plasma jet system, Plasma Process. Polym. 6 (2009) S530–S536. doi:10.1002/ppap.200931109.

[69] E.V. Kober, A.E. Chmel, Recording of IR Spectra of polymer specimen surfaces with a rough relief using thermoplastic ATR elements, 64 (1997) 140–145.

[70] R.O. Carter III, M.C. Paputa Peck, D.R. Bauer, The Characterization of Polymer Surfaces by Photoacoustic Fourier Transform Infrared Spectroscopy, Polym. Degrad. Stab. 23 (1989) 121–134.

[71] A.A. Kondyurin, M. Bilek, Ion Beam treatment of polymers, Second edi, Elsevier Ltd, University of Sydney, Australia, 2008. doi:http://dx.doi.org/10.1016/B978-0-08-099445-1.00015-8.

[72] A.J. Choudhury, S.A. Barve, J. Chutia, A.R. Pal, R. Kishore, Jagannath, M. Pande, D.S. Patil, RF-PACVD of water repellent and protective HMDSO coatings on bell metal surfaces: Correlation between discharge parameters and film properties, Appl. Surf. Sci. 257 (2011) 8469–8477. doi:10.1016/j.apsusc.2011.04.134.

[73] F. Fanelli, A.M. Mastrangelo, F. Fracassi, Aerosol-Assisted Atmospheric Cold Plasma Deposition and Characterization of Superhydrophobic Organic−Inorganic Nanocomposite Thin Films, Langmuir. 30 (2014) 857–865.

[74] H. Hamze, M. Jimenez, D. Deresmes, A. Beaurain, N. Nuns, M. Traisnel, Influence of processing gases on the properties of cold atmospheric plasma SiOxCy coatings, Appl. Surf. Sci. 315 (2014) 531–537. doi:10.1016/j.apsusc.2013.12.108.

[75] L. Yung-Sen, C. Ching-Lun, Wear Resistance of Low-Temperature Plasma-Polymerized Organosilica Deposited on Poly(ethylene terephthalate): The Effect of Discharge Powers, J. Appl. Polym. Sci. 110 (2008) 2704–2710. doi:10.1002/app.

[76] D.J. Marchand, Z.R. Dilworth, R.J. Stauffer, E. Hsiao, J.-H. Kim, J.-G. Kang, S.H. Kim, Atmospheric rf plasma deposition of superhydrophobic coatings using tetramethylsilane precursor, Surf. Coatings Technol. 234 (2013) 14–20. doi:10.1016/j.surfcoat.2013.03.029.

[77] S.J. Cho, I.S. Bae, Y.S. Park, B. Hong, W. Park, S.C. Park, J.H. Boo, The characteristics of organic-inorganic hybrid low-k thin films by PECVD, Surf. Coatings Technol. 202 (2008)

5654–5658. doi:10.1016/j.surfcoat.2008.06.105.

[78] H.J. Lee, K.S. Oh, C.K. Choi, The mechanical properties of the SiOC(-H) composite thin films with a low dielectric constant, Surf. Coatings Technol. 171 (2003) 296–301. doi:10.1016/S0257-8972(03)00289-5.

[79] S. Podgoric, B.J. Jones, R. Bulpett, G. Troisi, J. Franks, Diamond-like carbon/epoxy low-friction coatings to replace electroplated chromium, Wear. 267 (2009) 996–1001. doi:10.1016/j.wear.2009.01.014.

[80] G. Montay, A. Cherounat, A. Nussair, J. Lu, Residual Stresses in Coating Technology, J. Mater. Sci. Tecnol. 20 (2004) 81–84.

[81] A. Kariminejad, E. Taheri-Nassaj, M. Ghanbarian, S.A. Hassanzadeh-Tabrizi, Effects of PACVD parameters including pulsed direct current and deposition time on nanostructured carbon coating deposited on carbon fiber fabrics, Mater. Des. 106 (2016) 184–194. doi:10.1016/j.matdes.2016.05.072.

[82] A.E.A. Zeghni, The effect of thin film coatings and nitriding on the mechanical properties and wear resistance of tool steel, Dublin City University, 2003.

[83] R. Múgica-Vidal, F. Alba-Elías, E. Sainz-García, J. Ordieres-Meré, Atmospheric plasma-polymerization of hydrophobic and wear-resistant coatings on glass substrates, Surf. Coatings Technol. 259 (2014) 374–385. doi:10.1016/j.surfcoat.2014.10.067.

[84] A. Michelmore, P. Martinek, V. Sah, R.D. Short, K. Vasilev, Surface morphology in the early stages of plasma polymer film growth from amine-containing monomers, Plasma Process. Polym. 8 (2011) 367–372. doi:10.1002/ppap.201000140.

[85] S. Schlögl, R. Kramer, D. Lenko, H. Schröttner, R. Schaller, A. Holzner, W. Kern, Fluorination of elastomer materials, Eur. Polym. J. 47 (2011) 2321–2330. doi:10.1016/j.eurpolymj.2011.09.010.

[86] C.E. Nwankire, G. Favaro, Q.H. Duong, D.P. Dowling, Enhancing the mechanical properties of superhydrophobic atmospheric pressure plasma deposited siloxane coatings, Plasma Process. Polym. 8 (2011) 305–315. doi:10.1002/ppap.201000069.

[87] J.H. Yim, V. Rodriguez-Santiago, A.A. Williams, T. Gougousi, D.D. Pappas, J.K. Hirvonen, Atmospheric pressure plasma enhanced chemical vapor deposition of hydrophobic coatings using fluorine-based liquid precursors, Surf. Coatings Technol. 234 (2013) 21–32. doi:10.1016/j.surfcoat.2013.03.028.

[88] C.-L. Li, C.-Y. Tu, J.-S. Huang, Y.-L. Liu, K.R. Lee, J.-Y. Lai, Surface modification and adhesion improvement of expanded poly(tetrafluoroethylene) films by plasma graft polymerization, Surf. Coatings Technol. 201 (2006) 63–72. doi:10.1016/j.surfcoat.2005.10.041.

[89] Y. Chen, H. Kim, Preparation of superhydrophobic membranes by electrospinning of fluorinated silane functionalized poly(vinylidene fluoride), Appl. Surf. Sci. 255 (2009) 7073–7077. doi:10.1016/j.colsurfa.2010.04.004.

[90] L. Li, F.T. Zi, Y.F. Zheng, The characterization of fluorocarbon films on NiTi alloy by magnetron sputtering, Appl. Surf. Sci. 255 (2008) 432–434.

doi:10.1016/j.apsusc.2008.06.174.

[91] X. Jiang, J. Wang, J. Shen, R. Li, G. Yang, H. Huang, Improvement of adhesion strength and scratch resistance of fluorocarbon thin films by cryogenic treatment, Appl. Surf. Sci. 288 (2014) 44–50. doi:10.1016/j.apsusc.2013.09.103.

[92] R.G. Wankhede, S. Morey, A.S. Khanna, N. Birbilis, Development of water-repellent organic–inorganic hybrid sol–gel coatings on aluminum using short chain perfluoro polymer emulsion, Appl. Surf. Sci. 283 (2013) 1051–1059. doi:10.1016/j.apsusc.2013.07.066.

[93] T.-C. Wei, C.-H. Liu, Evaluation of plasma deposited fluorocarbon films using experimental design methodology, Surf. Coatings Technol. 200 (2005) 2214–2222. doi:10.1016/j.surfcoat.2005.04.028.

[94] R. Prikryl, V. Cech, R. Balkova, J. Vanek, Functional interlayers in multiphase materials, Surf. Coatings Technol. 174–175 (2003) 858–862. doi:10.1016/S0257-8972.

[95] C. Kang, H. Lu, S. Yuan, D. Hong, K. Yan, B. Liang, Superhydrophilicity/superhydrophobicity of nickel micro-arrays fabricated by electroless deposition on an etched porous aluminum template, Chem. Eng. J. 203 (2012) 1–8. doi:10.1016/j.cej.2012.06.128.

[96] D. Duday, C. Vreuls, M. Moreno, G. Frache, N.D. Boscher, G. Zocchi, C. Archambeau, C. Van De Weerdt, J. Martial, P. Choquet, Atmospheric pressure plasma modified surfaces for immobilization of antimicrobial nisin peptides, Surf. Coatings Technol. 218 (2013) 152–161. doi:10.1016/j.surfcoat.2012.12.045.

[97] M. Pantoja, N. Encinas, J. Abenojar, M.A. Martínez, Effect of tetraethoxysilane coating on the improvement of plasma treated polypropylene adhesion, Appl. Surf. Sci. 280 (2013) 850–857. doi:10.1016/j.apsusc.2013.05.074.

[98] Y.-S. Lin, M.-S. Weng, T.-W. Chung, C. Huang, Enhanced surface hardness of flexible polycarbonate substrates using plasma-polymerized organosilicon oxynitride films by air plasma jet under atmospheric pressure, Surf. Coatings Technol. 205 (2011) 3856–3864. doi:10.1016/j.surfcoat.2011.01.060.

[99] N. Encinas, J. Abenojar, M.A. Martínez, Development of improved polypropylene adhesive bonding by abrasion and atmospheric plasma surface modifications, Int. J. Adhes. Adhes. 33 (2012) 1–6. doi:10.1016/j.ijadhadh.2011.10.002.

[100] C. Wang, X. He, Preparation of hydrophobic coating on glass surface by dielectric barrier discharge using a 16 kHz power supply, Appl. Surf. Sci. 252 (2006) 8348–8351. doi:10.1016/j.apsusc.2005.11.042.

[101] Y.-F. Li, C.-J. Wu, Y.-J. Sheng, H.-K. Tsao, Facile manipulation of receding contact angles of a substrate by roughening and fluorination, Appl. Surf. Sci. 355 (2015) 127–132. doi:10.1016/j.apsusc.2015.07.078.

[102] L. Nobili, A. Guglielmini, Thermal stability and mechanical properties of fluorinated diamond-like carbon coatings, Surf. Coatings Technol. 219 (2013) 144–150. doi:10.1016/j.surfcoat.2013.01.018.

[103] H. Unal, U. Sen, A. Mimaroglu, Dry sliding wear characteristics of some industrial polymers against steel counterface, Tribol. Int. 37 (2004) 727–732. doi:10.1016/j.triboint.2004.03.002.

[104] S. Thongsang, W. Vorakhan, E. Wimolmala, N. Sombatsompop, Dynamic mechanical analysis and tribological properties of NR vulcanizates with fly ash/precipitated silica hybrid filler, Tribol. Int. 53 (2012) 134–141. doi:10.1016/j.triboint.2012.04.006.

PUBLICATION 1

Tribological behavior of plasma-polymerized aminopropyltriethoxysilane films deposited on thermoplastic elastomers substrates. F. Alba-Elías, E. Sainz-García, A. González-Marcos, J. Ordieres-Meré, Thin Solid Films 540 (2013) 125-134

PUBLICATION 2

Enhanced surface friction coefficient and hydrophobicity of TPE substrates using an APPJ system. E. Sainz-García, F. Alba-Elías, R. Múgica-Vidal, A. González-Marcos, Applied Surface Science 328 (2015) 554-567

PUBLICATION 3

Promotion of tribological and hydrophobic properties of a coating on TPE substrates by atmospheric plasma-polymerization. E. Sainz-García, F. Alba-Elías, R. Múgica-Vidal, M. Pantoja-Ruiz, Applied Surface Science 371 (2016) 50-60

PUBLICATION 4

Antifriction aminopropyltriethoxysilane films on thermoplastic elastomer substrates using an APPJ system. E. Sainz-García, F. Alba-Elías, R. Múgica-Vidal, A. González-Marcos, Surface & Coatings Technology 310 (2017) 239-250